Review

A Review of Multiscale Computational Methods in Polymeric Materials

Ali Gooneie *, Stephan Schuschnigg and Clemens Holzer

Chair of Polymer Processing, Montanuniversitaet Leoben, Otto Gloeckel-Strasse 2, 8700 Leoben, Austria; stephan.schuschnigg@unileoben.ac.at (S.S.); clemens.holzer@unileoben.ac.at (C.H.)
* Correspondence: ali.gooneie@unileoben.ac.at; Tel.: +43-3842-402-3509

Abstract: Polymeric materials display distinguished characteristics which stem from the interplay of phenomena at various length and time scales. Further development of polymer systems critically relies on a comprehensive understanding of the fundamentals of their hierarchical structure and behaviors. As such, the inherent multiscale nature of polymer systems is only reflected by a multiscale analysis which accounts for all important mechanisms. Since multiscale modelling is a rapidly growing multidisciplinary field, the emerging possibilities and challenges can be of a truly diverse nature. The present review attempts to provide a rather comprehensive overview of the recent developments in the field of multiscale modelling and simulation of polymeric materials. In order to understand the characteristics of the building blocks of multiscale methods, first a brief review of some significant computational methods at individual length and time scales is provided. These methods cover quantum mechanical scale, atomistic domain (Monte Carlo and molecular dynamics), mesoscopic scale (Brownian dynamics, dissipative particle dynamics, and lattice Boltzmann method), and finally macroscopic realm (finite element and volume methods). Afterwards, different prescriptions to envelope these methods in a multiscale strategy are discussed in details. Sequential, concurrent, and adaptive resolution schemes are presented along with the latest updates and ongoing challenges in research. In sequential methods, various systematic coarse-graining and backmapping approaches are addressed. For the concurrent strategy, we aimed to introduce the fundamentals and significant methods including the handshaking concept, energy-based, and force-based coupling approaches. Although such methods are very popular in metals and carbon nanomaterials, their use in polymeric materials is still limited. We have illustrated their applications in polymer science by several examples hoping for raising attention towards the existing possibilities. The relatively new adaptive resolution schemes are then covered including their advantages and shortcomings. Finally, some novel ideas in order to extend the reaches of atomistic techniques are reviewed. We conclude the review by outlining the existing challenges and possibilities for future research.

Keywords: computer simulations; computational methods; multiscale modelling; hierarchical structures; multiple scales; bridging strategies; polymers; nanocomposites

---

Contents

1. Introduction

Polymeric materials display distinguished characteristics which range from the angstrom level of an individual bond, to tens of nanometers of the chain gyration radius, to micrometers, millimeters and larger in melts, blends, solutions and polymer nanocomposites (PNCs). The corresponding time scales of the dynamics relevant to different material properties span an even wider range from femtoseconds to seconds or even hours for large-scale ordering processes such as phase separation in blends. In order to highlight the inherent multiscale nature of polymer systems, two interesting cases from the literature are briefly outlined. Indeed, many other examples from various fields of polymer science can be found elsewhere [1–13]. We believe that the selected examples should suffice to serve the purpose as well as the brevity.

As the first example, PNCs are considered due to their importance to many applications. The incorporation of nanoparticles in polymers has attracted substantial academic and industrial interest due to the dramatic improvements in the properties of the host polymers. The addition of only 1–10 vol % nanoparticles has been shown to be able to enhance various properties of the neat polymers [14–20]. These changes are often introduced into the polymer matrix while many benefits of the neat polymer including rather easy processability are still preserved [21,22]. Therefore, PNCs are ideal candidates for multiple applications like medical devices, aerospace applications, automobile industries, coatings, etc. Experience has shown that the property enhancement in PNCs is directly linked to the nanoparticles arrangement and dispersion [21,23]. A precise morphology control is of great significance in PNCs, otherwise the full property potential of these materials cannot be achieved.

The fact that many of the common nanoparticles possess strong van der Waals interactions promotes their aggregation and consequently diminishes their effectiveness. On the other hand, the role of polymer-particle interactions can either facilitate or complicate the aggregation process. Moreover, the geometrical characteristics of the nanoparticles, such as aspect ratio and structural flexibility, add to the complexity of their impact on the properties since it can alter surface energies as well as surface-to-volume ratio [24]. Therefore, the structural characterization and the detailed evaluation of the fabrication of PNCs are crucial to achieve the desired properties. Many studies are devoted to understand the effects of processing conditions on the final microstructure and the resulting properties of the PNCs [19–21,23–27]. The multiscale nature of PNCs simply divulges if one considers the interplaying role of the fabrication stage with macroscopic characteristics and the aforementioned submicron phenomena involved in the final outcome of PNCs.

A fascinating field of application for multiscale methods is in biological systems [3,4,7]. For instance, we take a single hair strand. It is well known that hairs, i.e., keratin fibers, exhibit a complex structure [28]. Filaments with a diameter of approximately 8 nm are tightly packed in a matrix, filling the approximately 2 nm gap in between which are later assembled into a so-called macrofibril. Often, several hundred filaments form one macrofibril. Various macrofibrils can be categorized based on how packed they are. These macrofibrils constitute the main part of the hair cells in the cortex. The remaining volume of the cell is comprised of the remnants and pigment granules. The cross-section of a hair typically has almost 100 cells, contained by a cell-membrane structure. Finally, the cortex is encapsulated by the cuticle which forms the surface of a hair fiber. It is of significance to be able to find the relation between the mechanical properties of these fibers and the structure of the keratin proteins, temperature, humidity and deformation rate. Obviously, such analysis necessitates a multiscale approach to capture the precise behavior of the hair mechanics as suggested by Akkermans and Warren [28].

In order to find appropriate solutions to these questions, several theories and computational methods were developed which could introduce new possibilities to design, predict and optimize the structures and properties of materials. At present, no single theory or computational method can cover various scales involved in polymeric materials. As a result, the bridging of length and time scales via a combination of various methods in a multiscale simulation framework is considered to be one of the most important topics in computational materials research. The resulting multiscale method is preferably supposed to predict macroscopic properties of polymeric materials from fundamental molecular processes. In order to build a multiscale simulation, often models and theories from four characteristics length and time scales are combined. They are roughly divided into the following scales.

1. The quantum scale (~10^{-10} m, ~10^{-12} s): The nuclei and electrons are the particles of interest at this scale and quantum mechanics (QM) methods are used to model their state. The possibility to study the phenomena associated with formation and rupture of chemical bonds, the changes in electrons configurations, and other similar phenomena are typical advantages of modelling at quantum scale.

2. The atomistic scale (~10^{-9} m, ~10^{-9}–10^{-6} s): All atoms or small groups of atoms are explicitly represented and treated by single sites in atomistic simulations. The potential energy of the system is estimated using a number of different interactions which are collectively known as force fields. The typical interactions include the bonded and nonbonded interactions. The bonded interactions often consist of the bond length, the bond angle, and the bond dihedral potentials. The most typically used nonbonded interactions are Coulomb interactions and dispersion forces. Molecular dynamics (MD) and Monte Carlo (MC) simulation techniques are often used at this level to model atomic processes involving a larger group of atoms compared with QM.

3. The mesoscopic scale (~10^{-6} m, ~10^{-6}–10^{-3} s): At mesoscopic scale, a molecule is usually described with a field or a microscopic particle generally known as a bead. In this way the molecular details are introduced implicitly which provides the opportunity to simulate the phenomena on longer length and time scales hardly accessible by atomistic methods. A good example for the field-based

description of polymer systems is the Flory-Huggins model for the free energy of mixing in which the details of the system are summed up in model parameters. On the other hand, in particle-based models collections of particles are accumulated in beads through a coarse-graining procedure. The interactions between the beads are then used to characterize the system. Various methods have been developed to investigate the mesoscopic structures in polymeric systems including dissipative particle dynamics (DPD), Brownian dynamics (BD), lattice Boltzmann (LB), dynamic density functional theory (DDFT), and time-dependent Ginzburg-Landau (TDGL) theory.

4. The macroscale (~10^{-3} m, ~1 s): At this scale, the system is treated as a continuous medium and the discrete characteristics of atoms and molecules are ignored. The behavior of such a system is governed by constitutive laws which are often coupled with conservation laws to simulate various phenomena. All functions such as velocity and stress components are continuous except at a finite number of locations which separate continuity regions. The fundamental assumption at this scale is in replacing a heterogeneous material with an equivalent homogeneous model. The most important methods used to simulate systems at this scale are finite difference method (FDM), finite element method (FEM), and finite volume method (FVM).

Although several review papers are available on the topic of multiscale simulations in materials [1–12,29–31], a comprehensive discussion of its various aspects in polymer science is still needed. Some reports approach the objective by introducing different case studies and never actually detailing various categories of multiscale methods, while some others focus only on a specific topic in multiscale simulations such as coarse-graining or concurrent simulations. Here, we aim to provide an opportunity for the interested reader to explore how such techniques might be applied in their own area of specialty by focusing on the core concepts of major trends in this field all in one place. Consequently, we outline the basics of the methods and illustrate each one with a few examples from the vast field of polymeric systems. We organize the review as follows. In Section 2, we introduce some of the most significant computational methods used so far to model different scales. This part is not intended to provide detailed description of each method. Instead, we aim to emphasize different approaches, challenges, restrictions, and opportunities that models of each scale could generally possess. Since such models are the building blocks for the multiscale methods, it is important to note how they convey their characteristics into a multiscale approach. We strongly advice the interested reader to refer to relevant literature, some significant ones introduced here, for further information. In Section 3, we discuss in detail various ideas to link scales in a multiscale package. Four major blocks are presented in this part: Sequential Multiscale Approaches, Concurrent Multiscale Approaches, Adaptive Resolution Simulations, and Extending Atomistic Simulations. This section is the core of the paper and therefore we attempt to deliver the most recent advances in each instance. In every case, the applications in polymer science are highlighted to serve the topic. It was a serious concern of ours to cite the outstanding studies that could cover from the classic fundamental works up to the latest publications. We hope this eases further pursue of the relevant works. It should be noted that the topic at hand is massive and there might be some significant studies which are left out despite our attempts. Finally, we conclude the review by emphasizing the current challenges and future research directions. Overall, the present review is meant to put forth the major directions in multiscale simulation strategies in polymer science.

2. Simulation Methods

In general, computational methods are categorized into either particle-based or field-based approaches [32,33]. The particle-based methods incorporate particles to represent the building blocks of polymers such as atoms, molecules, monomers, or even an entire polymer chain. These particles (and their combinations in the form of bonds, angles, dihedrals and so on) often interact with each other through certain forces which form a force field altogether [34]. By the application of a statistical mechanical sampling method, the particles are allowed to move within a certain thermodynamic ensemble and hence simulate a desired process [35]. Perhaps the most well-known

particle-based techniques are MD and its coarser versions such as DPD. In the second category, i.e., the field-based approaches, the system is typically described in terms of effective potentials, collective dynamic variables, and density fields which determine the degrees of freedom of the model [36]. Therefore, a reduced representation of the system is developed based on some phenomenological approximation [32]. The famous Flory approximation of the free energy of a polymer is a good example of the field-based strategy [37]. Another valuable field-based method is the polymer reference interaction site model (PRISM) which attempts to realize the polymer structure in terms of density correlation functions [38]. Other examples of such methods include density functional theory (DFT) [38–40], self-consistent field theory (SCFT) [32,33,38], and phase-field techniques [41–43]. In this section, we outline the details of some of the most important methods at different scales. These methods mainly belong to the particle-based approaches due to their relevance to the rest of the discussion as well as to our own research interest. For more details on the field-based methods, the reader is referred to the cited literature.

2.1. Quantum Mechanics

A precise treatment of atomistic scale phenomena requires the solution of the Schrödinger wave equations for all electrons and nuclei on the basis of a quantum scale modelling [44]. In QM, the time-independent form of the wave equation $\phi(\mathbf{r})_k$ for a particle in an energy eigenstate E_k in a potential $U(\mathbf{r})$ having coordinates vector $\mathbf{r}$ and mass m is

$$-\frac{h^2}{8\pi^2 m}\nabla^2\phi(\mathbf{r})_k + U(\mathbf{r})\phi(\mathbf{r})_k = E_k\phi(\mathbf{r})_k,$$ (1)

where h is Planck's constant. It can be shown that for a material having i electrons with mass m_{el} and the negative unit charge of $-e$ and the coordinates $\mathbf{r}_{el_i}$, and j nuclei with mass m_n and a positive unit charge of $z_n e$ with z_n being the atomic number, and the spatial coordinates $\mathbf{r}_{n_j}$, Equation (1) becomes

$$
\begin{aligned}
&-\frac{h^2}{8\pi^2 m_{el}}\sum_i \nabla_i^2\phi(\mathbf{r}_{el_1},\mathbf{r}_{el_2},\ldots,\mathbf{r}_{el_i},\mathbf{r}_{n_1},\mathbf{r}_{n_2},\ldots,\mathbf{r}_{n_j})_k \\
&-\frac{h^2}{8\pi^2}\sum_j \frac{1}{m_{n_j}}\nabla_j^2\phi(\mathbf{r}_{el_1},\mathbf{r}_{el_2},\ldots,\mathbf{r}_{el_i},\mathbf{r}_{n_1},\mathbf{r}_{n_2},\ldots,\mathbf{r}_{n_j})_k \\
&+\left(\sum_{\substack{i_1,i_2 \\ i_1\neq i_2}}\frac{e^2}{\left|\mathbf{r}_{el_{i1}}-\mathbf{r}_{el_{i2}}\right|}+\sum_{i,j}\frac{z_j e^2}{\left|\mathbf{r}_{el_i}-\mathbf{r}_{n_j}\right|}+\sum_{\substack{j_1,j_2 \\ j_1\neq j_2}}\frac{z_{j1}z_{j2}e^2}{\left|\mathbf{r}_{n_{j1}}-\mathbf{r}_{n_{j2}}\right|}\right)\phi(\mathbf{r}_{el_1},\mathbf{r}_{el_2},\ldots,\mathbf{r}_{el_i},\mathbf{r}_{n_1},\mathbf{r}_{n_2},\ldots,\mathbf{r}_{n_j})_k \\
&= E_k\phi(\mathbf{r}_{el_1},\mathbf{r}_{el_2},\ldots,\mathbf{r}_{el_i},\mathbf{r}_{n_1},\mathbf{r}_{n_2},\ldots,\mathbf{r}_{n_j})_k.
\end{aligned}
$$ (2)

In 1927, Born and Oppenheimer [45] proposed a strategy to separate the wave functions of the light electrons from the heavy nuclei considering that the electrons typically relax to some orders of magnitude faster than the nuclei. This strategy, known as the adiabatic Born-Oppenheimer approximation, assumes that the electrons always remain in their ground state irrespective of the positions of the nuclei by adiabatically adjusting to the movements of the nuclei. As a result of this assumption, one can define the wave function ϕ in Equation (2) as the product of two independent wave functions. In this approach, one function describes the dynamics of the electrons ϖ and the other function describes the dynamics of the nuclei φ. This can be shown as

$$\phi(\mathbf{r}_{el_1},\mathbf{r}_{el_2},\ldots,\mathbf{r}_{el_i},\mathbf{r}_{n_1},\mathbf{r}_{n_2},\ldots,\mathbf{r}_{n_j}) = \varpi(\mathbf{r}_{el_1},\mathbf{r}_{el_2},\ldots,\mathbf{r}_{el_i})\,\varphi(\mathbf{r}_{n_1},\mathbf{r}_{n_2},\ldots,\mathbf{r}_{n_j}).$$ (3)

Consequently, the corresponding wave function of the electrons with the eigenstate energy $E_{k_{el}}$ is

$$
\left(-\frac{h^2}{8\pi^2 m_{el}} \sum_i \nabla_i^2 + \sum_{\substack{i1,i2 \\ i1 \neq i2}} \frac{e^2}{\left| \mathbf{r}_{el_{i1}} - \mathbf{r}_{el_{i2}} \right|} + \sum_{i,j} \frac{z_j e^2}{\left| \mathbf{r}_{el_i} - \mathbf{r}_{n_j} \right|} \right) \varpi(\mathbf{r}_{el_1}, \mathbf{r}_{el_2}, \ldots, \mathbf{r}_{el_i})_{k_{el}} =
$$
$$
E_{k_{el}}^{el} \varpi(\mathbf{r}_{el_1}, \mathbf{r}_{el_2}, \ldots, \mathbf{r}_{el_i})_{k_{el}}, \tag{4}
$$

and the corresponding wave function of the nuclei with the eigenstate energy E_{k_n} is

$$
\left(-\frac{h^2}{8\pi^2} \sum_j \frac{1}{m_n} \nabla_j^2 + \sum_{i,j} \frac{z_j e^2}{\left| \mathbf{r}_{el_i} - \mathbf{r}_{n_j} \right|} + \sum_{\substack{j1,j2 \\ j1 \neq j2}} \frac{z_{j1} z_{j2} e^2}{\left| \mathbf{r}_{n_{j1}} - \mathbf{r}_{n_{j2}} \right|} \right) \varphi(\mathbf{r}_{n_1}, \mathbf{r}_{n_2}, \ldots, \mathbf{r}_{n_j})_{k_n} = E_{k_n}^n \varphi(\mathbf{r}_{n_1}, \mathbf{r}_{n_2}, \ldots, \mathbf{r}_{n_j})_{k_n}. \tag{5}
$$

It is worthy to note at this point that the use of the adiabatic Born-Oppenheimer approximation is justified only when the energy gap between ground and excited electronic states is larger than the energy scale of the nucleus motion. This assumption has been shown to fail in materials with zero energy gaps such as metals [46,47] and the free-state graphene [48]. Despite this, the adiabatic Born-Oppenheimer approximation has proved effective in the atomistic simulations of some metallic [49] and graphene-based systems [50] as well.

The quantum mechanical many-body problem was formulated by Kohn and Sham [40] in the density functional theory (DFT). In DFT, electrons were replaced by effective electrons with the same total density moving in the potential generated by the other electrons and ion cores. Later, DFT was modified by Car and Parrinello [51] which allowed for the movements to be incorporated into the DFT scheme, thus leading to the so-called ab initio MD (AIMD). Such methods have found useful applications in polymer science such as the simulation of mechanics of polyethylene (PE) macromolecules [52–54], conduction in polymers [55–57], polymerization [58,59], crystal structures [60], disordered conformations of poly(tetra fluoro ethylene) chains [61], and diffusion in polymers [62].

2.2. Atomistic Techniques

Atomistic scale simulations often benefit from Equation (5) to predict the initial atomic configurations assuming that the electrons are instantaneously equilibrated during the movements of the nuclei. The approximation methods of this equation are mainly divided into stochastic and deterministic approaches. The stochastic approaches are often referred to as MC methods which are well-credited to evaluate equilibrium states for certain distribution functions or to solve the equations of motion in their corresponding integral form. The deterministic approaches are typically referred to as MD which are mainly used to discretely solve the equation of motion. In general, simulations at this scale provide an atomistic picture of the interactions between components and conformational dynamics which could help uncover the underlying phenomena. By the way of illustration, we consider an example of the application of MD to PNCs in the work of Piscitelli et al. [63] who investigated the functionalization of sodium montmorillonite (Na-MMT) using three aminosilanes characterized by different lengths of the alkyl chains. It is known that the presence of negative charges on the surface of each MMT layer as well as counteracting cations such as sodium or potassium located in the vicinity of the platelets within the galleries produce highly polar pristine structures of Na-MMT [14,21,23]. These structures further lead to their incompatibility with the majority of polymers. Consequently, a simple dispersion of Na-MMT in a polymer results in the formation of aggregated structures within the matrix which is followed by the deterioration of the property enhancement in these PNCs. In order to avoid these structures, chemical functionalization of Na-MMT platelets like silylation reaction is often performed [14]. The X-ray diffraction (XRD) patterns of Piscitelli et al. [63] indicated that the silylation reaction results in the Na-MMT galleries to open up regardless of the type of the aminosilane. However,

it was observed that the *d*-spacing in the modified Na-MMT was reduced as the organic chain of the aminosilane molecule became longer. This outcome might not be expected before the experiments and therefore MD was incorporated to illuminate the underlying phenomena. The simulations revealed the increasing tendency of aminosilane molecules with increasing their length to interact among themselves by intermolecular hydrogen bonding as well as hydrophobic interactions. These interactions could eventually lead to the bridging of aminosilane molecules between two Na-MMT layers for longer chains. This situation not only does not improve the *d*-spacing of the modified Na-MMT compared with the unmodified nanoparticles, but also acts against any attempts from polymer macromolecules to open up the layers. As observed in these simulations, MD can play a key role in the understanding of molecular mechanisms involved in the intercalation process in polymer/clay nanocomposites. Without a thorough vision of such molecular processes in aminosilane-functionalized Na-MMTs, the designed PNC would fail due to this general belief that longer organic chains normally result in higher interlayer spacing. In the following, MC and MD techniques are revisited.

2.2.1. Monte Carlo

In general, the MC methods include a large number of stochastic computer experiments by incorporating uncorrelated random numbers. MC can be used to mimic stationary ensembles by exploring a multitude of states in the corresponding phase space. Therefore, one can obtain pseudo-time-averaged statistical data by calculating ensemble averages along trajectories in the phase space assuming the ergodic system behavior [64–66]. It should be noted that the MC methods are not restricted to the atomistic scale but can be used at any scale if an appropriate probabilistic model is provided.

MC methods often consist of three characteristic steps. These steps are: (i) translation of the physical phenomena under investigation into an analogous probabilistic or statistical model; (ii) solving the resulting probabilistic model by a large number of numerical stochastic sampling experiments; and (iii) analyzing the generated data utilizing statistical methods. The sampling method can follow either a simple sampling algorithm or a weighted sampling algorithm. The simple sampling uses an equal distribution of the random numbers while the weighted sampling develops random numbers based on a distribution which is accommodated to the problem being investigated. The weighted sampling algorithm is the underlying principle of the so-called Metropolis MC algorithm [67].

In Metropolis MC for canonical and/or microcanonical ensembles with N atoms, a new configuration of the atoms is achieved by randomly or systematically choosing one atom and moving it from its initial position *i* to the temporary trial position *j*. Consequently, the initial state $\mathbf{\Gamma}_i$ of the system in the corresponding phase space is changed to the trial state $\mathbf{\Gamma}_j$. This displacement alters the Hamiltonian of the system from $H(\mathbf{\Gamma}_i)$ to $H(\mathbf{\Gamma}_j)$ according to the particular interactions being considered in the model. Therefore, the change in the system Hamiltonian $\Delta H(\mathbf{\Gamma}_{i \to j})$ is

$$\Delta H(\mathbf{\Gamma}_{i \to j}) \;=\; H(\mathbf{\Gamma}_j) \;-\; H(\mathbf{\Gamma}_i). \tag{6}$$

If the imposed movement of the chosen atom brings the system to a lower state of energy, i.e., $\Delta H(\mathbf{\Gamma}_{i \to j}) \;<\; 0$, the movement is accepted and the displaced atom remains in its new position. Otherwise, the imposed movement is only accepted with a certain probability $p_{i \to j}$ which is proportional to

$$p_{i \to j} \;\propto\; \exp\left(-\frac{\Delta H(\mathbf{\Gamma}_{i \to j})}{k_B T} \right), \tag{7}$$

where k_B is Boltzmann's constant, and T is temperature. In Metropolis MC, a random number ζ between 0 and 1 is generated and used to test the new configuration. The imposed movement is accepted only if $\zeta \leq \exp\left(-\frac{\Delta H(\mathbf{\Gamma}_{i \to j})}{k_B T}\right)$. If the movement is not accepted, the initial position is assumed to be the new position and the entire procedure is repeated by considering another randomly chosen atom.

The Metropolis MC also suggests using the same strategy for the grandcanonical ensemble where the number of initial atoms might change. For this purpose, the change in the system energy due to the exchange of an arbitrarily chosen atom by an atom of a different kind is taken into account to determine whether the new configuration is accepted or not. The methodology is the same as before.

As a final remark on MC, it should be noted that the original MC methods were intrinsically designed to simulate the equilibrium states of a system. The extension of the MC predictions to the simulation of microstructure evolution was first promoted by the incorporation of Ising lattice model in Potts-type MC models [68–70]. In the sense of using an internal kinetic measure such as the number of MC steps, this class of MC models is often referred to as kinetic MC models [71–75].

MC simulations have been utilized to describe a variety of phenomena in polymeric materials. Its application covers a wide range of problems including study of polymer degradation [71,73], development of surface morphology in thin films [76–80], heterophase interfaces [81–94], crystal growth and melting [95–98], morphology evolution [99–106], fracture behavior [107], diffusion [108–111], study of polymer melt viscoelasticity by nonequilibrium MC [112,113], and prediction of phase diagrams [114,115].

2.2.2. Molecular Dynamics

The MD method is a deterministic simulation technique for the simulation of many-body interaction phenomena at the atomistic scale. It is based on substituting the quantum mechanical expression for the kinetic energy in Equation (5) by the classic momentum term and solving it for a nucleon using Newton's law of motion. Consequently, the simulation of a many-body system would require the formulation and solution of equations of motion of all constituting particles. The equation of motion of a particle *i* is

$$m_i \frac{d^2 \mathbf{r}_i}{dt^2} = \mathbf{f}_i, \tag{8}$$

where m_i is the particle mass and $\mathbf{r}_i$ is the particle position vector. $\mathbf{f}_i$ is the force acting on the *i*th particle at time t which is obtained as the negative gradient of the interaction potential U, i.e., $\mathbf{f}_i = -\nabla U = -\left(\frac{\partial U}{\partial x}\mathbf{i} + \frac{\partial U}{\partial y}\mathbf{j} + \frac{\partial U}{\partial z}\mathbf{k}\right)$. The underlying potentials are often quantified in terms of the relative position of two or more particles. This means that these potentials together with their parameters, i.e., the so-called force field, describe how the potential energy of a many-body system depends on the coordinates of the particles [34,116]. Such a force field can be obtained by QM, empirical methods, and quantum-empirical methods. It should be noted that the criteria for selecting an adequate force field should address the necessary precision in the system description, transferability, and computational speed.

The overall algorithm of MD is to simulate the evolution of particle configurations based on an adequate force field by integrating the equations of motion over discrete steps in time. The procedure is simply to calculate the position and velocity of every particle at present and a time step later. The system of equations of motion of N particles can be solved by utilizing FDM. The Verlet technique is possibly the most common integration scheme among all [117,118]. Utilizing the Taylor expansion, it uses the positions $\mathbf{r}_i(t)$ and accelerations $\mathbf{a}_i(t)$ at time t, and positions $\mathbf{r}_i(t - \Delta t)$ from the previous time step $t - \Delta t$, to calculate the new positions $\mathbf{r}_i(t + \Delta t)$ at the next time $t + \Delta t$ according to

$$\mathbf{r}_i(t + \Delta t) \approx 2\mathbf{r}_i(t) - \mathbf{r}_i(t - \Delta t) + \mathbf{a}_i(t)(\Delta t)^2. \tag{9}$$

The velocities $\mathbf{v}_i(t)$ and $\mathbf{v}_i\left(t + \frac{1}{2}\Delta t\right)$ at times t and $t + \frac{1}{2}\Delta t$ can be estimated as

$$\mathbf{v}_i(t) \approx \frac{\mathbf{r}_i(t + \Delta t) - \mathbf{r}_i(t - \Delta t)}{2\Delta t}, \tag{10}$$

$$\mathbf{v}_i\left(t + \frac{1}{2}\Delta t\right) \approx \frac{\mathbf{r}_i(t + \Delta t) - \mathbf{r}_i(t)}{\Delta t}. \tag{11}$$

A typical interaction potential U may consist of a number of bonded and nonbonded interaction terms. The bonded interactions may include bond stretching, bond angle bending, dihedral angle torsion, and inversion interaction potentials described by various functions such as harmonic functions. The nonbonded interactions contain electrostatic and van der Waals contributions and may consist of various potential types such as Lennard-Jones potential, Buckingham potential, Coulombic potential, etc. The concept of using interaction potentials makes it possible to carry out atomistic MD simulations which reveal the atomistic mechanisms and intrinsic structural properties by considering a relatively large number of particles.

While MD is shown to be a promising and reliable method in atomistic scale modelling, it has statistical limitations. A comparison of MC and MD methods suggests that in a phase space with 6N degrees of freedom, N being the total number of particles, MC allows one to investigate many more states than MD. Therefore, the validity of ensemble averages obtained by MD is limited to the assumption of system ergodicity; an assumption which is not unambiguously proven [64]. Still, the great power of MD is its proficiency to predict microstructure dynamics along its deterministic trajectory at an atomistic level. Applications of MD in the field of polymeric materials include topics such as macromolecular dynamics [119–124], intercalation phenomena in polymer/clay nanocomposites [63], structure of interfaces [125–127], polymer membranes [128,129], crystal structures [130–132], diffusion phenomena [133–136], segregation phenomena [137], tribological properties and crack propagation [138–140], thin films and surfaces [141–144], liquid crystalline polymers [145,146], rheology of polymeric systems [147–150], application of elongational flows on polymers using nonequilibrium MD [151,152], and the simulations of reactive systems such as crosslinking and decomposition of polymers using the ReaxFF force field [153–156].

2.3. Mesoscale Techniques

Atomistic simulations of complex systems including polymeric materials provide a detailed picture of, for instance, the interactions between components and conformational dynamics. Such information is often missing in macroscale models. On the other hand, the description of hydrodynamic behavior is relatively straightforward to handle in macroscale methods while it is challenging and expensive to address in atomistic models. Between the domains of these scale ranges, there is the intermediate mesoscopic scale which extends the time scale of atomistic methods. To show the importance of the time scale in the observed phenomena in soft matters, we take the lipid bilayers as an example. Bonds and angles of lipid molecules fluctuate within a time scale of a few picoseconds [157]. If the time scale is increased by an order of magnitude, trans-gauche isomerizations of dihedrals take place [158]. By further increasing the time scale to a few nanoseconds, the phospholipid molecule rotates around its axis. Moving on to longer time scales, two lipids can switch places in a bilayer on a time scale of tens of nanoseconds. Moreover, the individual lipid molecules orient and form membranes protrusions [159]. The peristaltic motions and undulations take place on a scale of 100 ns [160]. Finally, the steady transverse diffusion of lipids dominates on a time scale of 2 ms [161]. Simulating such a wide range of time scales in a single atomistic MD model needs large-scale computational resources. Consequently, the various mesoscale methods are developed which attempt to link atomistic and macroscale techniques and compensate for their shortcomings. Here, we briefly review BD, DPD and LB techniques which are often used at this scale. In addition to these methods, we also refer the interested reader to the stochastic multiparticle collision

model developed by Malevanets and Kapral [162] to investigate complex fluids such as polymers. This method was recently coupled with MD and an adaptive resolution hybrid model was achieved which is particularly interesting to study transport and hydrodynamic properties [163].

2.3.1. Brownian Dynamics

The motions of colloidal particles in dilute dispersions are a common example to introduce the BD method. Since the solvent molecules are often much smaller than the colloidal particles, the characteristic time of the motions of the solvent molecules is much smaller than that of the particles. Therefore, if one observes such dispersions based on the characteristic time of the solvent molecules in a MD framework, the suspended particles seem quiescent. In this case, a very long simulation time is necessary in order to observe the motions of particles. Hence, performing MD simulations is unrealistic when it is necessary, for instance, to trace a particle in time in order to calculate the diffusion coefficient. BD method overcomes this difficulty by replacing the explicit solvent molecules in MD with an implicit continuum medium. In BD simulations, the effects of the solvent molecules on the colloidal particles are defined by dissipative and random forces.

If the dispersion is dilute enough to neglect the hydrodynamic interactions between particles, the Brownian motion of particle i is generally described by the Langevin equation as [164]

$$m_i \frac{d^2 \mathbf{r}_i}{dt^2} = \mathbf{f}_i - \xi \mathbf{v}_i + \mathbf{f}_i^B. \tag{12}$$

In this equation, m_i, $\mathbf{r}_i$ and $\mathbf{v}_i$ are the mass, position and velocity vectors of the particle i, $\mathbf{f}_i$ is the sum of the forces exerted on particle i by the other particles, and ξ is the friction coefficient. Here, $\mathbf{f}_i^B$ is the random force inducing the Brownian motions of the particle due to the motions of solvent molecules. The random force should be independent of the particle position and velocity and is described by its stochastic properties

$$\left\langle \mathbf{f}_i^B(t) \right\rangle = 0, \tag{13}$$

$$\left\langle \mathbf{f}_i^B(t) \cdot \mathbf{f}_i^B(t') \right\rangle = A \delta(t - t'), \tag{14}$$

where $\delta(t - t')$ is the Dirac delta function and $A = 6 \xi k_B T$. The position and velocity of each particle in time is therefore described as

$$\mathbf{r}_i(t + \Delta t) = \mathbf{r}_i(t) + \frac{m_i}{\xi} \mathbf{v}_i(t) \left(1 - e^{-\frac{\xi}{m_i} \Delta t} \right) + \frac{1}{\xi} \mathbf{f}_i(t) \left(\Delta t - \frac{m_i}{\xi} \left(1 - e^{-\frac{\xi}{m_i} \Delta t} \right) \right) + \delta \mathbf{r}_i^B(t + \Delta t), \tag{15}$$

$$\mathbf{v}_i(t + \Delta t) = \mathbf{v}_i(t) e^{-\frac{\xi}{m_i} \Delta t} + \frac{1}{\xi} \mathbf{f}_i(t) \left(1 - e^{-\frac{\xi}{m_i} \Delta t} \right) + \delta \mathbf{v}_i^B(t + \Delta t). \tag{16}$$

The terms $\delta \mathbf{r}_i^B(t + \Delta t)$ and $\delta \mathbf{v}_i^B(t + \Delta t)$ represent a random displacement and velocity change due to the random forces. One can utilize a two-dimensional normal distribution to sample these terms based on random numbers [165]. Consequently, the positions and velocities of the particles can be updated in every time step during the simulations. It should be noted that the momentum is not conserved in the formulation of BD due to the random noise terms. As a result, BD cannot reproduce correct hydrodynamics and is limited to the prediction of diffusion properties [164,166,167].

If the dispersion is not dilute and the hydrodynamic interactions between the particles are not negligible, the above equations should be modified. Ermak and McCammon [168] have introduced such effects into BD. In their method, the diffusion tensor is utilized to re-write the Langevin equation. Recently, Ando et al. [169] suggested to use Krylov subspaces for computing Brownian random noise vectors. Their method facilitates performing large-scale BD simulations with hydrodynamic interactions. They showed that only low accuracy is required in the Brownian noise vectors to accurately evaluate dynamic and static properties of model polymer and monodisperse suspensions. BD has been incorporated to study a variety of phenomena including particle dispersions [170–177],

polymer solutions [178–181], confined suspensions [182], peeling behavior of polymer molecules from a surface [183], and translocation of complex molecules through nanopores [184,185].

2.3.2. Dissipative Particle Dynamics

DPD is a relatively new mesoscopic particle simulation method proposed by Hoogerbrugge and Koelman in 1992 [186]. Fundamentally, DPD is similar to MD except for the fact that individual DPD particles (which are often referred to as beads in the literature) represent the dynamic behavior of several atoms or molecules. This coarse-graining strategy along with the softer potential functions incorporated to represent bead-bead interactions allow for the simulation of dynamic processes over longer time scales [187,188].

In DPD, the motion of each bead is dominated by three pairwise forces. For bead i with the mass m_i and position vector $\mathbf{r}_i$, the Newton's equation of motion becomes

$$m_i \frac{d^2 \mathbf{r}_i}{dt^2} = \sum_j (F_{ij}^C + F_{ij}^D + F_{ij}^R), \tag{17}$$

in which F_{ij}^C, F_{ij}^D, and F_{ij}^R are respectively the conservative, the dissipative, and the random forces between bead i and its neighboring beads within a certain force cutoff radius r_{cut}. These forces are defined as [187]

$$F_{ij}^C = \mathbb{A}_{ij}\chi_{ij}\left(1 - \frac{r_{ij}}{r_{cut}}\right)\hat{\mathbf{r}}_{ij}, \tag{18}$$

$$F_{ij}^D = -\xi_{ij}\omega^D(\mathbf{r}_{ij})\mathbf{r}_{ij}[(\mathbf{v}_i - \mathbf{v}_j)\cdot\hat{\mathbf{r}}_{ij}]\hat{\mathbf{r}}_{ij}, \tag{19}$$

$$F_{ij}^R = \sigma_{ij}\omega^R(\mathbf{r}_{ij})\mathbf{r}_{ij}\zeta_{ij}\hat{\mathbf{r}}_{ij}. \tag{20}$$

Here, $\mathbf{r}_{ij}$ is the distance between the beads i and j, is the unit vector pointing from the center of bead j to that of bead i, χ_{ij} equals 1 for beads with a distance less than r_{cut} and equals 0 otherwise. $\mathbf{v}_i$ and $\mathbf{v}_j$ are the velocity vectors of the ith and jth beads, respectively. ζ_{ij} is a Gaussian random number with zero mean and unit variance. $\mathbb{A}_{ij}$ is the maximum repulsion between bead i and bead j. ξ_{ij} and σ_{ij} are the friction coefficient and the noise amplitude between bead i and bead j, respectively. $\omega^D(\mathbf{r}_{ij})$ and $\omega^R(\mathbf{r}_{ij})$ are dissipative and random weight functions, respectively. DPD simulations often obey the fluctuation-dissipation theorem in which one of the two weight functions fixes the other one [189]. This theory dictates that the random and dissipative terms must be administered in a particular way in order to maintain the correct Boltzmann distribution in equilibrium. As a consequent of this theory, one has

$$\omega^D(\mathbf{r}_{ij}) = \left[\omega^R(\mathbf{r}_{ij})\right]^2, \tag{21}$$

$$\sigma_{ij}^2 = 2\xi_{ij}k_B T. \tag{22}$$

These relationships ensure an equilibrium distribution of bead velocities for thermodynamic equilibrium. In many studies, the weight functions are

$$\omega^D(\mathbf{r}_{ij}) = \left[\omega^R(\mathbf{r}_{ij})\right]^2 = \chi_{ij}\left(1 - \frac{r_{ij}}{r_{cut}}\right)^2. \tag{23}$$

Due to the pairwise nature of the forces involved in DPD framework, all of the beads obey Newton's third law [190]. As a result, the sum of all forces in the system vanishes. Furthermore, any given volume of beads in the system is only accelerated by the sum of all forces that cross its boundaries. This is the fundamental assumption which results in the Navier-Stokes equation. Consequently, DPD formulation conserves hydrodynamics [187,190,191]. If the random force was not pairwise as in BD formulation see Equation (12), momentum would not be conserved [164,165].

At every time step during the simulation, the set of positions and velocities of the beads is updated utilizing the positions and velocities at the earlier time. In principle, all algebraic update algorithms from MD can be used in DPD. However, the dependence of forces on velocity in DPD complicates the algorithm. A common approach to solve this problem is to use a modified version of the velocity-Verlet algorithm [117,118,187]. For bead i with unit mass and the overall force $\mathbf{f}_i$ over a short interval of time Δt, the algorithm suggests

$$\mathbf{r}_i(t + \Delta t) \approx \mathbf{r}_i(t) + \mathbf{v}_i(t)\,\Delta t + \frac{1}{2}\mathbf{f}_i(t)(\Delta t)^2, \tag{24}$$

$$\tilde{\mathbf{v}}_i(t + \Delta t) \approx \mathbf{v}_i(t) + \lambda\,\mathbf{f}_i(t)\,\Delta t, \tag{25}$$

$$\mathbf{f}_i(t + \Delta t) \approx \mathbf{f}_i(\mathbf{r}_i(t + \Delta t), \tilde{\mathbf{v}}_i(t + \Delta t)), \tag{26}$$

$$\mathbf{v}_i(t + \Delta t) \approx \mathbf{v}_i(t) + \frac{1}{2}\Delta t\,(\mathbf{f}_i(t) + \mathbf{f}_i(t + \Delta t)). \tag{27}$$

In this algorithm, the velocity in the next time step is first estimated by a predictor method, i.e., $\tilde{\mathbf{v}}_i(t + \Delta t)$ and then corrected in the last step, i.e., $\mathbf{v}_i(t + \Delta t)$. If the forces were independent of velocity, the actual velocity-Verlet algorithm would be recovered for $\lambda = 0.5$. The parameter λ has been shown to affect the temperature in DPD simulations by Den Otter and Clarke [192]. Based on empirical observations, some authors suggest $\lambda = 0.65$ would yield an accurate temperature control probably due to the cancellation of errors [190].

In recent years, modified versions of DPD formulation have been developed. For instance, Pan et al. [193] formulated DPD by borrowing ideas from fluid particle model. This approach enabled an explicit separation of dissipative forces into central and shear components. As a further consequence of this methodology, the hydrodynamics of Brownian colloidal suspensions were correctly captured by redistributing and balancing the forces. In another study, Yamanoi et al. [194] replaced the conservative forces with entanglement forces in the force field to reproduce the physics of entangled polymers. In this way, they could successfully simulate static as well as dynamic behavior of linear polymer melts. Despite these efforts, the standard DPD has also shown quite capable of simulating complex systems such as compatibilized and uncompatibilized polymer/clay nanocomposites under shear flows [195,196]. Various polymeric systems have been successfully treated in the DPD framework such as blood rheology [197–199], rheology of ultrahigh molecular weight polymers [200], lipid bilayers [161], adsorption characteristics of confined PE glycols dissolved in water [201], crosslinking of thermoset resins and formation of a network in the bulk [202], structure of thermoset polymers near an alumina substrate [203], graphene structure [204], surfactant aggregation [205], photo degradation process of polymer coatings [71], distribution of nanoparticles in lamellar and hexagonal diblock copolymer matrices [206,207], surface segregation and self-repairing systems [208–210], and electrical percolation threshold in packed assemblies of oriented fiber suspensions [211].

2.3.3. Lattice Boltzmann

While BD and DPD techniques borrow ideas from MD to tackle the challenges at the mesoscale, some other methods such as lattice gas cellular automata (LGCA) and LB incorporate kinetic theory concepts. In this part of the paper, we briefly point out the fundamental ideas of LGCA at first and afterwards introduce LB as a pre-averaged version of LGCA.

LGCA was initially designed to overcome the computational limitations in the study of fluids at high Reynolds numbers (Re) [212]. In this method, the particles of fluid are bound to move on the nodes of a discrete lattice at discrete time steps. At each time step particles can move from one lattice node to a neighboring node according to a set of prescribed velocity vectors $\{v_k\}$ which connect the neighboring nodes. In addition, only single occupancy is allowed for each possible velocity at a given node. The dynamics has two steps according to LGCA: (i) a propagation step, and (ii) a collision step. In the propagation step, also known as the streaming step, the particles move from their current node to an empty neighboring node with respect to their velocity. In the collision step, the particles collide and scatter according to certain rules which honor the mass and momentum conservation. In this way the Navier-Stokes equations are simulated correctly provided that the lattice and the velocity space are chosen carefully [164,165]. Although LGCA is unconditionally stable, it does not allow as large Re as it was initially thought [166].

LB inherits the discretized lattice dynamics based on propagation and collision steps from LGCA. However, it incorporates a one-particle distribution function as the relevant dynamic variable instead of the particle-based dynamics in LGCA. Initially, the collisions in LB is modelled by pre-averaging the collision schemes in the underlying LGCA model [213]. The resulting collision mechanism is then presented by a linearized collision matrix in which the distribution function relaxes toward a local equilibrium distribution [214,215]. In the LB scheme, thermal noises are not present which makes it much more efficient in comparison with LGCA for hydrodynamic problems. On the other hand, the intrinsic stability of LGCA is lost in LB. It should be noted that both LGCA and LB methods suffer from Galilean invariance problems and should be corrected for these limitations [166].

The particle distribution function $\Psi_i(\mathbf{r}, t)$ used in LB gives the density of particles at node $\mathbf{r}$ at time t moving with velocity v_i in the *i*-direction. The lattice in which this density moves is characterized by both the sets of constructing nodes and the velocity subspace $\{v_k\}$. The velocity subspace determines the neighboring nodes to which a given density will be able to move in a time step. The lattice symmetry and the minimum allowed set of velocities should satisfy the requirement of a minimum set of symmetry properties. Otherwise, the underlying anisotropy of the lattice might affect the hydrodynamic behavior of the system. Figure 1 shows two lattice examples often used in two- and three-dimensional LB simulations. These lattices define 9 and 19 allowed velocities (including the quiescent state) and are thus named D2Q9 and D3Q19, respectively.
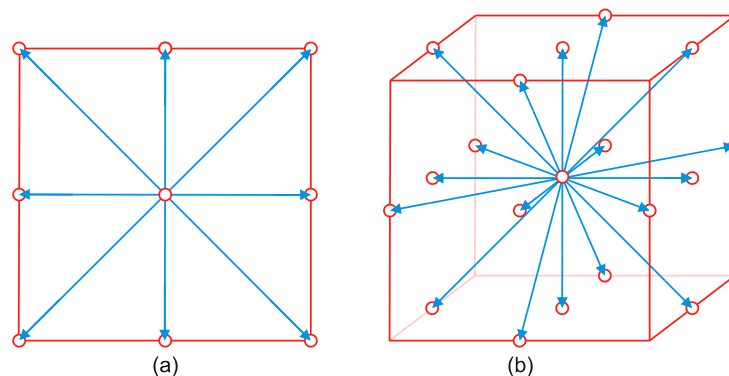

(a)　　　　　　　　　　　　　　　(b)

Figure 1. Two typical lattices often used in LB simulations: (**a**) D2Q9; and (**b**) D3Q19.

The densities $\Psi_i(\mathbf{r}, t)$ are the elementary dynamical variables in LB. The macroscopic local density $\rho(\mathbf{r}, t)$ and velocity $\mathbf{v}(\mathbf{r}, t)$ at position $\mathbf{r}$ can be evaluated based on $\Psi_i(\mathbf{r}, t)$ as

$$\rho(\mathbf{r}, t) = \sum_k \Psi_k(\mathbf{r}, t), \tag{28}$$

$$\rho(\mathbf{r}, t)\, \mathbf{v}(\mathbf{r}, t) \;=\; \sum_k \mathbb{v}_k \Psi_k(\mathbf{r}, t), \tag{29}$$

in which the summation is performed over all allowed velocities. It is obvious that the local macroscopic properties can be evaluated with time, if the evolution of the particle distribution function is known. In LB the elementary two-step evolution (i.e., propagation and collision) of the particle distribution function after a time step Δt can be written in a condensed format as

$$\Psi_i(\mathbf{r} + \mathbb{v}_k \Delta t,\, t + \Delta t) \;=\; \Psi_i(\mathbf{r}, t) + \sum_k \mathbf{\Lambda}_{ik}(\Psi_k(\mathbf{r}, t) - \Psi_k^{\text{eq}}(\mathbf{r}, t)), \tag{30}$$

where the index k spans the velocity subspace, $\Psi_k^{\text{eq}}(\mathbf{r}, t)$ is the equilibrium distribution function and $\mathbf{\Lambda}_{ik}$ is the collision matrix. The simplest form of the collision matrix was proposed by Bhatnagar, Gross, and Krook (BGK) as $\mathbf{\Lambda}_{ik} = -\frac{1}{\tau}\delta_{ik}$ where τ is the collision time [216,217]. This method produces reasonably accurate solutions despite its simplicity [164]. The simplified form of Equation (30), i.e., the BGK-LB method, consequently is

$$\Psi_i(\mathbf{r} + \mathbb{v}_k \Delta t,\, t + \Delta t) \;=\; \Psi_i(\mathbf{r}, t) + \frac{1}{\tau}(\Psi_i^{\text{eq}}(\mathbf{r}, t) - \Psi_i(\mathbf{r}, t)). \tag{31}$$

The equilibrium distribution function $\Psi_i^{\text{eq}}(\mathbf{r}, t)$ needs to be defined before one can use Equation (31) to simulate a system. This is done by requiring that mass and momentum must be conserved [166]. A suitable form for the equilibrium distribution is often a quadratic function in velocities as [164]

$$\Psi_i^{\text{eq}} = \rho w_i \left[1 + 3\frac{\mathbb{v}_i \cdot \mathbf{v}}{\mathbb{v}^2} - \frac{3}{2}\cdot\frac{\mathbf{v}^2}{\mathbb{v}^2} + \frac{9}{2}\cdot\frac{(\mathbb{v}_i \cdot \mathbf{v})^2}{\mathbb{v}^4} \right]. \tag{32}$$

Here, $\mathbb{v} = \sqrt{3}\,\mathbb{v}_s$ where $\mathbb{v}_s$ is the speed of sound, and w_i is the weighting constant. For D2Q9 lattice, w_i is

$$w_i = \begin{cases} \frac{4}{9} & \text{for } i = 0 \\ \frac{1}{9} & \text{for } i = 1,\,2,\,3,\,4 \\ \frac{1}{36} & \text{for } i = 5,\,6,\,7,\,8 \end{cases} \text{ and } |\mathbb{v}_i| = \begin{cases} 0 & \text{for } i = 0 \\ \mathbb{v} & \text{for } i = 1,\,2,\,3,\,4 \\ \sqrt{2}\mathbb{v} & \text{for } i = 5,\,6,\,7,\,8 \end{cases}, \tag{33}$$

and for D3Q19 lattice, it is defined as

$$w_i = \begin{cases} \frac{1}{3} & \text{for } i = 0 \\ \frac{1}{18} & \text{for } i = 1,\,2,\,\ldots,\,6 \\ \frac{1}{36} & \text{for } i = 7,\,8,\,\ldots,\,18 \end{cases} \text{ and } |\mathbb{v}_i| = \begin{cases} 0 & \text{for } i = 0 \\ \mathbb{v} & \text{for } i = 1,\,2,\,\ldots,\,6 \\ \sqrt{2}\mathbb{v} & \text{for } i = 7,\,8,\,\ldots,\,18 \end{cases}. \tag{34}$$

In the algorithm of BGK-LB method, one also needs to provide precise description of the boundaries of the system [164,165]. The discrete distribution function of LB on the boundaries has to be taken carefully so that it represents correct macroscopic boundaries of the system. LB has found various applications in polymer science [218], for instance, polymer solutions [133,178,219,220], simulation of complex flows [221,222], polymer electrolyte fuel cells [223], liquid crystals [224–226], deformation of droplets containing polymers and nanoparticles [227], and thermal conductivity and permeability of fibrous materials [228,229].

2.4. Macroscale Techniques

At the macroscopic scale, it is a common practice to disregard the discrete atomistic and molecular structures and assume that the material is continuously distributed throughout its volume. This approach is applicable provided that the behavior of the collections of atoms and molecules of the materials can be homogenized based on a proper understanding of the structures at the finer scales. Consequently, this scale is often referred to as the continuum scale in the literature. The continuum material is often assumed to possess average physical properties such as density, heat capacity, thermal

conductivity, etc. and can be subjected to body forces such as gravity and surface forces such as contact between two bodies.

In general, the macroscale methods obey several fundamental laws [2,30]. These laws are (i) conservation of mass; (ii) equilibrium, based on Newton's second law; (iii) the moment of momentum law, in which the moment is equal to the time derivative of angular momentum with respect to a reference point; (iv) conservation of energy; and finally (v) the conservation of entropy. Although these principles define the fundamentals for a macroscale model, they still need to be completed with suitable constitutive laws and the equations of state to provide all the information necessary in order to solve a macroscopic problem. It is noteworthy that the derivation of proper constitutive equations for polymeric systems has been an intriguing topic ever since the viscoelasticity concepts were introduced [230]. Various models are put forward with advantages as well as shortcomings often as a result of being limited to a certain class of either polymer systems or phenomena. Moreover, the implementation of usually complex viscoelastic constitutive equations results in extremely heavy calculations.

The continuum models often lead to a set of partial differential equations. In simple cases, it might be possible to find a closed-form analytical solution for the problem. However, it is often necessary to utilize appropriate numerical approaches to evaluate the solution due to the complexity of the involved phenomena. Finite difference method (FDM) is the simplest numerical method developed so far from a mathematical point of view. This simplicity comes with the price of losing flexibility for use with complicated geometries and phenomena compared with more elaborate numerical schemes such as finite element method (FEM) and finite volume method (FVM). It should be emphasized that all of these approaches are merely mathematical methods to estimate the solution of a set of partial differential equations and do not include a definite physical meaning in their bare core. Hence, they are not solely limited to the macroscale phenomena and the founding ideas behind them can also be applied to other scales. These numerical schemes ultimately transform the set of partial differential equations into a system of linear algebraic equations and solve it using either direct approaches, such as Gauss' method, or iterative approaches, such as Gauss-Seidel method [231].

It should be noted that the macroscale techniques do not always deal with a continuous medium. For instance, smoothed particle hydrodynamics (SPH) is one such particle-based method which has been applied to study a number of phenomena including viscoelastic flows [232,233]. Moreover, the thermodynamically consistent version of SPH is named smoothed dissipative particle dynamics (SDPD) and has been implemented in multiscale frameworks to link the macroscopic SPH to the mesoscopic DPD method [234–236]. In its essence, SPH utilizes particles moving with the flow which make it possible to evaluate hydrodynamic properties at particle positions by a weighted averaging of the local values. Therefore, every particle is practically "smoothed" over a finite volume with fixed mass. For this part of the paper, we focus our attention to two widely-used mathematical methods in macroscale calculations, i.e., FEM and FVM.

2.4.1. Finite Element Method

FEM is a powerful method to solve equations in integral form. Two possibilities exist for the application of FEM. In the first case, there exists an integral form of the physical problem. This integral form can be a result of a variational principle, the minimum of which corresponds to the solution, or more generally an integral equation to solve [231]. In the second case, an integral formulation must be obtained from an initial system of partial differential equations by a weak formulation, also called the weighted residual method [231].

A prerequisite of utilizing FEM is to decompose the spatial domain under consideration into a set of elements of arbitrary shape and size. This discretization is often called a grid or a mesh. In the decomposition procedure, the only restriction is that elements cannot overlap nor leave any zone of the domain uncovered. The definition of a mesh for FEM is more free compared with FDM for which the grid follows a coordinate system. For each element in FEM, a certain number of points, called nodes, must be defined which can be situated either on the edges of the element or inside it. The nodes are then used to construct the approximations of the functions under consideration over the entire domain by interpolation.

The approximation of a function $u(\mathbf{r})$, where $\mathbf{r}$ is the vector of spatial coordinates, on a geometric domain meshed with finite elements is obtained as a linear combination of interpolation functions $\psi_n(\mathbf{r})$ associated with the mesh. If $u_h(\mathbf{r})$ is the approximation of the function $u(\mathbf{r})$ under consideration, it can be expressed in the form of a sum over the nodes of the domain by

$$u_h(\mathbf{r}) = \sum_{n=1}^{N} u^n \psi_n(\mathbf{r}), \tag{35}$$

in which N is the total number of nodes. The interpolation functions $\psi_n(\mathbf{r})$ can be of diverse forms with different degrees of continuity and differentiability. In the standard FEM, these functions are defined locally at the level of each element. Therefore, if the node n belongs to element e, and if ψ_n^e is used to denote the restriction of ψ_n within the element, for every coordinate vector $\mathbf{r}$ outside the element e, one has

$$\psi_n^e(\mathbf{r}) = 0, \tag{36}$$

and for every coordinate vector $\mathbf{r}$ inside the element e,

$$u_h(\mathbf{r}) = \sum_{n=1}^{N} u^n \psi_n(\mathbf{r}) = \sum_{n \in e} u^n \psi_n^e(\mathbf{r}). \tag{37}$$

The last sum is performed only over the nodes that constitute the element e. Consequently, the interpolation used for approximation is locally defined at the level of each finite element. This way of decomposition and approximation thus distinguishes the standard FEM from other methods using interpolation functions defined over the entire domain. Moreover, in the standard FEM, the coefficients u^n are the values of the function u_h at the nodes of the mesh. As a result, the interpolation functions must satisfy two conditions in addition to Equation (36). First, if n and p are two nodes of the same element e, and $\mathbf{r}^p$ is the position vector of the node p, then

$$\psi_n^e(\mathbf{r}^p) = \delta_{np}, \tag{38}$$

where δ_{np} is the Kronecker delta function. Second, to exactly represent constant functions, for all $\mathbf{r}$ inside the element e including the borders

$$\sum_{n \in e} \psi_n^e(\mathbf{r}) = 1. \tag{39}$$

In most cases, the integral form of the problem should be also constructed from partial differential equations. For a simple case where the problem is limited to solve one partial differential equation of the form $R(u) = 0$ on domain Ω, one can utilize the weighted residual method to obtain the equivalent integral form. In the context of FEM, $R(u)$ is often called the residual value. Obviously, the solution of the problem zeros the residual and simultaneously satisfies the boundary conditions at $\partial\Omega$. The basic idea in FEM is to search for functions u which zero the integral form

$$\Phi(u) = \int_{\Omega} \rho \, R(u) \, dV = 0, \tag{40}$$

for every weighting function ρ belonging to a set of functions $\{S_\rho\}$, while u satisfies the boundary conditions at $\partial\Omega$. The equivalence between $R(u) = 0$ on Ω and Equation (40) is only true if the set $\{S_\rho\}$ has infinite dimensions and is composed of independent functions [231]. Otherwise, if $\{S_\rho\}$ is finite as in FEM, the solution u which satisfies Equation (40) is only an approximate solution to the problem.

It should be noted that the weighted residual method is not the only method which can be used to search for a function that zeros the residual $R(u)$ on Ω. For instance, the least-squares method can be applicable in some cases despite its limitations. The principle of least-squares consists of searching for the function u that minimizes the integral

$$f(u) = \int_\Omega (R(u))^2 \, dV, \tag{41}$$

and that respects the boundary conditions. However, it is often difficult to employ the boundary conditions in this formalism. Furthermore, the order of derivatives in R cannot be reduced which leads to high differentiability conditions on the finite element discretization [231]. For these reasons, the method of weighted residuals is often preferred.

For the discretization of the obtained integral form, *N* independent weighting functions ρ_1, ρ_2, ρ_3, ..., ρ_N are utilized. There are different approaches to define the type of ρ_i functions. The most used approach is the Galerkin method which defines the weighting functions precisely the same as the interpolation functions ψ_n of the approximation by finite elements [231]. Therefore, Equation (40) can be written as

$$\Phi(u) = \int_\Omega \psi_n \, R(\sum_{n=1}^N u^n \psi_n) \, dV = 0. \tag{42}$$

This integral equation is later turned into a sum of finite series over the nodes of the domain. The boundary conditions are usually implemented into this integral form benefitting from the divergence theorem [231]. In the algorithm of FEM, for every element *e* a mapping can be defined between the element in physical space and a reference element, which allows defining the interpolation functions universally for the diverse elements regardless of their coordinates [231]. This notion facilitates programming profoundly.

FEM has been implemented in several simulation packages and consequently can be easily used by both academic and industrial communities, in a variety of applications. To name a few instances in polymer science, we note the prediction of the failure behavior of adhesives [237,238], the study of elastic modulus of polymer/clay nanocomposites [239], the prediction of temperature distribution in a tissue-mimicking hydrogel phantom during the application of therapeutic ultrasound [240], the wall slippage in the extrusion of highly-filled wood/polymer composites [241,242], the torsional friction behavior in hydrogels [243], permeation analysis in polymer membranes [244], viscoelastic flow analysis [245–247], and droplet deformation [248]. A significant improvement of the precision of FEM was achieved by Patera [249] when it was combined with spectral techniques. The resulting algorithm is generally known as the spectral element method (SEM). SEM is more stable and accurate than FEM under a relatively broad range of conditions [250]. Due to its power and versatility, SEM has shown to be a promising candidate to solve the viscoelastic models in the simulations of complex polymer flows [251,252].

2.4.2. Finite Volume Method

FDM and FEM are admittedly the two most important classes of numerical methods for partial differential equations. However, they both suffer from serious shortcomings. The main defects of FDM are: (i) the considerable geometrical error of the approximation of curved domains by rectangular grids; (ii) the lack of an effective approach to deal with natural and internal boundary conditions; and (iii) the difficulty to construct difference schemes with high accuracy unless the difference equation is allowed to relate more nodal points and thus further complicating the incorporation of boundary conditions.

Classic FEM methods, i.e., Galerkin FEM (GFEM), perform successfully in fields such as solid mechanics and heat conduction where the problem is governed by self-adjoint elliptic or parabolic partial differential equations. Unfortunately, this success did not continue in the field of fluid dynamics. The reason was ascribed to the convection operators in the Eulerian formulation of the governing equations which render the system of equations non-self-adjoint [253]. Consequently, solutions to non-self-adjoint fluid dynamic problems by GFEM often suffer from node to node oscillations. This problem has motivated the development of alternatives to the GFEM which preclude oscillations without requiring mesh or time step refinement. The streamline-upwind/Petrov-Galerkin (SUPG) [254,255] and the least-squares finite element [231,256] methods are two examples of such approaches. Some authors also attempted to develop a strategy in FEM which employs a least-squares method for first-order derivatives and a Galerkin method for second-order derivatives in the governing Navier-Stokes equations [257]. Nevertheless, the simplicity of calculations and development of simulation algorithms is usually hindered by such approaches.

As a result, the search for a simple yet accurate alternative to FEM was carried out benefiting from FDM concepts and coupling it with finite element spaces in order to derive the so-called generalized differences methods (GDM) [253]. GDM provides several advantages such as small geometrical errors, easy handling of natural boundary conditions, and maintaining conservation of mass. With GDM, one is supplied with a method with the computational effort greater than classic FDM and less than FEM while the accuracy is higher than FDM and nearly the same as FEM. Due to its advantages, in particular its inheritance of the mass conservation law, GDM was rapidly developed in computational fluid dynamics (CFD) most popularly called FVM. FVM is also referred to as the finite control volume method which is a discrete estimation of a certain control equation in an integral form [258–260]. Hence, FVM is basically equivalent to GDM with piecewise constants and piecewise linear elements. Using FVM to develop numerical algorithms for nonlinear equations is in fact generalizing the classical difference schemes to irregular meshes. The equivalence of FDM and FVM has been shown in simple cases for instance by Rappaz et al. [231].

Although FVM has been applied to many applications including magnetohydrodynamics [261–263], structural dynamics [264,265], and semiconductor theory [266,267], its main field of application has been CFD mainly due to its conservative nature. Consequently, we restrict ourselves to this field in the rest of this section. Similar to FDM and FEM, FVM changes a set of partial differential equations with a system of linear algebraic equations. In order to do this, FVM utilizes a two-step discretization procedure [268]. First, the partial differential equations are transformed into balance equations by integration. In this transformation the surface and volume integrals are changed into discrete algebraic equations over individual elements benefitting from an integration quadrature. A set of semi-discretized equations is then produced. Second, the local values of the variables in the elements are approximated by using suitable interpolation profiles. For a general scalar variable ϑ, one can write the steady state conservation equation as

$$\nabla \cdot (\rho \mathbf{v} \vartheta) = \nabla \cdot (\mathbf{D}^{\vartheta} \nabla \vartheta) + Q^{\vartheta}, \tag{43}$$

where ρ is the fluid density, **v** is the fluid velocity vector, $\mathbf{D}^{\vartheta}$ is the diffusion coefficient of ϑ, and Q^{ϑ} is the generation/destruction of ϑ in the control volume per unit volume. By integrating the above equation over the element *e* and utilizing the divergence theorem, one finds

$$\oint_{\partial V_e} (\rho \mathbf{v}\vartheta)\cdot d\mathbf{S} = \oint_{\partial V_e} (\mathbf{D}^{\vartheta}\nabla\vartheta)\cdot d\mathbf{S} + \int_{V_e} Q^{\vartheta}\, dV, \tag{44}$$

in which **S** represents the surface vector, and ∂V_e shows that the integration is performed over all the surfaces surrounding the volume V_e. The semi-discrete steady state equation for *e* can be finally simplified to [268]

$$\sum_{\varepsilon \sim neighboring\ cells\ of\ e} (\rho \mathbf{v}\vartheta - \mathbf{D}^{\vartheta}\nabla\vartheta)_{\varepsilon}\cdot\mathbf{S}_{\varepsilon} = Q^{\vartheta}_{\varepsilon}V_{\varepsilon}, \tag{45}$$

by using the mid-point integration approximation. The summation is performed over the faces surrounding element *e* with its neighboring cells. Here, Q^{ϑ}_e is the contribution of element *e* to Q^{ϑ}. If one denotes the convection and diffusion flux terms by $\mathbf{J}^{\vartheta,C}$ and $\mathbf{J}^{\vartheta,D}$, respectively, one can write Equation (45) in the form

$$\sum_{\varepsilon \sim neighboring\ cells\ of\ e} (\mathbf{J}^{\vartheta,C} + \mathbf{J}^{\vartheta,D})_{\varepsilon}\cdot\mathbf{S}_{\varepsilon} = Q^{\vartheta}_{\varepsilon}V_{\varepsilon}, \tag{46}$$

where $\mathbf{J}^{\vartheta,C} = \rho\mathbf{v}\vartheta$ and $\mathbf{J}^{\vartheta,D} = -\mathbf{D}^{\vartheta}\nabla\vartheta$. In FVM, the transported variable ϑ is conserved in the discretized solution domain since the fluxes at a face of an element are calculated using the values of the elements which share that face [268]. As a result, for any mutual surface of two elements, the outwards flux from a face of an element is precisely equal to the inwards flux from the other element through that same face. Consequently, such fluxes are equal in magnitude but with opposite signs.

To get the fully-discretized steady state finite volume equation for element *e*, one needs to adjust proper interpolation profiles. The interpolation profiles are often different for diffusive and convective terms due to the distinct physical phenomena that these terms represent. For the diffusive term, a linear interpolation profile is often used [268]. The selection of an interpolation profile for the convective terms could be more challenging. The simplest interpolation scheme, i.e., the symmetrical linear profile or the central difference scheme, could be applied here. Despite its simplicity, this scheme can result in unbounded unphysical behavior at high Peclet numbers (Pe) due to the fact that it cannot describe the directional preference of convection [268]. Consequently, the upwind scheme was introduced to account for this directional preference and provide a better stability at the cost of the accuracy. This is due to the fact that the upwind scheme has a first order of accuracy whereas the linear scheme has a second order of accuracy [269]. In order to enhance the precision and stability of advection schemes, higher-order upwind biased interpolation profiles were incorporated in the calculations. Such higher-order schemes often produce at least a second-order accurate solution, while they are unconditionally stable. An example of such attempts is the quadratic upstream interpolation for convective kinematics (QUICK) scheme developed by Leonard [270]. In this method, the value of the dependent variable is interpolated at each element face using a quadratic polynomial biased towards the upstream direction. Further details can be found elsewhere [268].

In recent years, the application of FVM in CFD has been significantly accelerated, mostly because of the emerging open source software packages such as OpenFOAM® (Open Source Field Operation and Manipulation) [271,272]. Analysis of viscoelastic fluids [273–279], viscoelastic two-phase flows [280], mold filling in water-assisted injection molding of viscoelastic polymers [281], gas permeation in glassy polymer membranes [282], blood flow [283], development of droplet and co-continuous binary polymer microstructures [284] are some examples of FVM applications in polymer science.

3. Multiscale Strategies

The ultimate purpose of a multiscale modelling is to predict the macroscopic behavior from the first principles at the quantum scale. Finding appropriate protocols for multiscale simulations is on

the other hand a very challenging topic. This is due to the fact that polymeric materials often display phenomena on one scale that necessitate a precise description of other phenomena on another scale. Since none of the methods discussed before is sufficient alone to describe a multiscale system nor they are designed for such a purpose, the goal becomes to develop a proper combination of various methods specialized at different scales in a multiscale scheme. This scheme is also supposed to effectively distribute the computational power where it is needed most. By definition, such a multiscale approach can take advantage of the various methods it envelops at multiple scales and reaches the length and time scale that the individual methods fail to achieve. At the same time, this approach can retain the precision provided by the individual methods in their respective scales. Moreover, the multiscale approach should be flexible enough to allow for high accuracy in particular regions of the systems as required. Therefore, the overall objective of multiscale models is to predict the behavior of materials across all significant length and time scales while preserving a balance among precision, efficiency, and realistic description.

In general, there are three main categories of multiscale approaches: sequential, concurrent, and adaptive resolution schemes. The sequential approach links a series of computational schemes in which the operative methods at a larger scale utilize the coarse-grained (CG) representations based on detailed information attained from smaller scale methods. Sequential approaches are also known as implicit, serial, or message-passing methods. The second group of multiscale approaches, the concurrent methods, are designed to bridge the suitable schemes of each individual scale in a combined model. Such a model accounts for the different scales involved in a physical problem concurrently and incorporates some sort of a handshaking procedure to communicate between the scales. Concurrent methods are also called parallel or explicit approaches. It is noteworthy that multiscale simulations could principally utilize a hybrid scheme based on elements from both sequential and concurrent approaches. More recently, a new concept for multiscale simulations has been developed which resembles some characteristics of concurrent methods. In this approach, single atoms or molecules can freely move in the simulation domain and switch smoothly from one resolution to another, for instance based on their spatial coordinates, within the same simulation run. Consequently, these methods are generally referred to as the adaptive resolution simulations. Details of such techniques are provided in the following sections. Finally, there are a number of advanced techniques which allow for extending the reach of a single-scale technique such as MD within certain conditions. Such methods are also reviewed for the sake of completeness before closing the discussion of multiscale strategies.

3.1. Sequential Multiscale Approaches

In sequential approaches, calculations are often performed at a smaller scale (the more detailed, finer scale) and the resulting data are passed to a coarser model at a larger scale after leaving out unnecessary details for instance by coarse-graining. However, it will be shown that in some cases the reverse procedure can also be done. A sequential multiscale model requires a thorough understanding of the fundamental processes dominating the finest scale to yield accurate information. Afterwards, it is also crucial to have a well-founded approach to introduce this information into the coarser scales. Such a strategy is usually achieved by utilizing phenomenological theories which contain some key parameters. These parameters are then used as the linking bridges between the scales when their values are determined from the calculated data of the finer scale simulations. This message-passing method can be performed in sequence for multiple length scales. It is obvious that in this sequential approach the accuracy of the simulations at the coarser scale critically depends on the accuracy of the information from the finer scale simulations. Furthermore, the model at the coarser scale must be accurate itself so that it can provide reliable results. In this strategy, the relations between the scales must be invertible so that the results of the coarser scale simulations can be used to suggest the best choice for the finer scale parameters.

The sequential approach has generally proven effective in systems where the different scales are weakly coupled. Therefore, appropriate systems for such a methodology often share a common character by which the large-scale variations appear homogeneous and quasi-static from the small-scale perspective. The majority of the multiscale simulations that have been actually incorporated in materials research are in fact sequential. In order to highlight the sequential message-passing in a range of polymeric systems, a few examples are outlined here. To predict the morphology and mechanical properties of mixtures of diblock copolymers and rod-like nanoparticles, Shou et al. [285] coupled the self-consistent field theory with DFT to provide input information for the lattice spring model (LSM). In their sequential algorithm, the spatial morphology of different phases is mapped onto the coarser-scale lattice and the force constants are derived for the three-dimensional network of springs. In similar approaches, other methods including LB [286], MC [287], and MD [288,289], have also been used to produce appropriate morphological information for LSM in various systems including polymer blends and nanocomposite coatings. Recently, the classical fluids density functional theory was linked to MD simulations by Brown et al. [290] to study microphase separated states of both typical diblock and tapered diblock copolymers. The fluids density functional theory can predict the equilibrium density profiles of polymeric systems. The authors used the resulting density profiles of this theory to initialize MD simulations with a close to equilibrated structure and could speed up the simulations. In a study on the influence of self-assembly on the mechanical and electrical properties of PNCs, Buxton and Balazs [291,292] used a combination of Cahn-Hillard theory and BD at the finer scale to produce morphological data. The data were later fed either into LSM in order to determine the mechanical properties, or into FDM to calculate the electrical conductivity.

A number of studies have been devoted to characterize polymer/clay nanocomposites at different scales, spanning from quantum mechanical scale up to the macroscale. One such algorithm was developed by Suter et al. [293] which starts with the quantum theory, and transfers the key information through atomistic classical MD to a CG representation. This sequential procedure allowed for the study of the intercalation of molten polymers, poly(ethylene glycol) and poly(vinyl alcohol), within MMT tactoids and the larger scale ordering of these bridged tactoids, see Figure 2. In a separate multiscale study, Scocchi et al. [294] evaluated the rescaled energies of a CG DPD model from the energy values of their atomistic MD counterparts. Using this information, they could calculate the maximum repulsion coefficients for the corresponding DPD models of polyamide (PA)/clay and polypropylene (PP)/clay nanocomposites and reproduce experimentally observed microstructures. The same methodology was also applied in following works and was extended into the macroscale realm by linking to FEM in order to derive mechanical properties of polymer/clay nanocomposites as a function of the degree of exfoliation [295,296]. The DPD parameters of their work derived from MD simulations, were recently shown to be capable to capture the orientation dynamics of clays in polymer melts under various shearing flows, see Figure 3 [195].

The most common serial transfer of information from a finer scale method to a coarser one can be envisioned in the systematic development of CG models of polymer systems. The CG models are often designed to reproduce the configurations of more detailed descriptions in atomistic simulations as accurately as possible. In this way, a CG model with much less degrees of freedom is achieved which can access longer time scales appropriate for instance in dynamics simulations. It is worthy to note that the final conformations of such CG simulations could be translated back to its atomistic details based on a specific backmapping algorithm. These sequential procedures represent general characteristics of sequential multiscale approaches and could also be extended to more complex systems. Furthermore, these fields have witnessed a large amount of research activities in recent years. As a result, more details are provided on these topics to help the reader familiarize oneself with the underlying challenges and possibilities.
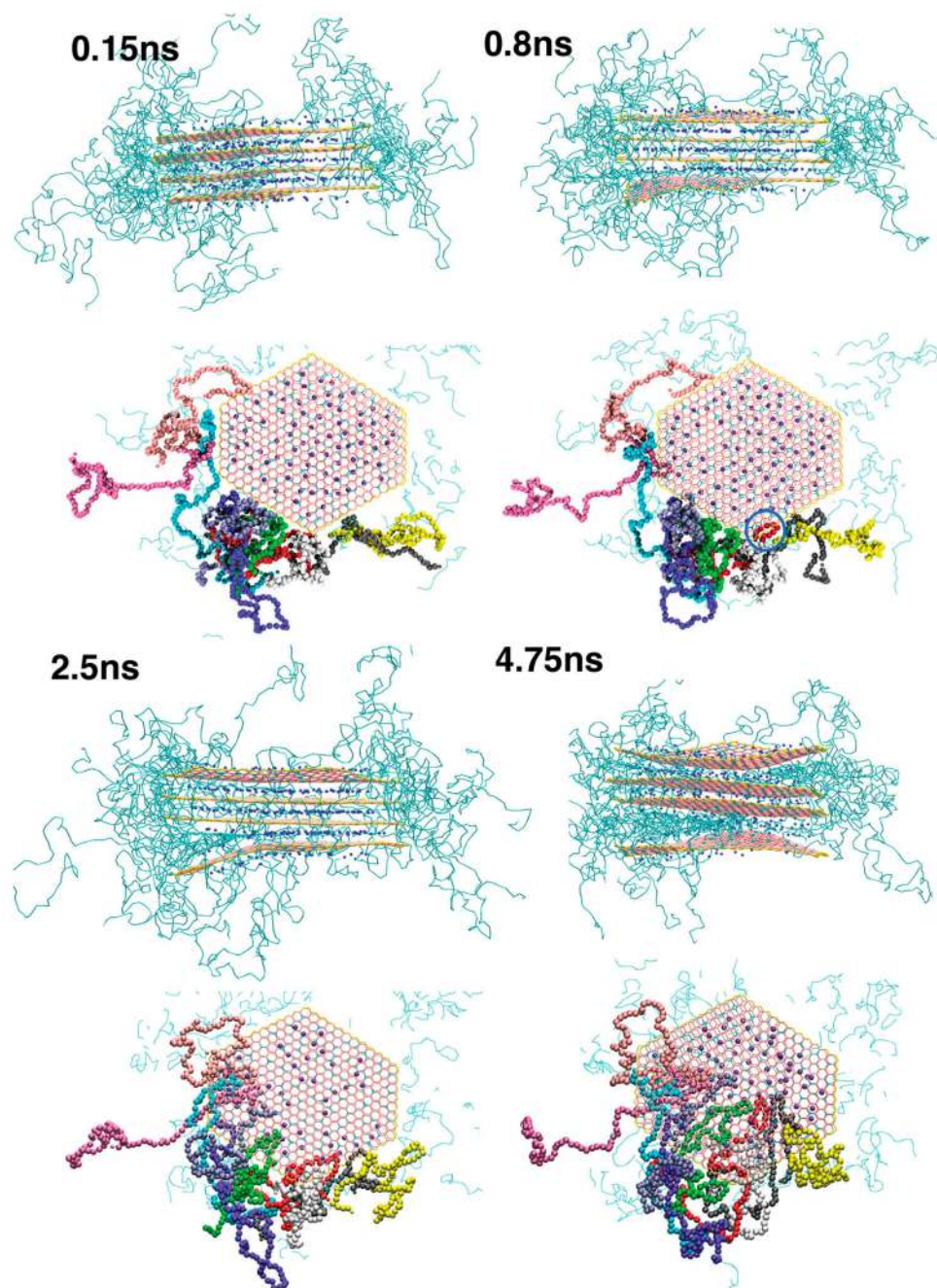
Figure 2. Pictorial overview of the intercalation of poly(vinyl alcohol) chains in a clay tactoid. The side and top views of the tactoids are illustrated at several snapshots. The macromolecules are shown by the green bonds in the side views. The color code for the clay particles are: pink: neutral clay; cyan: charged clay; yellow: edge of the clay; and blue: sodium. The bending of the lowermost clay due to the intercalation process of poly(vinyl alcohol) chains can be observed in the side view snapshots. For the top view, the intercalating polymers are colored based on their molecule number, to make the visualization easier. One can see that the polymer initially starts intercalating as short loops (for an instance see the blue circled chain at the 0.8 ns snapshot), and progresses further into the interlayer. Reprinted from Suter et al. [293] under the terms of the Creative Commons Attribution License.
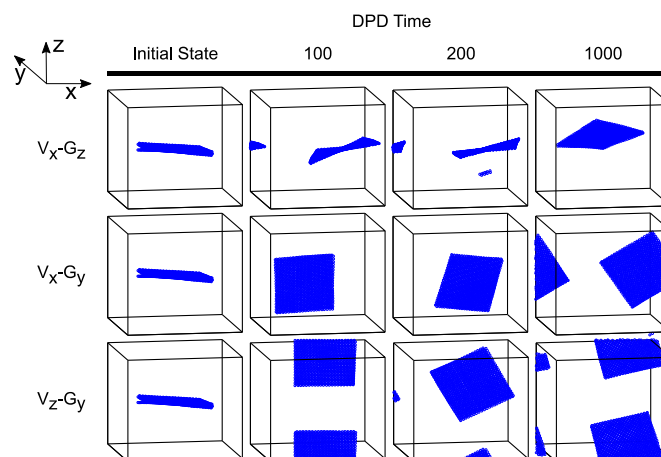
Figure 3. Snapshots of the clay platelets with time experiencing various flow directions. The applied shear-rate is 0.148 in DPD units and the flow of each row is defined in the figure; the velocity direction is shown by $V_{direction}$ and the velocity gradient direction by $G_{direction}$. Reprinted from Gooneie et al. [195]. Copyright 2016, with permission from John Wiley & Sons Inc.

3.1.1. Systematic Coarse-Graining Methods

A serious problem with polymeric materials in a sequential multiscale scheme is that the coarse-graining method from atomistic scale to mesoscale or from mesoscale to macroscale is not a straightforward procedure. The coarsening from QM to MD follows basic principles which can be formulated in a computational framework while it is system-specific at higher scales. All methods are based on the application of a force field which transforms information from quantum scale to atomistic simulations. From atomistic simulations to mesoscale model, critical features of the system such as the structure and/or thermodynamics have to be preserved while the degrees of freedom is reduced. The linking of scales through the mesoscale is addressed by many authors as the most challenging step towards developing reliable multiscale frameworks. Systematic coarse-graining methods are therefore developed to address these challenges. It is noteworthy that some mathematical aspects of various coarse-graining methods for equilibrium [297] and nonequilibrium [298] systems were addressed recently in details.

Systematic coarse-graining strategies attempt to extend the length and time scales of atomistic MD simulations by replacing several atoms with a single super atom and thus reducing the degrees of freedom. These approaches strictly attempt to preserve intrinsic properties of polymers such as radius of gyration, diffusion coefficient, etc. As a consequence, the results of such CG models can be directly compared with experiments. Depending on the number of atoms that are lumped into a single super atom, i.e., the degree of coarse-graining, the systemic coarse-graining methods are roughly divided into three major blocks; (i) low coarse-graining degrees where one or two monomers are coarse-grained into one super atom; for instance, in an iterative Boltzmann inversion (IBI) scheme; (ii) medium coarse-graining degrees where ten to twenty monomers are coarse-grained into one blob or bead, for instance, used in the so-called "blob model"; and (iii) high coarse-graining degrees where the whole chain is mapped to a single soft colloid in super coarse-graining methods. These variations provide access to a range of time and length scales from 10^{-6} s (10^{-6} m) to 10^{-2} s (10^{-2} m), particularly precious to simulate dynamic properties of polymeric systems [299]. In addition to the reduced number of degrees of freedom, CG models often benefit from simpler forms of interactions compared with the detailed models. This feature can promote the computational efficiency to a large extend. Besides, the free energy profiles of CG models are usually smoother due to the fact that many interaction centers are replaced with only a single site. Finally, the parametrization of the CG interactions is simpler than that of full atomistic systems since many chemistry-specific details are ignored during coarse-graining. Such features of CG models make them particularly appealing for many applications

in polymer systems. In the next sections, several methods for coarse-graining as well as various remaining challenges are discussed.

Low Coarse-Graining Degrees

Low degrees of coarse-graining with one or two monomers lumped into a single super atom are carried out by either parameterized or derived approaches [300]. The parameterized approaches utilize all-atomistic (AA) simulations to calculate some target property, such as a pair distribution function, and then the coarse-graining potentials are evaluated to reproduce the target quantities. One should note that the CG potentials can hardly reproduce all the original AA system specifications. On the other hand, in the derived methods the CG pair potentials are calculated in AA simulations from the direct interactions between the groups of atoms enveloped in super atoms. In these methods, the contribution of multibody interactions to the effective CG potentials is less significant in comparison with pair potentials. Consequently, the derived methods are often used to describe systems in which multibody interactions do not play a significant role. Examples of derived methods are the pair potential of mean force (pPMF) [301,302], the effective force CG (EFCG) [303], and the conditional reversible work (CRW) [300,304,305]. In the rest of this part, we focus on parametrized approaches since the derived methods are generally considered to be better-suited for small molecules even though they have recently found some applications in larger molecules [306,307].

The parameterized methods are divided into structure-based and force-based methods depending on the target quantities. As specified in the name, structure-based methods construct the CG potentials in order to reproduce a structural property of the AA system such as pair distribution functions [36,308–318]. The IBI method is undoubtedly the most significant example of such methods [308,319]. Other structure-based methods include the Kirkwood-Buff IBI method [320], the inverse Monte Carlo (IMC) method [309,310,313], the relative entropy method [321–324], and the generalized Yvon-Born-Green theory [325]. All of these methods are principally similar to the IBI method with minor differences in their optimization or mapping schemes. The force-based approaches, on the other hand, attempt to match the force distributions on a super atom from both the CG and AA representations. There are mainly two variations to force-based methods namely the force-matching method [3,326–331], and the multiscale coarse-graining method [328,329,332–335]. For the sake of completeness, we should mention that in some works a combination of the methods is used to derive the CG model. For instance, we refer to the recent study of Wu [336] who utilized a combination of IBI and CRW to find the CG potentials for morphological simulations of poly(vinyl chloride)/poly(methyl methacrylate) and PS/poly(methyl methacrylate) blends.

In the IBI method, one often assumes that the probability distribution function p^R depends on pair distance r, bond length l, bond angle θ, and dihedral angle $\mho$. These parameters are further taken to be independent from each other so that $p^R(r, l, \theta, \mho) = p^R(r) \times p^R(l) \times p^R(\theta) \times p^R(\mho)$ and the CG potential function becomes $U^{CG}(r, l, \theta, \mho) = U^{CG}(r) + U^{CG}(l) + U^{CG}(\theta) + U^{CG}(\mho)$. Through the simple Boltzmann inversion one has $U^{CG}(q) = -k_B T \ln p^R(q)$ with $q = r, l, \theta, \mho$. The iterative algorithm in IBI compares the probability distribution functions of the CG model with the corresponding target probability distribution functions of AA simulations p^R_{target}, and improves the calculated CG potential functions in a step-wise manner according to [299,337,338].

$$U^{CG}_{i+1}(q) = U^{CG}_i(q) + k_B T \ln \frac{p^R_i(q)}{p^R_{target}(q)} \tag{47}$$

The potential correction term, i.e., the second term on the right hand side of the equation, is sometimes multiplied by a relaxation factor between zero and one to avoid overshooting in the numerical procedure. The number of iterations required to reach satisfactory property reproduction in IBI is system-specific and depends on various factors like polymer structure, the definition of the super atom, the degree of coarse-graining, etc. and can take from a few to hundreds of

iterations to converge [327]. Li et al. [339] used such a strategy to reproduce viscoelastic properties of *cis*-polyisoprene. In their work, the authors reproduced CG distribution functions and those obtained from AA simulations. In this way, they could optimize the potential functions for the four independent parameters separately.

The IBI method is not the only way to optimize a CG model based on AA simulations. Here we take a quick look at two other methods namely IMC and force-matching methods. IMC or the Newton inversion method incorporates rigorous statistical mechanical arguments to update the potential functions of the CG model [309,310,313]. The optimization procedure in IMC poses an interdependent updating algorithm for pair potentials in multicomponent systems whereas in IBI method these potentials are updated separately which could lead to convergence problems. However, this feature is often computationally very expensive [327]. In the force-matching method, a variational approach is used to construct the CG potentials based on the recorded forces from AA simulations [3,326–331]. In this method, the difference between the average AA force on a particle and the corresponding force in the CG counterpart is minimized in order to find the optimized CG force field. Thus, the force-matching approach actually projects the full many-body force field onto the definitive potential functions of the CG force field [340]. Due to the fact that the CG force field is merely an approximation of the AA force field, the force-matching method may or may not reproduce the structural properties of the AA system perfectly. The incorporation of higher-order interactions in the definition of the CG force field could resolve this problem at the cost of lower computational efficiencies [341]. It should be noted that IBI and similar methods are usually not helpful in systems with a diluted component since the interactions between the diluted molecules cannot be readily obtained. In such cases one should compute the effective potentials for these interactions with more rigorous sampling schemes such as thermodynamic integration or umbrella sampling [306,342–344].

In the coarse-graining procedure, there is usually more than one way to define super atoms. Several important issues regarding the definition of super atoms should be addressed carefully, i.e., the shape of the super atom, the position of the center of a super atom on a molecule, the number of atoms which are enveloped by it, as well as the number of different super atoms associated with a molecule. The super atom is defined to be a spherical particle in most studies, but there are also some works which offer generalizations for anisotropic potentials [345,346]. This enforces additional complexity on the definition of potential functions as well as the performance of CG simulations only for a slightly increased accuracy. Therefore, it is generally advised to achieve higher precisions by incorporating additional spherical super atoms to characterize the molecules instead of utilizing non-spherical super atoms [299]. Considering the other parameters mentioned for the definition of super atoms, there is no general rule applicable for different cases. There are various ways to define the super atoms to represent a CG model of a system. However, it is crucial to ensure that the final CG model is capable to reproduce the static, dynamic or thermodynamic properties correctly before it is further applied. To give an example, we consider the various possibilities to develop CG models of polystyrene (PS), which has been extensively studied with different approaches in the definition of super atoms as illustrated in Figure 4. Müller-Plathe and his co-workers [347–349] adopted the CG structure shown in Figure 4a and could successfully reproduces the gyration radius and the Flory characteristic ratio of PS in melts at 500 K. Nevertheless, the entanglement length was estimated to be much smaller than the experiments. Spyriouni et al. [350] modified the CG potential functions of this model and could predict the correct entanglement length of PS melts as well as the packing length and the tube diameter. Still, the isothermal compressibility was largely different from experimental values indicating the poor transferability of the developed potentials to pressures other than the one used in AA simulations. Another CG representation was developed by Sun and Faller [351,352] as depicted in Figure 4b which could obtain the entanglement length at 450 K in agreement with experimental observations. The mapping scheme shown in Figure 4c was developed by Qian et al. [353] which yields potentials capable of reproducing the isothermal compressibility as well as structural properties of the PS melts from 400 to 500 K. Finally, in order to include the tacticity effects on the structural

and dynamic properties of PS, Harmandaris et al. [354,355] and Fritz et al. [356] used the CG models shown in Figure 4d. This model has been applied to study both the mechanical properties of PS glasses [357,358] and the dynamic properties of PS melts [359,360]. These works manifest the influence of the definition of super atoms on the final outcome of the simulations. Consequently, a CG model should be tested and validated for its predictive features and merits before any further use [361].
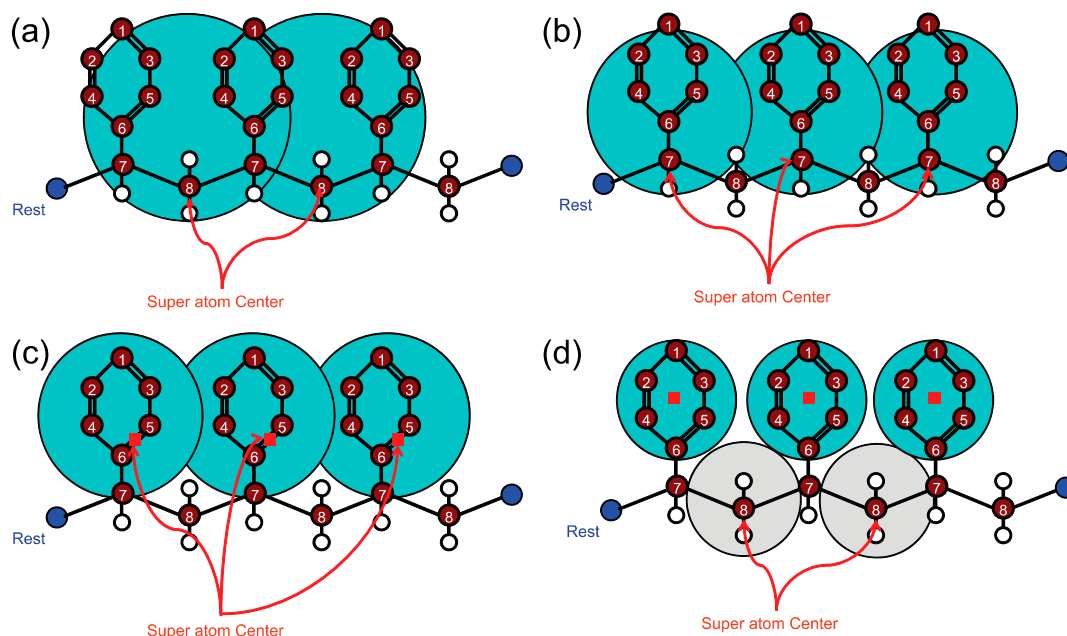

Figure 4. Different definitions for the super atoms of CG PS utilized by (**a**) Müller-Plathe and co-workers [347–349]; (**b**) Sun and Faller [351,352]; (**c**) Qian et al. [353]; and (**d**) Harmandaris et al. [354,355]. Reprinted from Li et al. [299] under the terms of the Creative Commons Attribution License.

The fact that several atoms are replaced with a super atom in CG models changes the entropy due to the deleted degrees of freedom. This leads to an altered internal dynamics after coarse-graining. This notion becomes more important as the degree of coarse-graining increases. In addition to this altered entropy, the coarse-graining procedure changes the amount of the surface of each molecule available to its surrounding molecules due to the fact that it simplifies a cluster of atoms into a spherical super atom. Consequently, the hydrodynamic radius of the CG super atom is strongly dependent on the coarse-graining methodology and in every case, it is different from its AA counterparts. Since the friction coefficient is related to the hydrodynamic radius according to Stokes's law [362], the coarse-graining procedure also changes the internal friction coefficient between monomers which leads to incorrect dynamic behavior of CG models [363–365]. Therefore, it is necessary to rescale the dynamics in order to simulate the correct behavior [366]. The dynamic rescaling can be performed utilizing a time-mapping factor defined, for instance, as the ratio of the friction coefficients [359,360], the ratio of decorrelation times utilizing the autocorrelation function [339], or numerically derived from the ratio of the mean square displacements (MSD) [354], between AA and CG models. In spite of these efforts, the correct definition of a time-mapping factor is still a challenge due to the fact that different modes of motions in a system should be scaled with different characteristic scaling factors, giving rise to the so-called "dynamical heterogeneity" issue [367–369].

Finally, the transferability and thermodynamic consistency of developed CG models should be ensured. In a coarse-graining procedure such as IBI, the effective potential functions are often evaluated based on target distribution functions, which are themselves derived for a specific set of thermodynamic conditions resembling a certain ensemble. Therefore, the derived potential functions from one state are not transferable to another state in most cases [337,370]. All CG models are

state-dependent and should not be transferred to another state without re-parametrization. The "state" contains information about temperature, density, concentration, system composition, phase, etc. as well as chemistry-specific details of the system. An example for the thermodynamic inconsistency of CG models and AA simulations is the missing long-range interactions between the super atoms leading to overestimations of the pressure. To compensate for such effects, some studies add a linear attractive tail function into the pair potential and recover the correct pressure for CG polymer systems [319,371,372]. Consequently, the effective potential functions should be optimized individually for each state of the CG system. Despite this general consideration, there are some instances in the literature where the effective potential functions of the CG model possess a range of transferability into a subset of thermodynamics states [353,373–375]. For instance, the effective CG potentials of homopolymer melts show a remarkable transferability over a large range of temperatures [376–378]. Such studies state that the definition of super atoms largely influences the transferability of the effective CG potentials derived by the IBI method. An interesting topic in the transferability of CG models is to find a methodology to derive CG potentials which are both thermodynamically and structurally consistent with the underlying AA description [317,318,338,344,379–382]. Such a method could ensure a certain state transferability for the constructed CG potentials. Using calibration methods in order to improve the transferability of derived CG potentials is also an interesting possibility. Recently, inspired by ideas from uncertainty quantification and numerical analysis, Patrone et al. [383] used a Bayesian correction algorithm [384] to efficiently generate transferable CG forces. Their method uses functional derivatives of CG simulations to rapidly recalibrate initial estimates of forces anchored by standard methods such as force-matching.

Medium Coarse-Graining Degrees

Since the definition of the super atom is not unique, it is possible to lump several monomers of the polymer chain into one single super atom. In this way, the approachable length and time scales of the CG simulations are significantly extended. Based on this idea, Padding and Briels lumped 20 monomers along a PE chain in a single spherical blob and developed the so-called "blob model" [385–387]. The potential functions of the blob model are optimized systematically based on AA simulations in a similar fashion to IBI. However, due to the larger number of lumped monomers in comparison with techniques for low coarse-graining degrees, the dihedral interactions between the blobs are negligible. Therefore, the potential functions of the blob model usually consist of nonbonded and bonded (i.e., bonds and bond angles) interactions. Padding and Briels write these interactions as

$$U^{CG}_{nonbonded}(r) = c_0 e^{-\left(\frac{r}{b_0}\right)^2}, \tag{48}$$

$$U^{CG}_{bond}(l) = c_1 e^{-\left(\frac{r}{b_1}\right)^2} + c_2 e^{-\left(\frac{r}{b_2}\right)^2} + c_3 l^{\mu}, \tag{49}$$

$$U^{CG}_{angle}(\theta) = c_4(1 - \cos\theta)^{\nu}, \tag{50}$$

in which $U^{CG}_{nonbonded}(r)$, $U^{CG}_{bond}(l)$, and $U^{CG}_{angle}(\theta)$ are the potentials of nonbonded, bond and angle interactions, respectively. c_0 to c_4, b_0 to b_2, μ and ν are fitting parameters derived from AA simulations. The potential functions for nonbonded and bonded interactions Equations (48) and (49), respectively are optimized against AA results for the blob representation of PE illustrated in Figure 5. Blob model has been applied in a number of studies including the investigation of transient and steady shear flow rheological properties of polymer melts [388], chain dynamics of poly(ethylene-*alt*-propylene) melts [389], and entangled star PE melts [390]. In the blob model, it is also necessary to rescale the dynamics to capture the behavior of the polymer chains correctly. The rescaling can be performed by adjusting the friction coefficient of the Langevin equation to the simulated value from the AA model [386]. Based on this rescaling strategy, the correct diffusion coefficients and scaling laws of the zero-shear viscosity of PE polymer melts were predicted correctly in the blob model as shown in Figure 6 [386].
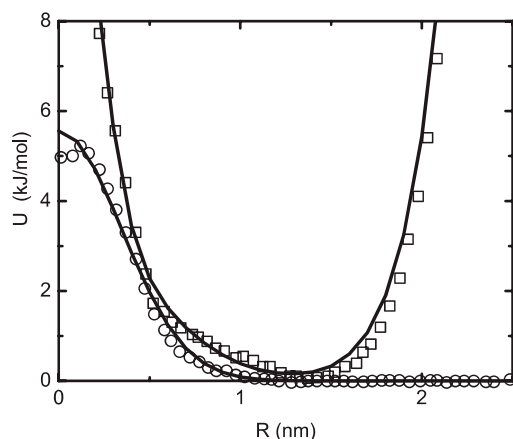
Figure 5. Potential functions for nonbonded (circles) and bonded (squares) interactions from AA simulations. The solid lines are fitted with Equations (48) and (49). Reproduced from Padding and Briels [385] with the permission of AIP Publishing.
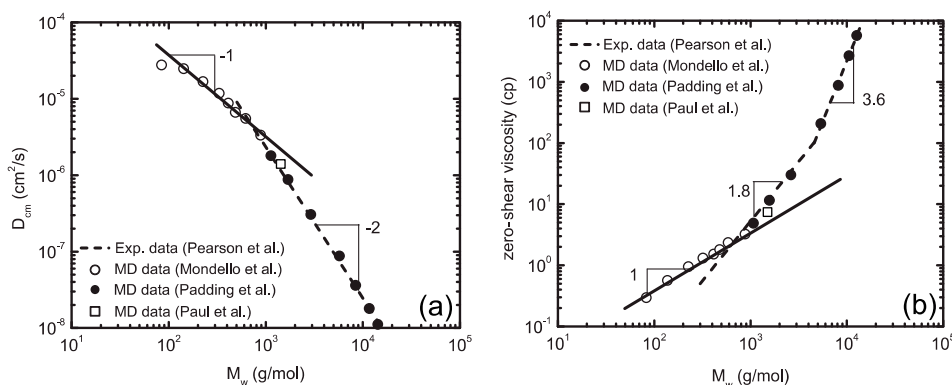

Figure 6. (**a**) Center-of-mass self-diffusion coefficient, D_{cm}; and (**b**) zero-shear viscosity versus molecular weight, M_w, for PE melts at 450 K. Reproduced from Padding and Briels [386] with the permission of AIP Publishing. For further information regarding the various sets of data shown in figure refer to the cited work and the references within it.

Another exciting method used to perform CG simulations with medium coarse-graining degrees is DPD which was introduced in Section 2.3.2. The conservative force in DPD algorithm was shown by Groot and Warren [187] to be connected to the Flory-Huggins parameters between components. This notion was further generalized to consider bead-size effects [391], variable bead volumes [392], as well as polymer blends [200]. The consideration of variable bead volumes in DPD facilitates the way to simulate more complex polymeric systems where beads can represent various functional chemical units with different volumes rather than polymers constructed from a single bead type [202]. In addition, an elaborate systematic strategy for parameterization of chain molecules in DPD simulations was recently proposed by Lee et al. [205] which successfully combines top-down and bottom-up approaches and benefits from experimental infinite dilution solubilities of the compounds to map the repulsion interaction parameters. There are rather simple relationships in the literature using which one can find the appropriate DPD conservative forces for all-fluid systems [202,203]. However, such relations cannot help in DPD studies where a fluid is interacting with a solid substrate. As a consequence, some authors developed an iterative approach to optimize the repulsive forces of DPD versus AA simulations based on a comparison of the density profiles of fluid particles on the solid substrate [201–203]. An example of such analysis is shown in Figure 7 for the parametrization of epoxy-alumina interactions as utilized by Kacar et al. [203]. A similar coarse-graining strategy was also incorporated by Johnston and

Harmandaris [393] to study model polystyrenes on a gold surface. In their methodology, the authors developed a hierarchical multiscale model in which DFT, MD, and CG models were combined to describe the interfacial properties.
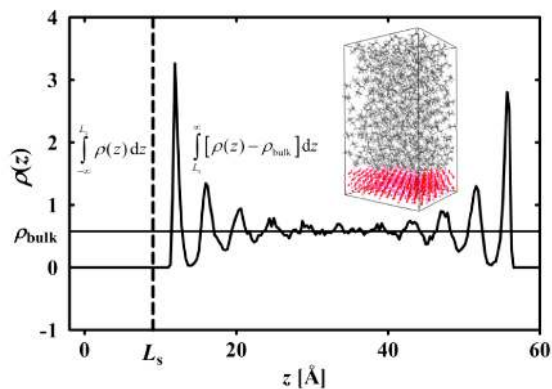

Figure 7. Number density profile from atomistic MD simulations. Molecular center-of-mass of a particular bead is used in computation of the profiles. Vertical line is the location of the substrate surface and defines the integration boundaries. A pictorial representation of the atomistic simulation box snapshot is given as the inset picture. Reprinted with permission from Kacar et al. [203]. Copyright 2016 American Chemical Society.

The distribution functions become broader as more atoms are coarse-grained into one super atom since more degrees of freedom are smeared out through averaging. Accordingly, the potential interactions become increasingly soft and therefore unphysical bond-crossings may occur in such systems. Such bond-crossings result in unrealistic predictions of the dynamics in the modelling of long polymer chains by reducing the number of entanglements. Hence, it is important to avoid the bond-crossing phenomenon in CG models. There are three main routes available to avoid (or to reduce in some cases) the bond-crossings in CG models. The first method was developed by Padding and Briels [385] for the blob model. They introduced an algorithm which prevents bond-crossings by considering a bond as an elastic band and applying the energy minimization (EM) criteria to predict the possible entanglement positions. The second method was proposed by Pan et al. [394] who added segmental repulsive forces to the force field in order to decrease the frequency of bond-crossings. Similar ideas were also put forward by Yamanoi et al. [194] and Sirk et al. [395]. While these approaches are promising, they are computationally expensive. Moreover, some parameters used in these models such as the cutoff distance of the segmental repulsions are physically ambiguous and need further explanation to avoid arbitrary choices. The third method was introduced by Nikunen et al. [396] who could prevent bond-crossings by incorporating simple topological constraints. Using this approach, Rouse as well as reptational dynamics [397] were simulated correctly for short and long chains, respectively. In spite of these attempts, there are still serious computational limitations regarding these methods which necessitate careful selection and implementation of such approaches [398].

High Coarse-Graining Degrees

The coarse-graining methods discussed so far often lump a few atoms up to several monomers into a single super atom. Since the polymer chain length is typically much longer than these coarse-graining limits, super coarse-graining models are necessary to approach extremely large spatial and temporal scales of polymers. In such models, an entire polymer chain is often represented by a single particle. The dynamics of polymer chains is strictly defined by the dynamics of the centers of mass of these particles and all the high-frequency motions associated with macromolecules are dropped out. Based on these ideas, a super CG model was developed by Murat and Kremer [399] in which polymer chains were replaced by soft ellipsoidal particles. The size and shape of the particles is determined based

on the conformations of the underlying chains. The internal energy of a particle with a given size is characterized by the probability of occurrence of that particle. Furthermore, the density of monomers within each particle is calculated from all conformations that have the same size. The spatial overlap of the monomer density distributions of two particles defines the interaction between them. For a large number of contacting particles, the interactions between the particles forces them to adjust the equilibrium size distribution. Their simulations showed that the generic Gaussian random walk scheme appropriately defines the behavior of the chains in the melt [399]. They argue that a large number of long chains can be simulated within a reasonable computation time on a single workstation processor due to the fact that the internal degrees of freedom of the chains are severely smeared out [399]. Extensions of this method are available in which a chain of such soft particles can be considered for the simulations of high molecular weight polymers [400–403]. For instance, Zhang et al. [403] used such a strategy in combination with the mapping of the density distributions onto a lattice in the framework of MC schemes and could develop a particle-to-mesh approach for high molecular weight polymers. The authors propose that such a grid-based scheme could be a viable candidate to produce equilibrated models of long polymer chains useful in the setting of a general multiscale study [403].

An interesting super CG model was developed by Kindt and Briels [404] in which a single particle was ambitiously used to study the dynamics of entangled polymer chains. In this model, a set of entanglement numbers are used for each pair of particles to describe the deviation of the CG model (with the ignored degrees of freedom) from the equilibrium state. Such deviations give rise to transient forces in the system. The displacements of the particles are governed by these transient forces as well as the conservative forces derived from the potential of mean force. This deviation-displacement analysis is performed for any given configuration of the centers of mass of the polymers. Due to the core role of the transient forces in the simulation strategy, it has been called the "transient force model" [405]. The authors applied this model to a melt of $C_{800}H_{1602}$ chains at 450 K and examined radial distribution functions, dynamic structure factors, and linear and nonlinear rheological properties. In general, they could achieve good qualitative, and to a large extent quantitative, agreement with experiments and more detailed simulations. Figure 8 illustrates typical linear and nonlinear rheological properties for $C_{800}H_{1602}$ chains at 450 K calculated by Kindt and Briels [404]. The surprising observation that a single particle could capture the correct reptation behavior was qualitatively linked to the transient forces being quadratic in the deviations of entanglement numbers and thus resembling the confined motions of a chain in a tube [405]. This model has been further applied to study rheological properties of various polymer systems [406–412].
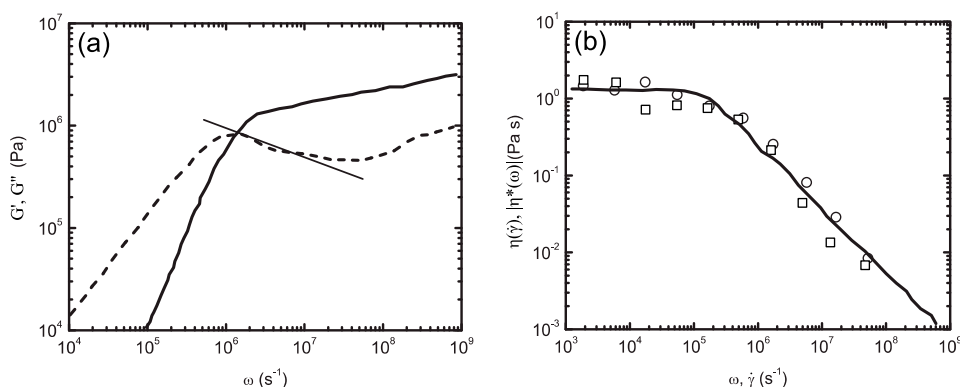

Figure 8. (**a**) Storage G′ and loss G″ moduli (full and dashed lines, respectively); and (**b**) the flow curve for $C_{800}H_{1602}$ melt at 450 K. Reprinted from Kindt and Briels [404] with the permission of AIP Publishing. The solid line in (**b**) is derived in equilibrium simulations using the Cox-Merz rule. The circles and squares are simulation results under shear benefitting from linear background and variable flow field methods, respectively. For further information regarding the data shown in figure refer to the cited work and the references within it.

Based on analytical calculations through the Ornstein-Zernike equation [413], a super coarse-graining model was developed by Guenza and her co-workers [363–365,414–419] which does not need any further optimization against a more detained model. This model provides analytical expressions for various thermodynamic and physical quantities which are especially useful when dealing with rescaling issues. As it was noted before, once a molecule is coarse-grained its entropy as well as accessible surface to the surrounding molecules are changed. The entropy change becomes important in such super CG models in comparison with low coarse-graining degrees such as IBI. The present model provides analytic expressions for the scaling factors from each contribution as [363,365]

$$s_{entropy} = R_g \sqrt{\frac{3MN_c}{2k_BT}}, \tag{51}$$

$$s_{friction} = \frac{\xi}{N\xi_m}, \tag{52}$$

with $s_{entropy}$ and $s_{friction}$ as the rescaling factors for the entropy and surface changes, respectively. Here, M is the molecular weight of the chain with radius of gyration R_g, and N_c is the number of monomers per chain. ξ and ξ_m are the friction coefficients of the super CG and freely-rotating chain systems, respectively.

3.1.2. Reverse Mapping

While the coarse-graining procedure helps accessing longer time scales in simulations, it also removes detailed atomistic features necessary for precise evaluations of the structure. Since CG models have proven extremely useful in various simulations, such as generating equilibrated structures for further analysis and simulation runs [350,420–422], there is a general tendency towards employing them upon possibility. Consequently, a reverse mapping is also needed to reproduce atomistic details such as chemical characteristics from the CG model. The reverse mapping procedure is also referred to as fine-graining or backmapping in the literature [423,424].

Early attempts for reverse mapping are dated back to Tschöp et al. [425] and Kotelyanskii et al. [426]. In general, a reverse mapping operation includes (i) the reconstruction of CG particles with possible atomistic structures from a bank of templates; followed by (ii) performing EM, MD, or MC simulations to guarantee collectively and locally relaxed atomistic structures. In the first step, the fitting templates are often extracted from a preceding atomistic equilibrium simulation. The chosen template for a given CG particle should not only fit the contour of the underlying CG molecule, but also allow the best superposition for the neighborhood CG particles. In order to achieve a high backmapping efficiency, the fitting procedure is usually based only on geometrical criteria and no force and energy calculations are involved. In some cases where the CG particle represents a complex structure with bulky side groups, one must be careful to avoid interlocking of side groups [420]. In the second step, it is necessary to run post-processing calculations due to the fact that the CG force field is derived from average atomic distributions and therefore may easily lead to overlapping structures [427]. Such artefacts could happen more frequently in coarser CG models.

Several backmapping approaches are proposed for different polymers in the literature [420,425,428–431]. Often, when the CG model is constructed based on the atomistic simulations, the zoom-in back to the atomistic description is simply a geometrical problem [430]. However, a more sophisticated procedure must be followed in some cases where the model is significantly coarse or the CG particles include asymmetric atoms and the polymer chain shows a specific tacticity [420,431]. An example for the first case was given by Karimi-Varzaneh et al. [430] who used a simple backmapping algorithm to reinsert the atomistic details of a PA-66 in its corresponding CG model. As for the latter, Wu [431] utilized a special backmapping procedure to capture tacticity effects on the structure and dynamics of poly(methyl methacrylate) melts. Moreover, a general backmapping technique to prepare equilibrated polymer melts was proposed by Carbone et al. [424] which consists of (i) the generation of random

walk chains with various Kuhn lengths; and (ii) the insertion of atoms on the underlying random walk chains. The steps of this approach for PA-66 are shown in Figure 9. The authors showed that well-equilibrated melts of PE, atactic PS and PA-66 can be achieved using this method. The structural properties of such relaxed melts were shown to be in good agreement with previous AA simulations and experimental data on short as well as long spatial ranges. Some cases with special reverse mapping algorithms are also found in literature. For instance, in order to generate realistic amorphous polymer surfaces, Handgraaf et al. [432] developed a special mapper which takes the CG structure as input and uses the MC technique to generate the atomistic structure. The mapped atomistic structure is later equilibrated by performing a short MD simulation.
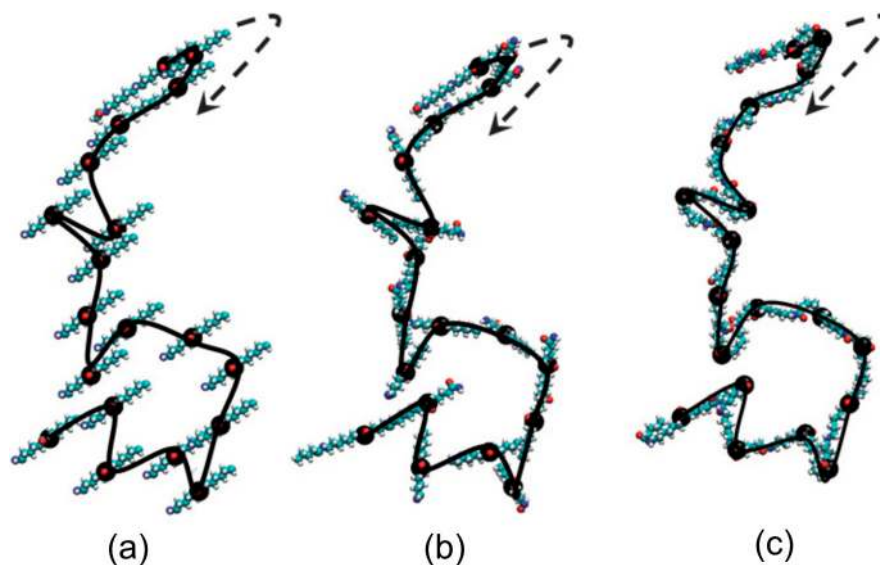

Figure 9. Reverse-mapping procedure for PA-66: (**a**) insertion of the atomistic segments (colored beads) on the underlying random walk chain (solid black line); (**b**) re-orientation of the atomistic segments; (**c**) final configuration of the reconstructed atomistic chain. The arrow indicates the grow direction of the chain. Reproduced from Carbone et al. [424] with permission of The Royal Society of Chemistry.

It should be noted here that the reverse mapping of a nonequilibrium CG system differs from an equilibrium run to some extent. Since molecular deformations are significant in the CG model due to the nonequilibrium simulations, a proper backmapping procedure should translate these deformations into the atomistic model. Furthermore, the atomistic model must also contain information about the stored deformation energy in the CG model of the polymer. Obviously, a simple backmapping cannot meet these requirements since during the post-processing step, i.e., EM or MD or MC simulations, the energetically unstable deformed structure relaxes quickly. A backmapping method was proposed by Chen et al. [423] to overcome this problem for polymer chains experiencing sheared nonequilibrium conditions. Their methodology mixes the general concepts of backmapping with the new idea of applying position restraints to preserve the deformed configurations. In order to preserve the stretched chain configuration obtained in the CG simulation, position restraints with a harmonic potential are applied to all the atoms coinciding with CG particles locations. The globally deformed structure is allowed to relax locally using a molecular mechanics approach [433]. By changing the position restraint scheme and re-optimizing the structure through an iterative procedure, it is possible to minimize the isolation of segments from the rest of the chain. The workflow of the backmapping procedure of Chen et al. [423] is illustrated in Figure 10.
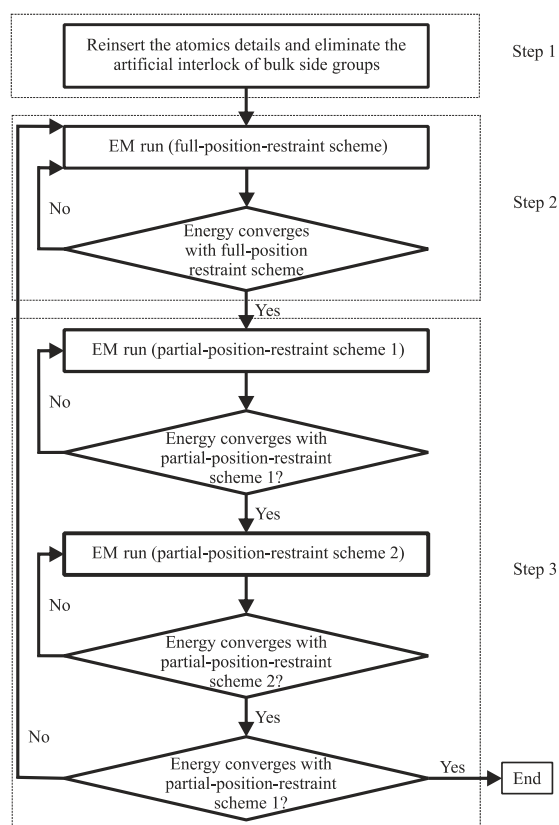
Figure 10. The workflow used in the backmapping procedure of nonequilibrium CG simulations as proposed by Chen et al. [423]. Notice that schemes 1 and 2 in step 3 are two variants of the main scheme in step 2 in order to minimize the isolation of segments from the rest of the chain. Reproduced from Chen et al. [423] with permission of the PCCP Owner Societies.

Finally, the validity of a reverse-mapped atomistic structure is often tested by comparing relevant structural information simulated using atomistic models based on the reverse-mapped configurations with the original AA simulations initially used to develop the CG force field [424,430,434]. Radial distribution function of a specific chemical group, bond and angle distributions, torsion angle distribution, and the number of hydrogen bonds are mostly used for such comparisons. In some studies, the results of a reverse-mapped atomistic simulation are also directly compared with the available experimental data [424].

3.2. Concurrent Multiscale Approaches

The concurrent approaches define the system under consideration through a genius combination of several methods and solve them simultaneously instead of a hierarchical procedure as in sequential approaches. The resolution of the solution is adapted to provide an accurate representation of those regions of the system which are of particular interest. A common field of application for such strategies is the analysis of crack propagation in materials. During the crack propagation the immediate neighborhood of the crack tip, where the bond breaking is taking place, demands a higher precision in the models representation whereas a coarser model could suffice for further away from this region. An example of the concurrent methodology used in the crack analysis is shown in Figure 11. In this multiscale simulation, the concurrent approach combines tight binding (TB), MD, and FEM techniques to study crack propagation in silicon [435]. The vicinity of the crack should be simulated at a finer resolution since it exhibits significant nonlinearity. Therefore, atomistic MD method could provide a more precise representation of the crack surrounding whereas FEM can still accurately describe

the rest of the system further away from the crack. In order to provide a reliable description of the underlying physics, the formation as well as the rupture of covalent bonds must be treated with quantum mechanics rather than empirical potentials. This is due to the fact that bonds are principally the sharing of valence electrons at a quantum mechanical scale [436]. Consequently, it is crucial to apply a TB modelling to a small region in the immediate vicinity of the crack tip, where bond breaking prevails during fracture, while the empirical potential description of MD is adequate further away from this region.
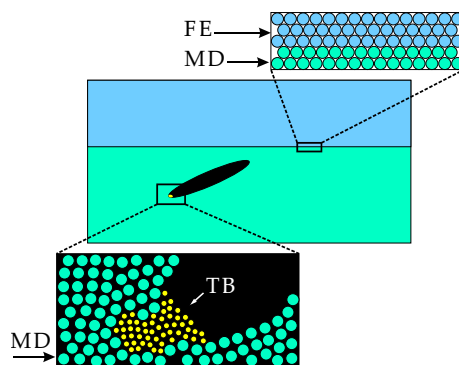

Figure 11. A hybrid FE/MD/TB simulation. The FE, MD, and TB approaches compute forces on particles (either FE nodes or atoms) in their respective domains of application. These forces are then incorporated to calculate the updated positions and velocities of the particles in a time-stepping algorithm.

The concurrent approach is best suitable for the systems with an inherent multiscale character. In such systems, the behavior at each scale depends strongly on the phenomena at other scales. Moreover, this approach can be of a more general nature due to the fact that it does not often rely on any system-specific assumptions such as a particular coarse-graining model. Therefore, a well-defined concurrent model can be applied to many different systems within the limits of common phenomena involved as long as it incorporates all the relevant features at each level. In contrast to sequential methods, concurrent models are not usually constructed based on a detailed prior knowledge of the physical quantities and processes involved. As a result, such models are particularly useful when dealing with new emerging problems about which little is known, for instance, at the atomistic level and its connection to larger scales. However, the coupling between the different regions treated by different methods is a critical challenge remaining in the core of concurrent approaches. A successful multiscale model seeks a smooth coupling between these regions. Here, we address some of the concepts and strategies developed in the concurrent framework.

3.2.1. The Concept of Handshaking

In concurrent simulations, often two distinct domains with different scales are linked together benefitting from a region called the "handshake" region. The handshake region generally bridges the atomistic and continuum domains of the multiscale model [437,438]. However, there are studies where it has been used to link quantum mechanical TB calculations to atomistic domains [438,439], or atomistic MD models to their equivalent CG descriptions [437].

The handshake region transfers information from one domain to the other and thus provides the possibility to overlap, usually, atomistic and continuum domains. This overlap is defined with a field variable, often the potential energy, taking a weighted form of the magnitude of the same variable in each domain. The weighting is usually in the form of a function which decreases monotonically from one to zero in the overlap. As a result, the control variable has its corresponding values in each domain with a gradual transition between the domains. The form of the weighting function is not determined by the formulation and is arbitrary. Consequently, the modelling quality of the handshake region is strongly dependent on a smooth and gradual shift of control variables from one domain to the other

domain. In the handshake algorithm, it is assumed that the properties of each domain are independent from one another. Due to this assumption, one has to be concerned particularly whether or not the material properties of both domains are truly equivalent. In addition, physical complications in the handshake region might necessitate more complex algorithms to obtain a precise representation of it. For instance, nodal displacements of the continuum domain should be influenced by the displacements of molecules inside the neighboring atomistic domain if the node and the molecules are within the cutoff distance of the molecular interactions.

The handshaking approach has been applied to combine TB/MD/FEM in order to study crack propagation and crystal impact in silicon [438,439]. A combination of TB/MD/FEM has also been utilized in a handshaking framework to characterize submicron micro-electro-mechanical systems by Rudd et al. [437]. Based on the works of Abraham et al. [439,440] the unifying theme for such a multiscale model is the total Hamiltonian H$_{tot}$ defined throughout the entire system. This Hamiltonian is a function of the atomic positions $\mathbf{r}_j$ and their velocities $\mathbf{v}_j$ in the TB and MD regions for all *j* atoms, and the displacements $\mathbf{u}_\alpha$ and their time rates of change $\dot{\mathbf{u}}_\alpha$ in the finite element (FE) regions for all *α* nodes. Within this scheme, the Hamiltonian is divided into FE, MD, TB and handshaking contributions from FE/MD and MD/TB during the domain decomposition. It is assumed that the atomic and nodal movements are not necessarily exclusive to a single domain, but their interactions are. In this way, H$_{tot}$ may be written as

$$\mathrm{H}_{tot} = \mathrm{H}_{FE}(\mathbf{u}_\alpha, \dot{\mathbf{u}}_\alpha) + \mathrm{H}_{FE/MD}(\mathbf{r}_j, \mathbf{v}_j \mathbf{u}_\alpha, \dot{\mathbf{u}}_\alpha) + \mathrm{H}_{MD}(\mathbf{r}_j, \mathbf{v}_j) + \mathrm{H}_{MD/TB}(\mathbf{r}_j, \mathbf{v}_j) + \mathrm{H}_{TB}(\mathbf{r}_j, \mathbf{v}_j), \quad (53)$$

with the Hamiltonian of different contributions depicted with appropriate indices. Rudd et al. [437] explain that the FE/MD as well as MD/TB handshakes must successfully address the fundamental issues of (i) matching the degrees of freedom and (ii) defining consistent forces at the corresponding interfaces. Despite this similarity, it should be emphasized that each handshake obliges a somewhat different approach in order to answer the requirements. This is due to the fact that the MD/TB handshake occurs across an interface of atoms whereas the interface at the FE/MD handshake is between planes of atoms [437]. Appropriate derivatives of this Hamiltonian function can be used to define the equations of motion in a standard Euler-Lagrange routine. The time evolution of all the variables can then proceed to the next step using the same integrator. The interested reader is referred to the work of Rudd et al. [437] for further information.

3.2.2. Linking Atomistic and Continuum Models

It is frequently observed in large-scale atomistic simulations that only a small subset of atoms actively participate in the evolving phenomenon. This allows for the majority of atoms to be effectively represented by continuum models. Hence, a considerable reduction of computation and storage resources is guaranteed if only novel multiscale approaches could reduce the number of degrees of freedom in atomistic simulations. There is a tremendous amount of concurrent multiscale modelling methods developed in the last twenty years which couple atomistic simulations such as MD with continuum simulations such as FEM [441,442]. The idea behind these methods, not unlike all multiscale strategies, is to focus the available computation power where it is needed by applying atomistic simulations, whereas an approximate solution is provided for the rest of the system by continuum simulations. Therefore, both atomistic details as well as the macroscopic properties of materials can be obtained simultaneously from these simulations. Such models are mostly designed for crystalline materials such as metals or carbon nanomaterials. Unfortunately, their application in polymeric materials is still limited, possibly due to the unfamiliarity of these models to polymer researchers. Although some authors have referred to such methods in recent reports on polymer simulations [32,299], the fundamentals of the methods are not brought to discussion. We believe that the basic ideas of these methods can be extended to study polymeric materials. Here a brief description of these methods is provided with emphasis on the fundamentals. At the end of this section,

several studies in polymeric systems are listed where such methods or a modified version of them are incorporated to address the phenomena. It is our hope that it will help guide future improvements.

Certain categories of problems such as fracture and nanoindentation possess the characteristics of localized deformation where it is possible to address the system by a dual-domain or partitioned-domain approach; one with an atomistic description B^A, and the other with continuum approximation B^C. The two domains are linked by an interfacial region B^I across which compatibility and equilibrium are enforced. An important distinction among various methods is the way they treat the interfacial region. Most methods follow one of the strategies demonstrated in Figure 12. The interfacial region is shown by the dashed lines. In part (a) of the figure, B^I has been further subdivided into two parts: (i) the handshake region B^H, and (ii) the padding region B^P. As explained before, the handshake region provides a mixing between the two scales. The padding region is continuum in nature and provides the boundary conditions to the atoms in B^A and B^H with a certain range of atomistic interactions, r_{cut}. The thickness of this region depends on r_{cut} and the motions of atoms in B^P are calculated, in different ways for different methods, based on the continuum displacement fields at the positions of the padding atoms. It is also possible to eliminate the handshake region as shown in part (b) of Figure 12. Models that do not use a handshake region mostly incorporate a direct atom-node correspondence at the edge of the FE region to impose the displacement compatibility across the interface. This necessitates that the mesh is refined down to the atomic scale on the continuum side of the interface and hence introduces difficulties in mesh generation.
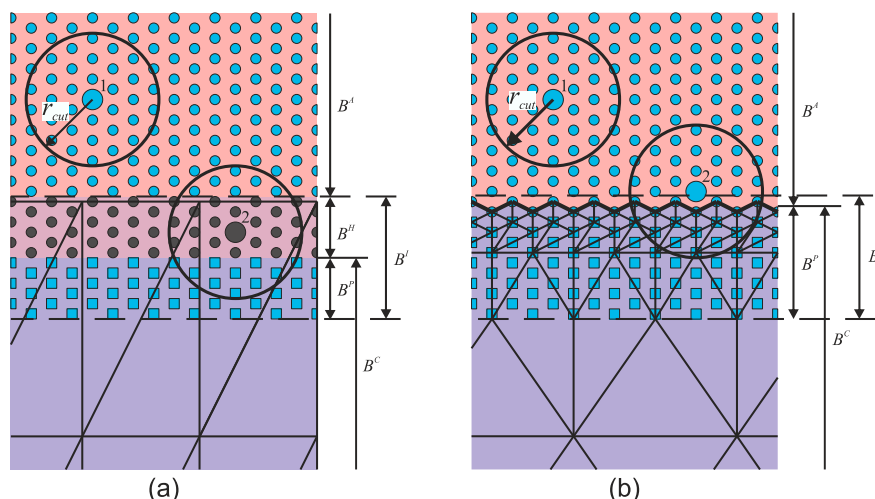

Figure 12. Schematic representation of generic interfaces used in coupled atomistic/continuum simulations: (**a**) with the handshake region; and (**b**) without the handshake region. Atom 1 does not influence the continuum directly (while atom 2 does) because of the finite cutoff length. Padding, handshake, and regular atoms are depicted by blue squares, black circles, and blue circles, respectively.

The coupling between the B^A and B^C domains necessitates compatibility conditions in each direction. Therefore, the displacements of atoms in B^P must be determined from the nodal displacements in B^C. Moreover, the displacement boundary conditions need to be defined for the B^C nodes at the edge of the mesh closest to the B^A. The compatibility criteria can be either strong or weak. The strong compatibility is when the padding atoms move in the same as the finite elements in which they reside. In this type of compatibility, subsets of nodes are defined that coincide with some of the atoms in B^A. The displacement boundary condition is therefore imposed on B^C with the motion of the overlaying atoms from B^A. The weak compatibility, on the other hand, utilizes some sort of an averaging or penalty method to enforce the displacement boundary conditions. Strong compatibility introduces complications in mesh definition near the interface while it also yields relatively more accurate results [442].

The simulation algorithm often finds the equilibrium by either minimizing an energy functional or driving the set of forces on all degrees of freedom to zero. Consequently, there are two major categories of the governing formulation i.e., the energy-based and the force-based approaches. The major drawback of the energy-based method is that it is extremely complicated to remove the non-physical artifacts of the coupled energy functional. This problem, often referred to as the "ghost forces", stems from trying to combine two energy functionals from different models into a single coupled energy expression [442–444]. The force-based approaches, on the other hand, have no well-defined total energy functional and are considered to be non-conservative in general. These approaches can be numerically slow and unstable and could converge to unstable equilibrium states. However, force-based methods can eliminate the ghost forces due to access to the direct definition of the forces.

Several methods are proposed in literature to correct the ghost forces artifact in energy-based models. These methods take various actions in order to eliminate or at least mitigate for ghost forces [445–449]. One such approach with general characteristics is the deadload ghost force correction [444]. In this approach, the ghost forces are explicitly computed and the negative of these forces are added as deadloads to the affected atoms or nodes. The deadload ghost force correction has shown great promise in some static simulations [442]. However, the deadload correction is only an approximation for the simulations where ghost forces change during the calculation progress.

The general algorithm for energy-based methods defines the total potential energy of the entire system U^{tot} as the sum of the potential energies of the atomistic U^A, continuum U^C and handshake U^H regions, as

$$U^{tot} = U^A + U^C + U^H, \tag{54}$$

and minimizes it to reach equilibrium. These energies are described by [442]

$$U^A = \sum_{\alpha \in B^A} E_\alpha - \sum_{\alpha \in B^A} \mathbf{f}_\alpha \cdot u_\alpha, \tag{55}$$

$$U^C = \sum_{e=1}^{N_e} \sum_{q=1}^{N_q} \omega^q V_e W(\Delta(\mathbf{r}_e^q)) - \bar{\mathbf{f}}^T \mathbf{u}, \tag{56}$$

$$U^H \approx \sum_{\alpha \in B^H} (1 - \Theta(\mathbf{r}_\alpha)) E_\alpha + \sum_{e \in B^H} \Theta(\mathbf{r}_e^{cent}) W(\Delta(\mathbf{r}_e^{cent})), \tag{57}$$

where the energy, spatial coordinates, displacement and applied forces of atom α are shown by E_α, $\mathbf{r}_\alpha$, $\mathbf{u}_\alpha$, and $\mathbf{f}_\alpha$, respectively. N_e is the number of elements, V_e is the volume of element e, N_q is the number of quadrature points in the numerical integration, $\mathbf{r}_e^q$ is the position of quadrature point q of element e in the reference configuration, and ω^q is the associated Gauss quadrature weights. $\bar{\mathbf{f}}$ and $\mathbf{u}$ are the vector of applied forces and nodal displacements in the FE region, respectively. W is a function of the deformation gradient Δ. $\mathbf{r}_e^{cent}$ is the coordinates of the Gauss point in element e which is taken at the centroid of the triangular elements in this specific case shown in Figure 12. One should notice that the energy of the continuum region is approximated due to the fact that a continuous integral has been replaced by a discrete numerical method. Consequently, the handshake region is also approximated since it also uses such a numerical approach for the continuum energy contribution. In the energy equation for the handshake region, both the continuum and atomistic energies are used in a weighted fashion according to a function Θ which varies linearly from one at the edge of B^H closest to the continuum region, to zero at the edge closest to the atomistic region. Indeed, for methods with no handshake region, U^H is taken zero and only the continuum and atomistic regions contribute to U^{tot}. Moreover, one should note that the padding atoms have no contribution to the formulation of the potential energy. Therefore, these atoms only provide an appropriate boundary condition for the atoms in B^A.

The force-based methods are based on two independent potential energy functionals. The first one calculates an energy functional U^{atom} assuming the entire system is modelled using atoms. The second energy functional U^{FE} on the other hand, provides a description of the system if it was modelled

entirely in a FEM framework. The forces for all α atoms, $\mathbf{f}_\alpha$, and all i nodes, $\mathbf{f}_i$, are simply found by differentiating the corresponding energies with respect to the atomic or nodal displacements, $\mathbf{u}_\alpha$ and $\mathbf{u}_i$ respectively, as

$$\mathbf{f}_\alpha = \frac{\partial \mathrm{U}^{atom}}{\partial \mathbf{u}_\alpha}, \tag{58}$$

$$\mathbf{f}_i = \frac{\partial \mathrm{U}^{FE}}{\partial \mathbf{u}_i}. \tag{59}$$

It is important to note that the difference between energy-based and force-based methods stems from the fact that in the second approach one does not attempt to minimize the combined energy functional. In the following, some relevant approaches which are used to link atomistic and continuum models are discussed.

Quasicontinuum Approach

Quasicontinuum (QC) method is a particularly interesting approach by Tadmor et al. [450–452] which seamlessly couples the atomistic and continuum realms. In QC approach, the atomistic description of the system is systematically coarsened by the introduction of kinematic constraints designed carefully so that the full atomistic resolution is preserved where required, for instance in the vicinity of large deformations, and to treat collectively large numbers of atoms in regions further away. QC was firstly developed to investigate defects in solids considering the interaction of dislocations [444,450,451,453–456]. However, it has also found applications in fracture and crack mechanics [457,458], and nanoindentation [459].

In QC method, there is no handshake region. Since there is no separation of the domains in QC, there are no needs for separate sets of material data in this multiscale approach. This is a significant advantage of QC. The calculation domain is partitioned into non-overlapping cells similar to the FEM. These cells then cover the constituting molecules of the material while their vertices coincide with some representative atoms from the molecules. The local density of such representative atoms is larger in regions with high deformations compared with the regions experiencing low deformations. Figure 13 shows an example for the selection of representative atoms in the vicinity of a crack. QC takes the degrees of freedom in a cell the same as the degrees of freedom of the representative atoms of that cell. In addition, the movement of molecules is usually calculated from the representative atoms utilizing interpolation functions. QC also approximates the average energy of a cell from its representative atoms. The method eventually looks for the arrangement of representative atoms which minimizes the potential energy of the domain.
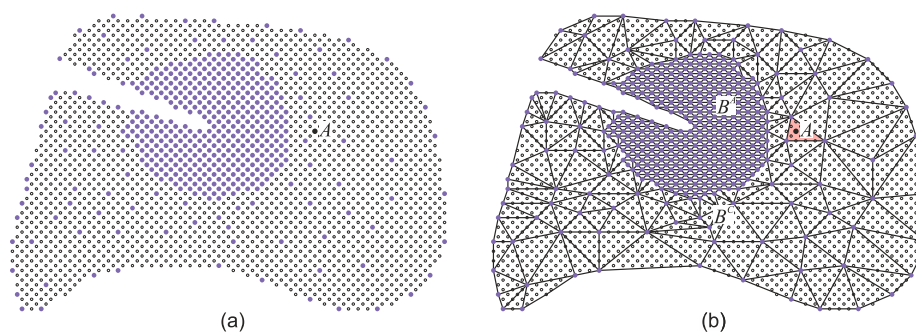

(a) (b)

Figure 13. For an irregular domain which includes a crack, part (**a**) shows the representative atoms near the crack tip; Part (**b**) demonstrates the domain meshed by linear triangular elements. The density of representative atoms is adjusted to correspond to the variation in the deformation gradient. In order to calculate the displacement of atom A in part (**b**), one can use a linear interpolation of the displacements of the three representative atoms which form the highlighted element.

Variants of the QC model have been developed and applied in different situations [450,451,460,461]. In general, the QC approach includes three major blocks: (i) the constrained minimization of the atomistic energy of the system; (ii) the computation of the effective equilibrium equations based on appropriate summation rules; and (iii) the design of the computational mesh representing the structure of the system based on proper adaptation criteria. The QC model initially provides a full atomistic description of the system which is later scaled down to a subset of representative atoms. The positions of the remaining atoms are obtained by piecewise linear interpolations of the representative atoms. Afterwards, the effective equilibrium equations are obtained by minimizing the potential energy of the system based on the scaled-down configuration space. A precise evaluation of the total energy of the system E^{tot} is often performed over the full collection of atoms as

$$E^{tot} \; = \; \sum_{i=1}^{N} E_i, \tag{60}$$

in which N is the total number of atoms, and E_i is the energy of the ith atom at its corresponding position in the system. This comprehensive formula is approximated in QC models benefitting from the concept of representative atoms with

$$E^{tot} \; \approx \; \sum_{i=1}^{N_r} \omega_i \overline{E_i}, \tag{61}$$

where ω_i and $\overline{E_i}$ are the quadrature weight which shows the number of the atoms that a given representative atom stands for in the definition of the total energy, and the energy of the ith representative atom, respectively. Here, the summation is only performed over N_r representative atoms and thus the calculation effort is reduced. The representative atoms are usually adaptively selected so that an accurate description of the critical positions with larger deformation fields is obtained. QC approach often incorporates FEM to determine the displacement fields and combines it with an atomistic technique which is used to determine the energy of a given displacement field. One can compare it with the standard FEM in which a constitutive law is coupled with it through a phenomenological model.

The concepts of QC could be extended to include a coupling between atomistic calculations and QM as well. Such an strategy was initially introduced to study fracture in silicon and the method was named coupling of length scales (CLS) [437,439,440]. There are small differences between QC and CLS. Initially CLS method used a small strain approximation to describe the continuum region rather than the Cauchy-Born rule used in QC [442,462]. However, conceptually the methods are similar since the original CLS approach could be generalized to provide a nonlinear Cauchy-Born description for the continuum region. Furthermore, minor differences between the methods exist in the way they treat the interface. Still, these differences are believed to have slight influences on the error and rate of convergence [442,463].

QC suffers from the ghost forces like any other energy-based method. An idea to reduce these forces was initially put forward by introducing a handshake region to the QC models. This idea along with minor changes in the manipulation of forces at the interface constructed the bridging domain method (BDM) [464]. At the interface, BDM uses weak compatibility which eliminates the need for one-to-one correspondence between atoms and nodes. This weak compatibility imposes some loss of accuracy on BDM. Another approach to correct for ghost forces is the iterative minimization of two energy functionals used in composite grid atomistic/continuum method (CACM) [465]. CACM is a highly modular method with weak compatibility and no handshake region. It provides the possibility to separately solve energy functionals of different regions. However, this could lead to longer computation times especially for nonlinear problems.

Coarse-Grained Molecular Dynamics

Coarse-grained molecular dynamics (CGMD) was originally developed to model the nano-electro-mechanical systems (NEMS) [437,452,466]. In this technique, conventional MD is coupled

with a CG description of the system. The CG regions are modeled on a mesh in a formulation that generalizes conventional FEM of continuum elasticity. The significant aspect of CGMD is that it is derived solely from the MD model and has no continuum parameters. In other words, this method is notably different from the other coupled atomistic/continuum methods presented in this manuscript in the way that it constructs the continuum model only based on the atomistic information. As a result, it offers a smooth coupling and provides control of errors that arise at the coupling between the atomistic and CG regions. A more general version for the dynamics of CGMD is also proposed by Curtarolo and Ceder [467].

In CGMD the domain is partitioned into cells with variable sizes. This provides the possibility to assign a mesh node to each atom in important positions whereas in other regions the cells could contain several atoms and the nodes are not necessarily coincident with atoms. CGMD follows a detailed statistical coarse-graining prescription which particularly results in scale-dependent constitutive equations for different regions of the domain [466]. In CGMD, the CG mesh is refined to the atomic scale where it joins with the MD lattice. This refined mesh with no handshake region as well as the fact that CGMD adopts an effective field model suggests a strong resemblance to QC. In addition to the point made earlier on the use of atomistic constitutive equations in CGMD, this method is also designed for finite-temperature simulations. On the contrary, the classic QC is mainly applicable to zero-temperature simulations. It is interesting to note that according to Rudd and Broughton [466] the classic QC is closely related to the zero-temperature rigid approximation of CGMD. It should be noted that finite-temperature versions of QC are developed in recent years [468–470]. These methods often benefit from coarse-graining concepts similar to CGMD. Finally, CGMD is free from the ghost forces which is a desirable feature missing in QC.

Finite-Element/Atomistic Method

The finite-element/atomistic (FEAt) method is a force-based method first introduced by Kohlhoff et al. [471]. FEAt uses no handshake region and strong compatibility is enforced between the domains. To compensate for the absence of the handshake region, FEAt incorporates a nonlocal elasticity formulation in the finite elements and mitigates the abrupt transition from B^C to B^A. In general, the forces on every atom α in B^A and B^P are calculated independently from B^C, from the derivative with respect to atom positions of an energy functional $U^{A \cup P}$ of the form

$$U^{A \cup P} = \sum_{\alpha \in \{B^A \cup B^P\}} E_\alpha - \sum_{\alpha \in \{B^A \cup B^P\}} \mathbf{f}_\alpha \cdot \mathbf{u}_\alpha. \tag{62}$$

This energy functional looks very similar to the one used in energy-based methods, but it is fundamentally different since it also contains the padding atoms. The energy functional of the continuum domain is similar to the energy functional of the energy-based methods described in Equation (56). The forces on the nodes are therefore simply obtained from its derivative with respect to nodal displacements. Based on these forces, the atoms and nodes are moved and the forces are re-calculated for the new atom and node positions.

Some variations to FEAt are found in the literature. In the presence of dislocations in the continuum, one can use discrete dislocation methods in the description of the continuum region. The resulting continuum region could be coupled with the atomistic region in a force-based algorithm just like FEAt to yield coupled atomistic and discrete dislocation (CADD) approach [472,473]. In order to remove the strong compatibility from FEAt and CADD, the hybrid simulation method (HSM) uses the same approach as BDM by including a handshake region in the system [474]. A variation of HSM is the concurrent atomistic/continuum (AtC) method in which a blending of forces is performed at the interface [443,475,476].

Bridging Scale Method

The bridging scale method (BSM) is an energy-based technique with no handshake region. In this method, the FE mesh exists throughout the entire domain in order to store a part of the final solution, see Figure 14. The central idea behind BSM is derived from classical works in decomposing a complete solution of the total displacement field into fine and coarse scales and solving for the fine scale only in regions that require it [477–479]. The coarse scale solution is that part of the solution which is normally represented by a set of FE shape functions. The fine scale solution on the other hand, is defined as the part of the solution whose projection onto the coarse scale is zero.
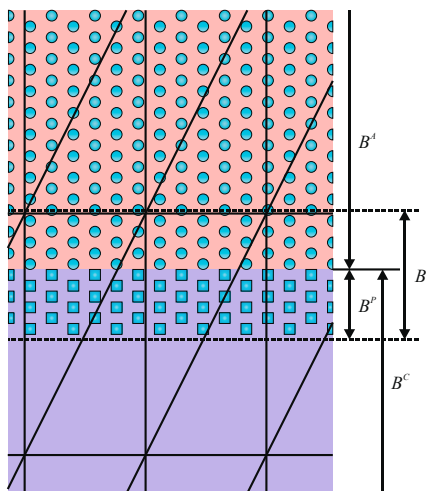

Figure 14. The BSM interfacial region. The interface has no handshake region and the finite elements cover the entire body which allows to store the coarse scale displacement field.

In BSM framework, the coarse scale solution $\gamma \mathbf{r}_\alpha$ is taken to be a function of the initial positions of the atoms $\mathbf{r}_\alpha$ and is defined by

$$\overline{\gamma}\mathbf{r}_\alpha = \sum_i \sigma_i^\alpha \mathbf{u}_i, \tag{63}$$

where σ_i^α is the shape function of node i evaluated at point $\mathbf{r}_\alpha$, and $\mathbf{u}_i$ is the FE nodal displacement associated with node i. Using a mass-weighted least-squares fitting of the coarse scale solution to the total solution, Park and Liu [480] showed that the fine scale solution γ' can be defined based on a projection matrix $\mathbf{P}$ as

$$\gamma' = \gamma - \mathbf{P}\gamma. \tag{64}$$

Here, γ is the exact solution determined from an underlying atomistic technique such as MD. Therefore, the total solution can be found by summing up both fine and coarse scale contributions. Such an approach is sometimes referred to as the projection method in the literature due to the fact that atomistic and continuum regions are coupled by projecting a fine scale solution onto a finite dimensional solution space [481].

Applications in Polymeric Materials

In this part of the paper, we give several examples for the applications of coupled atomistic/continuum models in polymeric systems. In the studies outlined here, one can find applications of the methods explained so far; either it is directly used, or a modified version is developed to capture the correct physics involved, or a concept is borrowed to propose new models for polymers. The reader should note that our goal is not to provide a comprehensive list here but merely to raise attention towards the opportunities. We hope that the polymer researcher finds it useful in order to navigate through these multiscale approaches and further develop new strategies for one's own problem.

Generally, it is more difficult to model polymers than crystalline materials due to their amorphous nature. A methodology to solve this problem was formulated by Theodorou and Suter [482,483] in which a parent chain of atoms is attached to an Amorphous Cell (AC). The AC then experiences deformations while periodic boundary conditions are applied to all sides. Tan et al. [481] incorporated the concept of AC and developed it based on the adaptive scaling resolution ideas similar to CGMD and introduced the Pseudo Amorphous Cell (PAC) multiscale approach for amorphous polymers. PAC algorithm includes: (i) generating a configuration of polymer chains in the domain; (ii) applying linear molecular mechanics for regions with small deformations; (iii) reducing the degrees of freedom in such regions; and (iv) coupling of linear and nonlinear molecular mechanics equations. In their method, the regions with large deformations are represented with nonlinear molecular mechanics and thus provide a finer solution. The authors showed that PAC can successfully simulate the nanoindentation of amorphous polymers and the indentation force was predicted with a good precision comparable to a full molecular mechanics simulation [481]. Later Su et al. [484] applied the PAC approach to correlate the movements of atoms of an amorphous material within a representative volume element (RVE) to the its overall deformation.

The ground idea of projection methods was first introduced in details by Hughes et al. [477] as the variational multiscale methods (VMS) which allows a complete model to be described by orthogonal subscale models. Utilizing this property, Codina [485] presented a method to deal with numerical instability of the Stokes problem due to the incompressibility constraint and convection. He proposed using orthogonal subscales in FEM through the pressure gradient projection. This approach has been developed recently by Castillo and Codina [486,487] to present stabilized VMS formulations to solve the quiescent three-field incompressible flow problems of viscoelastic fluids as well as fluids with nonlinear viscosity. The authors were able to successfully capture the distributions of streamlines in a sudden contraction flow for an Oldroyd-B fluid at Re of 1 at various Weissenberg numbers (We). It was observed that the size of the vortex appearing in the bottom corner decreases as We increases.

In a recent MD study of brittle fracture in epoxy-based thermoset polymers under mechanical loading, Koo et al. [488] introduced an EM step into the virtual deformation test to maintain the system temperature at zero. They stated in the paper that this idea was borrowed from QC which bridges atomistic scale to continuum scale by decoupling temperature effects. The possibilities of incorporating multiscale approaches to connect MD and FEM such as QC, in investigations of structure at epoxy-silica interface are also emphasized by Büyüköztürk et al. [489].

Jo and Yang [490] utilized an atomistic/continuum model to predict the mechanical properties of semicrystalline poly(trimethylene terephthalate) (PTT). Their approach includes an EM process similar to energy-based methods. The semicrystalline PTT includes an amorphous matrix represented as a continuum, and the crystalline phase represented by a spherical inclusion modelled in atomistic detail. The degree of crystallinity of PTT is altered by changing the volume fraction of an inclusion.

In order to model the compressive behavior of carbon nanotube PNCs, Li and Chou [491,492] developed a multiscale strategy in which the nanotube is modelled at the atomistic scale, and the matrix deformation is analyzed by the continuum FEM. Their methodology is similar to other atomistic/continuum coupling themes except for the fact that they adopt a so-called truss rod model to correctly represent van der Waals interactions at the interface. The multiscale scheme developed by Li and Chou was later incorporated by Montazeri and Naghdabadi [493] to study the stability of carbon nanotube PNCs with a viscoelastic matrix. They coupled molecular structural mechanics to FEM and simulated the buckling behavior of the system.

A multiscale simulation strategy was proposed by De et al. [494] to determine the mesoscopic velocity development in polymer fluids with large stress relaxation times. The incorporation of a constitutive viscosity equation is not sufficient in such systems to produce the correct rheology. The authors introduced a scale bridging concept in which small parts of the system were simulated with MD. These parts could communicate with each other through a continuum approach. During the passing of information, the continuum approach provides precise means of interpolating between these

points. They described the coupling of atomistic and continuum regions in a Lagrangian framework so that the memory effects are included in the calculations.

3.3. Adaptive Resolution Simulations

It was already discussed in the concurrent multiscale approaches that there is a category of systems in which the phenomenon of interest is focused in a subregion of the entire domain. Consequently, it would be computationally efficient if the irrelevant AA representation of molecules far from this subregion were replaced with an alternative less expensive model. However, the common limitation in all concurrent methods (introduced so far) is that particle exchange is not allowed in the fixed regions of the system treated at different resolutions. The relatively new class of multiscale simulation approaches, i.e., the adaptive resolution simulations, provides this possibility. Several papers have been devoted to address different aspects of these methods in recent years showing their increasing popularity [337,495–498]. It should be noted that these methods can be principally considered to be concurrent since they often couple the simultaneous run of two techniques with different levels of resolution using a transition region. Furthermore, the transition region usually uses an either force or energy interpolation criterion to link different resolutions somewhat similar to the concurrent methods. However, in adaptive resolution simulations, an atom or a molecule is free to smoothly switch its resolution within the same simulation run depending on its spatial coordinates. Therefore, it allows for an adaptive modification of the resolution within the coexisting models which promotes the accuracy where needed and provides the required precision. In concurrent approaches, on the other hand, different scales are coupled often by a step-wise transfer of information between different methods, for instance we refer to Youn Park et al. [499]. Therefore, some authors introduce adaptive resolution simulations as a separate class of multiscale approaches to emphasize these different aspects [32]. Here, we also follow this notion.

The adaptive resolution simulations often divide a domain into an AA and a CG region and link them using a transition region, see Figure 15, hence are sometimes referred to as the double-resolution simulation methods. Examples for the appropriate systems to investigate with such a strategy include the studies of macromolecules embedded in a solvent (see Figure 16) [500], and liquids near surfaces [501]. The transition region provides the basis for a smooth interpolation from a certain structural representation of a molecule to another depending on the properties that have to be preserved in the CG region. A complete methodology should address the interactions between the atoms or molecules in different domains as well as the property change in crossing the transition region. Moreover, it is central to adaptive resolution simulations that the molecules should be able to diffuse freely between different regions of the simulation box. Other constraints could include thermal equilibrium and uniform density profile across the entire domain which along with certain region-specific properties lead to a formulation of an adaptive resolution scheme.
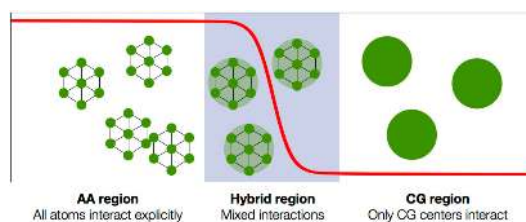

Figure 15. Representation of an adaptive resolution simulation in which a high-resolution region (AA region) is coupled to a low-resolution region (CG region). In the AA region, the structure of the molecules are described in their full atomistic details. In the CG region, however, a simpler representation of the structure and interactions of the molecules are utilized. A transition region is used to connect these regions. The novelty as well as difficulty of adaptive resolution schemes depends strongly on the properties of the transition region, i.e., the way molecules change their resolution. Reprinted from Potestio et al. [337] under the terms of the Creative Commons Attribution License.
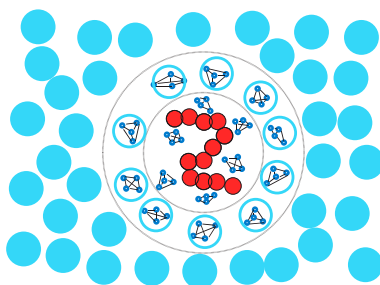
Figure 16. A schematic representation of a generic polymer solution. The structural resolution of the solvent molecules adaptively change based on their distance from the center of the mass of the polymer chain. The polymer beads are represented smaller than the solvent molecules to preserve clarity. Reprinted from Praprotnik et al. [500] with the permission of AIP Publishing.

3.3.1. The Adaptive Resolution Scheme

The Adaptive Resolution Scheme (AdResS) was developed by Kremer and co-workers [500,502–507] to simulate systems in which an AA and a CG model are incorporated to model different subregions of the simulation domain at the same time. The atoms and molecules are allowed to diffuse freely from one region to the other using a smooth transition region which links the subregions. AdResS is principally based on the assumption that Newton's third law should be satisfied the entire simulation box. Additionally, the method assumes that a molecule in the CG subregion contains no information about its atomistic details and interacts with other molecules, either in AA or CG regions, only via its center of mass. An interpolation scheme for the force field across the domain defining the force $\mathbf{f}_{\alpha\beta}$ acting between molecules α and β can be formulated considering the aforementioned assumptions as

$$\mathbf{f}_{\alpha\beta} = \psi(\mathbf{R}_\alpha)\,\psi(\mathbf{R}_\beta)\,\mathbf{f}_{\alpha\beta}^{\mathrm{AA}} + (1 - \psi(\mathbf{R}_\alpha)\,\psi(\mathbf{R}_\beta))\,\mathbf{f}_{\alpha\beta}^{\mathrm{CG}}, \tag{65}$$

where $\mathbf{R}_\alpha$ and $\mathbf{R}_\beta$ are the center of mass coordinates of molecules α and β, respectively. $\mathbf{f}_{\alpha\beta}^{\mathrm{AA}}$ and $\mathbf{f}_{\alpha\beta}^{\mathrm{CG}}$ are the atomistic and CG forces acting on molecule α due to the interaction with molecule β, respectively. Here, ψ is a spatial interpolation function that goes from 1 in the AA region to 0 in the CG region smoothly. In the transition region, atomistic details are explicitly integrated and the CG force is computed between the centers of mass of the molecules and then redistributed to the atoms weighted by the ratio of the atom's mass to the mass of molecule [508]. In the CG region, the CG force is directly applied to the center of mass coordinates of the molecules and there is no need to conserve the molecules internal structure. When a molecule enters the CG region its atomistic details are removed and reintroduced again, through some sort of reservoir of equilibrated atomistic structures, as soon as it approaches the transition region.

The central requirement of satisfying Newton's third law in AdResS is demonstrated to rule out any form of potential energy interpolation and vice versa [509]. Consequently, energy-conserving simulations in the microcanonical ensemble cannot be performed using AdResS. Due to the non-conservative nature of the forces in the transition region, molecules receive an unreal excess energy when crossing this region. This energy can be removed utilizing a local thermostat in order to keep the temperature constant everywhere in the system. The equilibrium configurations of the system are then sampled according to Boltzmann distribution [500,502,503,505,510,511].

The different resolution of the utilized models typically results in a pressure difference between the corresponding regions which further leads to a non-uniform density profile in the system. Kremer and co-workers [508,512,513] modify the CG potential by introducing a thermodynamic force $\mathbf{f}^{th}$ which counterbalances the high pressure of the CG model. This force is obtained in an iterative procedure as

$$\mathbf{f}_{i+1}^{th} = \mathbf{f}_i^{th} - \frac{\nabla \rho_i(\mathbf{r})}{\rho^* \mathbf{k}_T}, \tag{66}$$

where ρ^* is the reference molecular density, k_T is the system's isothermal compressibility and $\rho_i(r)$ is the molecular density profile. This profile is taken as a function of the position in the normal direction to the CG/AA interface. The iterative procedure converges once the density profile is flat, i.e., $\nabla\rho(r) = 0$. The resulting thermodynamic force produces a flat density profile and preserves the thermal compressibility of the system as well as the structure of the system in the CG region. Principally, this method allows one to use any CG force field. As a result, the AA region exchanges energy and molecules with a reservoir like an open system. Such an approach yields a relatively small AA region with the corresponding molecule number fluctuations and all relevant thermodynamic quantities the same as a large AA simulation [508]. It is only because of the thermodynamic driving force that this condition can be achieved independent of the CG model used.

AdResS provides the possibility to perform simulations of the spatial extension of correlations in the system. Particularly, the structural properties of the AA region can be monitored as a function of its size in order to examine their dependency on the interactions with molecules in the bulk region. For instance, Lambeth et al. [514] used this notion to study the ordering degree of the hydrogen bond network of a molecule with hydrophilic and hydrophobic bonds dissolved in water as a function of the size of the AA region. The extent of spatial correlations in low-temperature para-hydrogen has also been studied with the same approach [515,516]. In some systems, it is critical to have access to a large number of particles, for instance, to precisely evaluate the solvation free energies in mixtures. Thus, a standard AA simulation could lead to extremely costly computations in such cases. Naturally, AdResS has shown to be a viable candidate for these systems as well, as evidenced in some works on methanol-water mixtures [517], and triglycine in aqueous urea [513]. Another interesting possibility for such a case to even further accelerate the simulations was incorporated by Mukherji and Kremer [518] to study a coil-globule transition of a biomolecule in aqueous methanol. In their simulations, the usual closed boundary CG reservoir was replaced with a much smaller open boundary CG reservoir in which particles can be exchanged at the eight corners of the simulation domain, see Figure 17. Through this particle exchange adaptive resolution scheme (PE-AdResS), the depletion effects were avoided during the simulations. This type of *open system* MD simulations have raised attraction in recent years. We refer to the work of Agarwal et al. [519] for instance. Recently, a variation of AdResS formulation was developed by Alekseeva et al. [163] which presents a coupling strategy between the stochastic multiparticle collision dynamics and the deterministic MD methods. In this way, the authors were able to successfully demonstrate that hydrodynamic properties of the mixed fluid are conserved by a suitable coupling of the two particle-based methods.
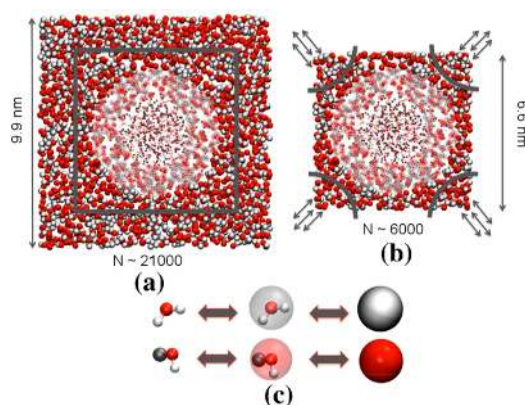

Figure 17. Simulations of a biomolecule dissolved in aqueous methanol: (**a**) Conventional AdResS approach; (**b**) PE-AdResS approach; and (**c**) Mapping scheme of the smooth transition between AA and CG representations. Reprinted with permission from Mukherji and Kremer [518]. Copyright 2016 American Chemical Society.

3.3.2. The Hamiltonian Adaptive Resolution Scheme

A theoretical analysis of the AdResS double-resolution scheme can show that with a local thermostat and the thermodynamic force the atomistic region is equivalent to an open region of a fully atomistic simulation up to second order correlation functions, i.e., the density profile and radial distribution functions [520]. Nonetheless, the lack of a global energy function makes it impossible to perform simulations in the microcanonical ensemble. Consequently, different strategies were employed to formulate an energy conserving version of adaptive resolution simulations including the healing region concept with a space-dependent interpolation of the AA and CG potential energies [521], and the combination schemes for the sum of the Lagrangians of all possible groupings of atomistic and CG molecules [522,523]. Unfortunately, these methods are either inaccurate or extremely complicated to be readily used [337,506]. Recently, an energy-based version of the AdResS method was developed namely the Hamiltonian adaptive resolution scheme (H-AdResS) [524,525]. H-AdResS defines the total Hamiltonian of each molecule with a position-dependent function H^{tot} as

$$H^{tot} = K + U^{int} + \sum_{\alpha} \left\{ \psi_\alpha U_\alpha^{AA} + (1 - \psi_\alpha) U_\alpha^{CG} \right\}, \tag{67}$$

in which K is the all-atom kinetic energy of the molecules, U^{int} is the contribution from internal interactions of the molecules, N is the number of molecules, and

$$U_\alpha^{AA} = \frac{1}{2} \sum_{\beta, \beta \neq \alpha}^{N} \sum_{ij} U^{AA}(|\mathbf{r}_{\alpha i} - \mathbf{r}_{\beta j}|), \tag{68}$$

$$U_\alpha^{CG} = \frac{1}{2} \sum_{\beta, \beta \neq \alpha}^{N} U^{CG}(|\mathbf{R}_\alpha - \mathbf{R}_\beta|), \tag{69}$$

$$\psi_\alpha = \psi(\mathbf{R}_\alpha). \tag{70}$$

U_α^{AA} and U_α^{CG} represent the potential energies of molecule α in its AA and CG representations, respectively. The force acting on atom *i* in molecule α can be obtained through differentiation of this Hamiltonian function [337,524,525]. The differentiation operation results in a drift force F_α^{drift} in the transition zone which is proportional to the difference between U_α^{AA} and U_α^{CG}, by

$$F_\alpha^{drift} = -\left[U_\alpha^{AA} - U_\alpha^{CG} \right] \nabla_{\alpha i} \psi_\alpha. \tag{71}$$

The definition of the drift force implies that the molecules are pushed into one of the regions if the potentials of the AA and CG regions are different. It is obvious from the mathematical expression of the drift force that it is not possible to write it as a sum of antisymmetric terms with molecule label exchange. Consequently, it results in a local breakdown of Newton's third law at the transition region. One can deduce that the drift force vanishes if the CG potential perfectly reproduces the many-body potential of mean force in the AA model. Since this is almost never true, a thermodynamic imbalance is always to be expected between the two regions in the form of different pressure and density levels [337,524]. Potestio et al. [524] used a compensation term $\Delta H(\psi_\alpha)$ in the Hamiltonian, as was done in the AdResS method with the thermodynamic force, to correct for this imbalance. The Hamiltonian is therefore modified as [524]

$$\widehat{H} = H^{tot} - \sum_{\alpha=1}^{N} \Delta H(\psi_\alpha). \tag{72}$$

The authors then obtained an approximate function $\Delta H(\psi_\alpha)$ to cancel out the drift force on average, as

$$\Delta H(\psi_\alpha) = \frac{\Delta F(\psi_\alpha)}{N}, \tag{73}$$

in which the suitable compensation term is related to the Kirkwood's thermodynamic integration for the free energy difference $\Delta F(\psi_\alpha)$ between a hybrid system with a position-independent coupling parameter ($\psi_\alpha \leq 1$) and a CG system ($\psi_\alpha = 0$) at the reference density ρ^* [524]. The authors include a further compensation term to ensure that both the AA and CG subregions coexist at the same reference density ρ^* by considering the effect of pressure difference along the interface $\Delta p(\psi_\alpha)$ and re-formulating $\Delta H(\psi_\alpha)$ in terms of the chemical potential gradient $\Delta\mu(\psi_\alpha)$, as [524]

$$\Delta H(\psi_\alpha) = \Delta\mu(\psi_\alpha) = \frac{\Delta F(\psi_\alpha)}{N} + \frac{\Delta p(\psi_\alpha)}{\rho^*} \tag{74}$$

The H-AdResS method was utilized with both a free energy and a chemical potential compensation strategy to study their effects on the density and pressure profiles [524]. The results showed that with the application of the free energy compensation Equation (73) the pressure profile became flat, but the density was still higher in the AA region. On the other hand, when the chemical potential compensation Equation (74) was applied, the densities of the AA and CG regions attained the same value with a small deviation due to the fluctuations present in the transition region. This was achieved by modifying pressures in each region to correspond to the desirable reference state of density and temperature.

The existence of a Hamiltonian in H-AdResS allows for the precise formulation of a statistical physics theory of double-resolution systems, providing a deep insight into the properties of a given AA model, its CG counterpart and the relation between them. In addition, H-AdResS makes it possible to perform simulation in the microcanonical ensemble as well. Some simulation techniques such as MC can also be incorporated in H-AdResS in contrast to AdResS [525]. It should be noted that H-AdResS along with its compensation strategy can be extended to multicomponent systems. In order to illustrate the routine, a simple case was outlined by Potestio et al. [337] for a liquid composed of two types of molecules.

3.4. Extending Atomistic Simulations

Besides the methods that are explicitly designed to link computational techniques from different realms together, there are some approaches to extend the reaches of a specific technique such as MD. As it was noted before, MD plays a critical role in the modelling of materials problems because MD simulations can follow the actual dynamical evolution of the system along its deterministic pathway. However, MD is strictly limited to very short time scales due to its full atomistic representation of the molecules. Therefore, some researchers studied different methods to address the time scale problem including hyperdynamics [526–528], parallel replica dynamics [529], and temperature-accelerated dynamics [530]. These methods are based on the transition state theory in which the system trajectory is simulated to find an appropriate pathway to escape from an energy well [528,531]. The simulation walks through this pathway with a process that takes place much faster than the direct MD.

The hyperdynamics is an accelerating approach for MD simulations which needs no prior information about the possible state trajectories of the system in the phase space. The method raises the energy of the system in regions other than at the dividing surfaces of the initial and final configurations in the phase space by applying a bias potential. Consequently, an accelerated transition is achieved from one equilibrium state to another equilibrium state [528]. The parallel replica dynamics method was incorporated for a system with infrequent events in which successive transitions are uncorrelated [529]. In such a system, running a number of independent MD simulations in parallel gives the exact dynamical evolution between the states. For a system with correlated crossing events, the state-to-state transition sequence is still correct. However, the error associated with the simulation time should be eliminated. Finally, in the temperature-accelerated dynamics method, the state-to-state transition is accelerated by increasing the temperature followed by filtering out the transitions that should not have occurred at the original temperature [530]. Consistent with other accelerated dynamics methods, the trajectory of the system is allowed to wander on its own to find an appropriate escape path. Consequently, no prior information is required about the nature of the involved phenomena [528].

The accelerated dynamics methods are formulated in order to find transition pathways between two known equilibrium states via effective MD simulations. Other approaches to extend atomistic simulations are also available which often require no preconceived mechanism or transition state. In order to find the transition pathway, one such method minimizes the average of the potential energy along the path instead of finding the path with the lowest barrier [532–534]. Another approach utilizes statistical sampling of the dynamical paths i.e., MC sampling of MD trajectories introducing transition path-sampling methods [535–539]. In addition to these methods, a finite-temperature string method is also available which represents the collection of the hyperplanes normal to the pathways of a system by a string [540–543]. In this method, the string is constantly updated during the simulations to capture the correct coordinate associated with the phenomenon. Finally, some works try to find dynamical paths that could connect an initial state to a final state in general terms [544–550]. Such methods often offer good numerical stability, efficient parallelizability, and high quality trajectories.

A class of methods attempts to address the systems with a free-energy surface which could possess several local minima in the free-energy surface. These strategies are generally known as the methods to escape the free-energy local minima [551]. For instance, a proper combination of CG dynamics with the adaptive bias potential methods could allow for the system to avoid local minima in the free-energy surface [551]. At the same time, the system provides a quantitative description of the free-energy surface through the integrated process. Such an approach has especially found application in biological systems [552–554].

In a category of systems an inherent dispersity in some characteristic details results in a natural disparity in time scales. A well-known example of such a case was already discussed in Section 2.1, i.e., the Born–Oppenheimer approximation [45], in which the electrons move independently from the nuclei due to their largely different masses. Another scenario which could lead to the separation of time scales is when a subset of forces is much stronger than the rest of the forces, while the masses of the constituents are almost equal. In order to deal more efficiently with such systems, various integration algorithms with multiple time steps have been developed [555]. This idea is particularly useful in polymers in which the bonds vibrate often much faster than they translate and rotate. Consequently, the configuration space as well as the forces can be divided into fast and slow components. As a result of this separation, a set of equations of motion are derived for the development of the fast and slow processes. This set of equations are solved using the multiple-time-step integration in which a small time step Δt to advance the fast processes by n steps while holding the slow variables fixed. The slow processes are then updated using a time step of $n\Delta t$. In the case that an analytic solution of high-frequency motions is available, this solution can be incorporated into an integration scheme for the entire system. Therefore, a time step can be defined based on the slow processes and used for the simulation of entire system with a much smaller number of cycles [555].

In order to extend the time scale of MD simulations, a method was developed based on optimization of the action functional [534]. The method parametrizes the system trajectory as a function of length rather than time. In order to achieve this goal, this approach optimizes an action term defined based on the stochastic time-dependent difference equation rather than solving the Newton equations in MD simulations. A similar idea was recently proposed in which the trajectories of the orientation process of weakly-interacting layered silicates were parametrized as a function of the shear strain instead of the time [196]. The idea of using the applied strain was motivated by the experimental reports supporting strain-dependent structure developments in such non-Brownian materials. Benefitting from the notion that the orientation kinetics is principally determined with respect to strain, the applied strain was selected to pass the orientation parameters to an upper scale through a simple combination of affine and nonaffine deformations, see Figures 18 and 19. This methodology could be also incorporated to develop multiscale models of orientation process provided that the interactions between the components are carefully defined in the unit cell.
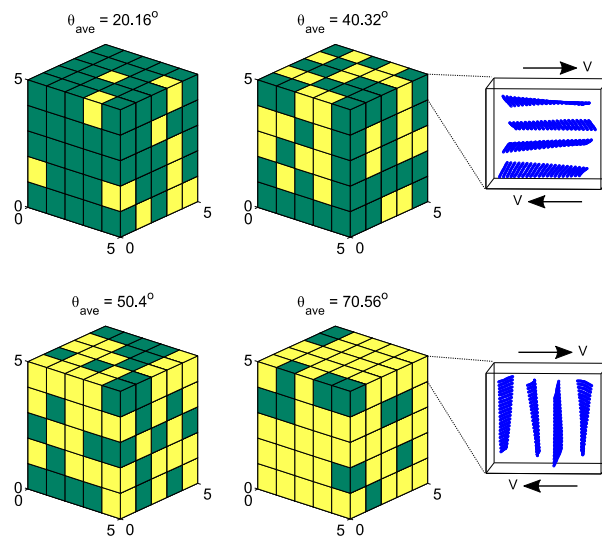
Figure 18. Examples of construction of a large cell for the upper scale simulation benefitting from a random mixing of unit cells resulting in various average initial orientation angles, θ$_{ave}$. The initial configurations of the unit cells before the flow starts are also given. Reprinted from Gooneie et al. [196]. Copyright 2016, with permission from John Wiley & Sons Inc.
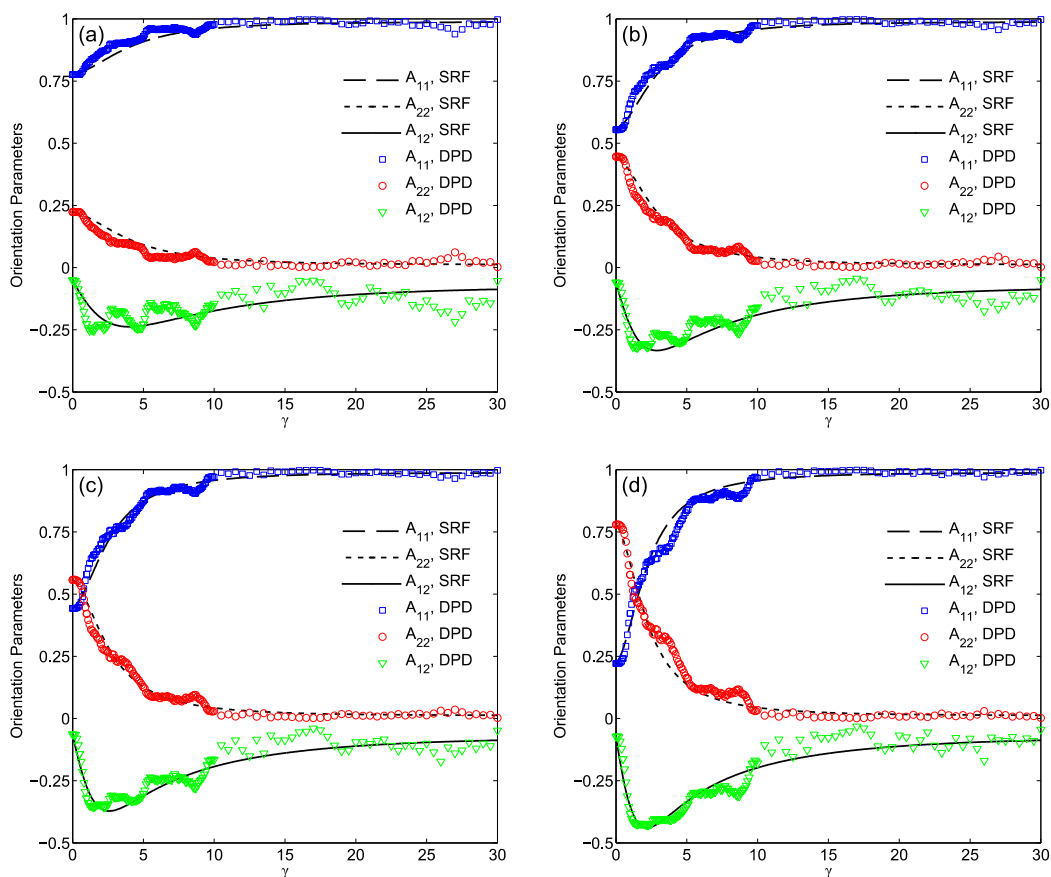

Figure 19. The orientation process defined by the orientation parameters as a function of the shear strain, γ. The results are derived from DPD models and strain reduction factor (SRF) model for various average initial orientation angles of (**a**) 20.16°; (**b**) 40.32°; (**c**) 50.40°; and (**d**) 70.56°. Reprinted from Gooneie et al. [196]. Copyright 2016, with permission from John Wiley & Sons Inc.

4. Conclusions and Outlooks

The development of polymeric materials necessitates a comprehensive understanding of the phenomena at different time and length scales. This need has significantly accelerated the progress in theoretical and computational methods to capture the inherent hierarchical phenomena in such materials. In this field, the development of efficient multiscale approaches could lead to the design of materials simultaneously on many scales instead of trial-and-error experimentations. The present review attempted to survey the state-of-the-art of various multiscale simulation approaches as applied to polymer science.

Within the context of an overall multiscale simulation perspective, various approaches for modelling relevant processes in polymer science are classified into three major categories, namely sequential, concurrent, and adaptive resolution approaches. This classification provides the opportunity to easily examine these methods and the systems to which they have been often applied. It is fairly clear from this review that different multiscale approaches provide precious insights into the structure and dynamics of polymeric materials.

In general, the sequential techniques are more popular in polymer science. However, *a priori* knowledge of relevant physical quantities is a prerequisite in these methods. The bridging of various scales in a sequential method is often implicit. A successful sequential modelling depends critically on the accuracy of the finer scale model as well as the reliability of the message-passing algorithms. The link between QM data and atomistic models should be further developed to reproduce the correct structure and thermodynamics. Phenomena which might involve the breaking of bonds require a reactive force field of MD in combination with QM which further complicates the computations as well as the derivation of such a force field from the parametrization of QM data in the first place. Moreover, the construction of CG potentials from atomistic data might necessitate more rigorous strategies particularly in systems with variant local structures and properties. Systematic coarse-graining and backmapping schemes were revisited as major routes towards a sequential model generation in polymers. An inevitable question that arises with the coarse-graining procedure is the question of transferability of the final CG model. As an advantageous aspect, however, the investigation of transferability conditions could help to gain insight into fundamental principles that control the behavior of the system. It is expected that a general prescription for coarse-graining should be developed which ensures a wide range of transferability. In the context of systematic coarse-graining methods, it is interesting to extend super CG models to describe phenomena, such as flow birefringence and systems such as multicomponent mixtures.

The concurrent multiscale methods are a lot more complicated and computationally expensive than sequential approaches particularly when it comes to simulating flow problems. Nevertheless, they do not depend on *a priori* knowledge of relevant physical quantities supplied from smaller-scale simulations. In concurrent methods, it is significant that the problem is carefully posed to make the method practical. The common problem in a concurrent approach is usually associated with the partitioning of domains in the system. More importantly, an appropriate handshaking strategy in a concurrent approach between different domains, which is both mathematically accurate and physically consistent, is challenging and critical. There is no general consensus on what a proper coupling of domains is. Therefore, a general criterion that measures the quality of handshaking between domains would be extremely beneficial. Additionally, there is plenty of room for innovative research on the issue of domain coupling. Although many concurrent approaches exist which are very desirable and appealing in metals and carbon nanomaterials, their use in polymeric systems is still limited to a large extend. In this paper, we have devoted an entire section to cover the fundamentals of several concurrent methods and introduce the existing possibilities to polymer scientists. In order to better illustrate the outlooks, several examples from relevant areas of polymer research are provided so that the reader is persuaded to follow these highlights.

A third group of multiscale simulation strategies was also noted as the adaptive resolution schemes in which a molecule can freely move in space and change its resolution depending on

spatial criteria. There is plenty of room in this class of methods for future innovation, either in its methodological aspects or its extension to different materials and phenomena. The method is fundamentally developed for quiescent conditions and the application of flow is yet to be added to these schemes. Even for the simulation of equilibrium conditions, these schemes show noticeable discontinuities in pressure and density profiles at the transition region between the high and low resolutions. Furthermore, the combination of mixed resolution concurrent methods and adaptive resolution schemes can potentially become an increasingly robust multiscale simulation methodology for complex polymer systems. Future work in this area appears to be promising.

When dealing with computer simulations, the role of the computer itself should be also noted including both hardware and software characteristics. Computer technology develops at an astonishing rate. It is believed that the progress in graphics processing units (GPUs) along with the development of GPU-oriented molecular simulation algorithms should extend our reach to yet unexplored spatial and temporal scales in the simulations of polymer systems. Such computational resources along with advanced simulations schemes can closely mimic the problem at hand on engineering time scales in a computer experiment. As a possible area for future endeavors, it would be ideal to compile a combination of atomistic methods with mesoscale and even continuum methods within one simulation package instead of many scattered codes which are available today, each coming with its certain advantages and shortcomings. Such a package could ultimately use the strengths from various individual codes to mitigate for the shortcomings of others. Even more important is the development and implementation of seamless multiscale modelling techniques in this hypothetical package. In addition, it is expected that the qualitative description of fundamental processes will be replaced with the quantitative prediction of material properties with the introduction of exascale computing. First-principle simulations are expected to play an increasing role in these areas. However, the availability of increased computing power will not be sufficient on its own and advanced strategies and techniques are an indispensable part of extreme-scale computing architectures.

Although multiscale methods have brought about substantial developments in the field, the challenge of bridging the time scale of atomic motions to the typical experimental and engineering scales is still far from completion. For instance, in a number of polymer systems such as PNCs, suitable theoretical frameworks are still missing which can provide insights into the nonequilibrium phenomena and the impact of external fields on the morphology and dynamics of the system. Moreover, more rigorous and direct quantitative analysis of nonequilibrium atomistic polymeric models and their CG counterparts is still needed. Various topics still remain to be disclosed in future research including new emerging possibilities to pass the information from the atomic to macroscopic scale and back. Multiscale modelling techniques are yet to be applied to characterize many interesting systems such as polymer flow in dilute and concentrated solutions, characteristics of a polymer layer next to the surface of nanoparticles in PNCs, the molecular roots of the viscoelasticity in filled elastomers, dynamics of confined polymers, etc. These examples are just a few among many topics for the future research on polymer systems. With the progress in theoretical as well as experimental techniques, finding answers to such challenges shall result in a comprehensive knowledge of various material properties of polymeric systems across a range of length and time scales. Moreover, it will bring forth directions to design new systems with desired or yet unexplored properties in the future.

In the framework of multiscale methods, one should not forget that there is also a critical necessity to design new and improved simulation methods at individual time and length scales. From the discussions provided in this review, it is clear that multiscale modelling is a heavily active field in modern science with a multidisciplinary character. The actual power of multiscale strategies is only truly appreciated by overcoming traditional barriers between various scientific disciplines. The computational multiscale approaches should eventually fulfill their philosophy which is to enhance our knowledge of, and ability to control complex processes, even in life sciences. Developing proper multiscale methods is extremely difficult but undeniably represents the future of polymer science as well as computer simulation and modelling.

Appendix A. Acronyms and Nomenclature

Acronyms

Acronym	Full phrase
AA	All-Atomistic
AC	Amorphous Cell method
AdResS	Adaptive Resolution Scheme
AIMD	Ab Initio Molecular Dynamics
AtC	Atomistic/Continuum method
BD	Brownian Dynamics
BDM	Bridging Domain Method
BGK-LB	Bhatnagar, Gross, And Krook LB method
BSM	Bridging Scale Method
CACM	Composite Grid Atomistic/Continuum Method
CADD	Coupled Atomistic and Discrete Dislocation method
CFD	Computational Fluid Dynamics
CG	Coarse-Grained
CGMD	Coarse-Grained Molecular Dynamics
CLS	Coupling of Length Scales method
CRW	Conditional Reversible Work
D2Q9	2-dimensional lattice with 9 allowed velocities used in LB simulations
D3Q19	3-dimensional lattice with 19 allowed velocities used in LB simulations
DDFT	Dynamic Density Functional Theory
DFT	Density Functional Theory
DPD	Dissipative Particle Dynamics
EFCG	Effective Force CG
EM	Energy Minimization
FDM	Finite Difference Method
FE	Finite Element
FEAt	Finite-Element/Atomistic method
FEM	Finite Element Method
FVM	Finite Volume Method
GDM	Generalized Differences Methods
GFEM	Galerkin Finite Element Method
GPU	Graphics Processing Unit
H-AdResS	Hamiltonian Adaptive Resolution Scheme
HSM	Hybrid Simulation Method
IBI	Iterative Boltzmann Inversion
IMC	Inverse Monte Carlo
LB	Lattice Boltzmann
LGCA	Lattice Gas Cellular Automata
LSM	Lattice Spring Model
MC	Monte Carlo
MD	Molecular Dynamics
Na-MMT	Sodium Montmorillonite

NEMS	Nano-Electro-Mechanical Systems
OpenFOAM	Open Source Field Operation And Manipulation
PA	Polyamide
PAC	Pseudo Amorphous Cell method
Pe	Peclet number
PE	Polyethylene
PNC	Polymer Nanocomposite
PP	Polypropylene
pPMF	Pair Potential of Mean Force
PRISM	Polymer Reference Interaction Site
PS	Polystyrene
PTT	Poly(Trimethylene Terephthalate)
QC	Quasicontinuum method
QM	Quantum Mechanics
QUICK	Quadratic Upstream Interpolation for Convective Kinematics
Re	Reynolds number
RVE	Representative Volume Element
SCFT	Self-Consistent Field Theory
SDPD	Smoothed Dissipative Particle Dynamics
SEM	Spectral Element Method
SPH	Smoothed Particle Hydrodynamics
SRF	Strain Reduction Factor model
SUPG	Streamline-Upwind/Petrov-Galerkin
TB	Tight Binding
TDGL	Time-Dependent Ginzburg-Landau
VMS	Variational Multiscale methods
We	Weissenberg number
XRD	X-Ray Diffraction

Nomenclature

Symbol	Meaning
A	$A = 6\xi k_B T$ in BD method
$\mathbb{A}_{ij}$	maximum repulsion between bead i and bead j in DPD method
a_i	acceleration of ith particle
B^A	atomistic domain in concurrent simulations
B^C	continuum domain in concurrent simulations
B^H	handshake region in concurrent simulations
B^I	interfacial region in concurrent simulations
B^P	padding region in concurrent simulations
b_i	fitting parameter
c_i	fitting parameter
D^ϑ	the diffusion term of ϑ
D_{cm}	center-of-mass self-diffusion coefficient
e	element
$\mathbb{e}$	absolute unit charge of an electron
E_f	Young's modulus
E_i	energy of atom, particle, or node i
$\overline{E_i}$	energy of the ith representative atom in QC method
E_k	eigenstate of energy
$E_{k_{el}}$	eigenstate energy of an electron

E_{k_n}	eigenstate energy of a nucleon
E^{tot}	total energy
$\Delta F(\psi_\alpha)$	free energy difference in H-AdResS method
F_{ij}^C	conservative force between bead i and its neighboring bead j within the force cutoff radius r_{cut}
F_{ij}^D	dissipative force between bead i and its neighboring bead j within the force cutoff radius r_{cut}
F_{ij}^R	random forces between bead i and its neighboring bead j within the force cutoff radius r_{cut}
F_α^{drift}	drift force of molecule α
$\bar{f}$	vector of applied forces in the FE region of a concurrent simulation
f_i	force acting on the ith atom, particle, or node
$f_{\alpha\beta}$	force acting between molecules α and β
f^{th}	thermodynamic force
f_i^B	Brownian random force acting on the ith particle
$f_{\alpha\beta}^{AA}$	atomistic forces acting on molecule α due to the interaction with molecule β
$f_{\alpha\beta}^{CG}$	CG forces acting on molecule α due to the interaction with molecule β
G'	storage modulus
G''	loss modulus
$H(\Gamma_i)$	Hamiltonian of the system at system state Γ_i
$\hat{H}$	modified Hamiltonian of the H-AdResS method
$\Delta H(\Gamma_{i \to j})$	change in the system Hamiltonian for going from system state Γ_i to Γ_j
$\Delta H(\psi_\alpha)$	compensation term in the Hamiltonian of the H-AdResS method
$H_{FE}(u_\alpha, \dot{u}_\alpha)$	Hamiltonian of the FE region as a function of the nodal displacements u_α, and time rate of nodal displacements $\dot{u}_\alpha$
$H_{FE/MD}(r_j, v_j, u_\alpha, \dot{u}_\alpha)$	Hamiltonian of the FE/MD handshake region as a function of the atomic positions r_j, atomic velocities v_j, nodal displacements u_α, and time rate of nodal displacements $\dot{u}_\alpha$
$H_{MD}(r_j, v_j)$	Hamiltonian of the MD region as a function of the atomic positions r_j, and atomic velocities v_j
$H_{MD/TB}(r_j, v_j)$	Hamiltonian of the MD/TB handshake region as a function of the atomic positions r_j, and atomic velocities v_j
$H_{TB}(r_j, v_j)$	Hamiltonian of the TB region as a function of the atomic positions r_j, and atomic velocities v_j
H_{tot}	total Hamiltonian
h	Planck's constant
$J^{\vartheta,C}$	convection flux term in FVM formulation
$J^{\vartheta,D}$	diffusion flux term in FVM formulation
K	the all-atom kinetic energy of the molecules
k_B	Boltzmann's constant
k_T	isothermal compressibility
l	bond length
M, M_w	molecular weight
m	mass of an atom or particle
m_{el}	mass of an electron
m_n	mass of a nucleon
N	number of atoms, particles, or nodes
N_c	number of monomers per chain
N_e	number of elements

N_q	number of quadrature points in the numerical integration
N_r	number of representative atoms in QC method
P	the projection matrix
$\Delta p(\psi_\alpha)$	pressure difference along the interface in H-AdResS method
$P_{i \rightarrow j}$	probability of accepting a new configuration for going from system state Γ_i to Γ_j
p^R	probability distribution function
p^R_{target}	the target probability distribution function of AA simulations
Q^ϑ	the generation/destruction of ϑ within the control volume per unit volume
$R(u)$	residual form of a partial differential equation in terms of the unknown function u in FEM scheme
R_g	radius of gyration
R_i	center of mass coordinates of the ith molecule
$\mathbf{r}$	coordinates vector of an atom, or particle, or node
r	distance
r_{cut}	force cutoff radius
r_{el_i}	spatial coordinates of an electron
$\hat{r}_{ij}$	unit vector pointing from the center of bead j to that of bead i
r_{n_j}	spatial coordinates of a nucleon
r_e^{cent}	coordinates of the Gauss point in element e taken at the centroid of the triangular elements
r_e^q	position of quadrature point q of element e in the reference configuration
$\delta r_i^B(t + \Delta t)$	random displacement of the ith particle due to the random forces during time step Δt
S	surface vector
S_i	ith subregion
$\{S_\rho\}$	set of weighting functions in FEM
$s_{entropy}$	rescaling factor for the entropy change
$s_{friction}$	rescaling factor for the friction change
T	temperature
t	time
Δt	time step
$U(r)$	potential energy
U^A	potential energies of the atomistic region
U^{atom}	energy functional of a systems assuming it is entirely modelled using atoms
U^C	potential energies of the continuum region
$U^{CG}(r, l, \theta, \upsilon)$	general form of the CG potential function in IBI method
U^{FE}	energy functional of a systems assuming it is entirely modelled using FEM
U^H	potential energies of the handshake region
U^{int}	energy of internal interactions
U^{tot}	total potential energy of the entire system
$U^{CG}_{angle}(\theta)$	bond angle potential in the blob model
$U^{CG}_{bond}(l)$	bond potential in the blob model
$U^{CG}_{nonbonded}(r)$	potential of nonbonded interactions in the blob model
U^{AA}_α	potential energy of molecule α in the AA representation
U^{CG}_α	potential energy of molecule α in the CG representation
u	vector of nodal displacements in the FE region of a concurrent simulation

$u(r)$	the unknown function in FEM which one needs to find
$u_h(r)$	approximation of the function $u(r)$ under consideration in FEM
u_α	displacements of atom, particle, or node α
$\dot{u}_\alpha$	rate of displacements of atom, particle, or node α
u^n	values of the function u_h at node n of the mesh
V_e	volume of element e
dV	volume element of the simulation domain in FEM
∂V_e	surfaces surrounding the volume v_e of element e
v	macroscopic velocity magnitude
$\mathbb{v}$	$\mathbb{v} = \sqrt{3}\,\mathbb{v}_s$ in LB method
$v(r, t)$	macroscopic local velocity at node r at time t in LB
$\tilde{v}(t + \Delta t)$	estimated velocity in the next time step using a predictor method in DPD velocity-Verlet algorithm
$\delta v_i^B(t + \Delta t)$	Random velocity change of the ith particle due to the random forces during time step Δt
v_i	velocity of ith atom, particle, or node
$\lvert \mathbb{v}_i \rvert$	velocity magnitude in i-direction in LB method
$\{\mathbb{v}_k\}$	set of prescribed velocity vectors connecting the neighboring nodes in LB method
$\mathbb{v}_s$	speed of sound
W	a function of deformation gradient Δ
w_i	weighting constants used in LB method
$z_n\mathbb{e}$	positive unit charge of a nucleon
Γ_i	system state in a phase space at position i
γ	exact solution in the projection method
$\dot{\gamma}$	shear-rate
$\overline{\gamma}(r_\alpha)$	coarse scale solution of a problem in the projection method
γ'	fine scale solution of a problem in the projection method
Δ	deformation gradient
δ	delta function
$\Delta\mu(\psi_\alpha)$	chemical potential gradient in H-AdResS method
ε	neighboring cells of a specific element in FVM
ζ	random number between 0 and 1 which is to determine the acceptance or rejection of a new configuration
ζ_{ij}	a Gaussian random number with zero mean and unit variance used in the definition of the random forces between beads i and j in DPD method
η	viscosity
Θ	a weighting function to link FE and atomistic models in concurrent simulations
θ	bond angle
θ_{ave}	averaged initial orientation angle
Λ_{ik}	collision matrix used in LB method
λ	multiplication parameter in in DPD velocity-Verlet algorithm
μ	fitting parameter
ν	fitting parameter
ϑ	a general conserved scalar variable in FVM scheme
ξ	friction coefficient between atoms or particles
ξ_{ij}	friction coefficient between bead i and bead j in DPD method
ξ_m	friction coefficient between particles of freely-rotating chains
$\mathbb{w}$	wave function of electrons

ρ	fluid density in CFD
$\rho(r, t)$	macroscopic local density at node r at time t in LB method
$\rho_i(r)$	molecular density profile in the *i*th iteration step as a function of the position in the direction perpendicular to the interface, in AdResS method
ρ^*	reference molecular density
ρ_i	*i*th weighting function in FEM
σ_{ij}	noise amplitude between bead *i* and bead *j* in DPD method
σ_i^α	shape function of node *i* evaluated at the point with coordinates r_α
τ	characteristic collision time in LB method
$\Phi(u)$	integral form of the weighted residuals in FEM
$\phi(r)_k$	wave function in Schrödinger's equation
φ	wave function of the nuclei
χ_{ij}	a parameter in DPD formulation which equals 1 for beads with a distance less than r_{cut} and equals 0 otherwise
$\Psi_i(r, t)$	particle distribution function used in LB at node r at time t moving with velocity v_i In the *i*-direction
$\Psi_i^{eq}(r, t)$	equilibrium particle distribution function used in LB at node r at time t moving with velocity v_i In the *i*-direction
ψ	spatial interpolation function in AdResS method
$\psi_n(r)$	interpolation functions in FEM for node *n*
$\psi_n^e(r)$	interpolation functions in FEM for node *n* in element *e*
Ω	simulation domain in FEM
$\partial\Omega$	boundaries of the simulation domain in FEM
$\mho$	dihedral angle
ω	Frequency
ω_i	quadrature weight signifying how many atoms a given representative atom stands for in the description of the total energy, in QC method
$\omega^D(r_{ij})$	dissipative weight function in DPD method
ω^q	associated Gauss quadrature weights of quadrature point *q* of element *e*
$\omega^R(r_{ij})$	random weight function in DPD method

References

1. Elliott, J.A. Novel approaches to multiscale modelling in materials science. *Int. Mater. Rev.* **2011**, *56*, 207–225. [CrossRef]
2. Zeng, Q.H.; Yu, A.B.; Lu, G.Q. Multiscale modeling and simulation of polymer nanocomposites. *Prog. Polym. Sci.* **2008**, *33*, 191–269. [CrossRef]
3. Ayton, G.S.; Noid, W.G.; Voth, G.A. Multiscale modeling of biomolecular systems: In serial and in parallel. *Curr. Opin. Struct. Biol.* **2007**, *17*, 192–198. [CrossRef] [PubMed]
4. Ayyaswamy, P.S.; Muzykantov, V.; Eckmann, D.M.; Radhakrishnan, R. Nanocarrier hydrodynamics and binding in targeted drug delivery: Challenges in numerical modeling and experimental validation. *J. Nanotechnol. Eng. Med.* **2013**, *4*. [CrossRef] [PubMed]
5. Raabe, D. Challenges in computational materials science. *Adv. Mater.* **2002**, *14*, 639–650. [CrossRef]
6. Kremer, K.; Müller-Plathe, F. Multiscale problems in polymer science: Simulation approaches. *MRS Bull.* **2001**, *26*, 205–210. [CrossRef]
7. Murtola, T.; Bunker, A.; Vattulainen, I.; Deserno, M.; Karttunen, M. Multiscale modeling of emergent materials: Biological and soft matter. *Phys. Chem. Chem. Phys.* **2009**, *11*, 1869–1892. [CrossRef] [PubMed]
8. Peter, C.; Kremer, K. Multiscale simulation of soft matter systems—From the atomistic to the coarse-grained level and back. *Soft Matter* **2009**, *5*, 4357–4366. [CrossRef]
9. Sherwood, P.; Brooks, B.R.; Sansom, M.S. Multiscale methods for macromolecular simulations. *Curr. Opin. Struct. Biol.* **2008**, *18*, 630–640. [CrossRef] [PubMed]

10. Steinhauser, M.O.; Hiermaier, S. A review of computational methods in materials science: Examples from shock-wave and polymer physics. *Int. J. Mol. Sci.* **2009**, *10*, 5135–5216. [CrossRef] [PubMed]

11. Fermeglia, M.; Posocco, P.; Pricl, S. Nano tools for macro problems: Multiscale molecular modeling of nanostructured polymer systems. *Compos. Interfaces* **2013**, *20*, 379–394. [CrossRef]

12. Fermeglia, M.; Pricl, S. Multiscale molecular modeling in nanostructured material design and process system engineering. *Comput. Chem. Eng.* **2009**, *33*, 1701–1710. [CrossRef]

13. Johnston, K.; Harmandaris, V. Hierarchical simulations of hybrid polymer-solid materials. *Soft Matter* **2013**, *9*, 6696. [CrossRef]

14. Chiu, C.-W.; Huang, T.-K.; Wang, Y.-C.; Alamani, B.G.; Lin, J.-J. Intercalation strategies in clay/polymer hybrids. *Prog. Polym. Sci.* **2014**, *39*, 443–485. [CrossRef]

15. Gao, D.; Li, R.; Lv, B.; Ma, J.; Tian, F.; Zhang, J. Flammability, thermal and physical-mechanical properties of cationic polymer/montmorillonite composite on cotton fabric. *Compos. Part B* **2015**, *77*, 329–337. [CrossRef]

16. Lowe, D.J.; Chapman, A.V.; Cook, S.; Busfield, J.J.C. Micromechanical models of young's modulus of NR/organoclay nanocomposites. *J. Polym. Sci. Part B* **2011**, *49*, 1621–1627. [CrossRef]

17. Mattausch, H.; Laske, S.; Duretek, I.; Kreith, J.; Maier, G.; Holzer, C. Investigation of the influence of processing conditions on the thermal, rheological and mechanical behavior of polypropylene nanocomposites. *Polym. Eng. Sci.* **2013**, *53*, 1001–1010. [CrossRef]

18. Decker, J.J.; Meyers, K.P.; Paul, D.R.; Schiraldi, D.A.; Hiltner, A.; Nazarenko, S. Polyethylene-based nanocomposites containing organoclay: A new approach to enhance gas barrier via multilayer coextrusion and interdiffusion. *Polymer* **2015**, *61*, 42–54. [CrossRef]

19. Nguyen, Q.T.; Ngo, T.D.; Tran, P.; Mendis, P.; Bhattacharyya, D. Influences of clay and manufacturing on fire resistance of organoclay/thermoset nanocomposites. *Compos. Part A* **2015**, *74*, 26–37. [CrossRef]

20. Gooneie, A.; Nazockdast, H.; Shahsavan, F. Effect of selective localization of carbon nanotubes in PA6 dispersed phase of PP/PA6 blends on the morphology evolution with time, part 1: Droplet deformation under simple shear flows. *Polym. Eng. Sci.* **2015**, *55*, 1504–1519. [CrossRef]

21. Kotal, M.; Bhowmick, A.K. Polymer nanocomposites from modified clays: Recent advances and challenges. *Prog. Polym. Sci.* **2015**, *51*, 127–187. [CrossRef]

22. Sepahvand, R.; Adeli, M.; Astinchap, B.; Kabiri, R. New nanocomposites containing metal nanoparticles, carbon nanotube and polymer. *J. Nanopart. Res.* **2008**, *10*, 1309–1318. [CrossRef]

23. Pavlidou, S.; Papaspyrides, C.D. A review on polymer-layered silicate nanocomposites. *Prog. Polym. Sci.* **2008**, *33*, 1119–1198. [CrossRef]

24. Moniruzzaman, M.; Winey, K.I. Polymer nanocomposites containing carbon nanotubes. *Macromolecules* **2006**, *39*, 5194–5205. [CrossRef]

25. Gooneie, A.; Nazockdast, H.; Shahsavan, F. Effect of selective localization of carbon nanotubes in PA6 dispersed phase of PP/PA6 blends on the morphology evolution with time, part 2: Relaxation of deformed droplets after cessation of flow. *Polym. Eng. Sci.* **2016**, *56*, 51–60. [CrossRef]

26. Sinha Ray, S.; Okamoto, M. Polymer/layered silicate nanocomposites: A review from preparation to processing. *Prog. Polym. Sci.* **2003**, *28*, 1539–1641. [CrossRef]

27. Lecouvet, B.; Gutierrez, J.G.; Sclavons, M.; Bailly, C. Structure-property relationships in polyamide 12/halloysite nanotube nanocomposites. *Polym. Degrad. Stab.* **2011**, *96*, 226–235. [CrossRef]

28. Akkermans, R.; Warren, P.B. Multiscale modelling of human hair. *Philos. Trans. R. Soc. A Math. Phys. Eng. Sci.* **2004**, *362*, 1783–1793.

29. De Borst, R. Challenges in computational materials science: Multiple scales, multi-physics and evolving discontinuities. *Comput. Mater. Sci.* **2008**, *43*, 1–15. [CrossRef]

30. Gates, T.S.; Odegard, G.M.; Frankland, S.J.V.; Clancy, T.C. Computational materials: Multi-scale modeling and simulation of nanostructured materials. *Compos. Sci. Technol.* **2005**, *65*, 2416–2434. [CrossRef]

31. Karakasidis, T.E.; Charitidis, C.A. Multiscale modeling in nanomaterials science. *Mater. Sci. Eng. C* **2007**, *27*, 1082–1089. [CrossRef]

32. Khalatur, P.G. Molecular Dynamics Simulations in Polymer Science: Methods and Main Results. In *Polymer Science: A Comprehensive Reference, 10 Volume Set*; Elsevier: Spain, 2012; Volume 1, pp. 417–460.

33. Fredrickson, G.H. *The Equilibrium Theory of Inhomogeneous Polymers*, 2nd ed.; Clarendon Press: Oxford, UK, 2006.

34. González, M.A. Force fields and molecular dynamics simulations. *Écol. Thémat. Soc. Fr. Neutron.* **2011**, *12*, 169–200. [CrossRef]

35. Raabe, D. *Computational Materials Science*; Wiley-VCH Verlag: Darmstadt, Germany, 1998.

36. Müller-Plathe, F. Coarse-graining in polymer simulation: From the atomistic to the mesoscopic scale and back. *ChemPhysChem* **2002**, *3*, 754–769. [CrossRef]

37. Flory, P.J. *Principles of Polymer Chemistry*, 1st ed.; Cornell University Press: Ithaca, NY, USA, 1953.

38. Ganesan, V.; Jayaraman, A. Theory and simulation studies of effective interactions, phase behavior and morphology in polymer nanocomposites. *Soft Matter* **2014**, *10*, 13–38. [CrossRef] [PubMed]

39. Alkorta, I.; Elguero, J. Review on DFT and ab initio calculations of scalar coupling constants. *Int. J. Mol. Sci.* **2003**, *4*, 64–92. [CrossRef]

40. Kohn, W.; Sham, L.J. Self-consistent equations including exchange and correlation effects. *Phys. Rev.* **1965**, *140*, A1133–A1138. [CrossRef]

41. Steinbach, I. Phase-field models in materials science. *Model. Simul. Mater. Sci. Eng.* **2009**, *17*, 73001. [CrossRef]

42. Wang, X.; Ouyang, J.; Zhou, W.; Liu, Z. A phase field technique for modeling and predicting flow induced crystallization morphology of semi-crystalline polymers. *Polymers* **2016**, *8*, 230. [CrossRef]

43. Kim, J. Phase-field models for multi-component fluid flows. *Commun. Commut. Phys.* **2012**, *12*, 613–661. [CrossRef]

44. Schrödinger, E. Quantisierung als Eigenwertproblem. *Ann. Phys.* **1926**, *384*, 361–376. [CrossRef]

45. Born, M.; Oppenheimer, R. Zur quantentheorie der molekeln. *Ann. Phys.* **1927**, *389*, 457–484. [CrossRef]

46. Ponosov, Y.S.; Bolotin, G.A.; Thomsen, C.; Cardona, M. Raman scattering in Os: Nonadiabatic renormalization of the optical phonon self-energies. *Phys. Status Solidi B* **1998**, *208*, 257–269. [CrossRef]

47. White, J.D.; Chen, J.; Matsiev, D.; Auerbach, D.J.; Wodtke, A.M. Conversion of large-amplitude vibration to electron excitation at a metal surface. *Nature* **2005**, *433*, 503–505. [CrossRef] [PubMed]

48. Pisana, S.; Lazzeri, M.; Casiraghi, C.; Novoselov, K.S.; Geim, A.K.; Ferrari, A.C.; Mauri, F. Breakdown of the adiabatic Born-Oppenheimer approximation in graphene. *Nat. Mater.* **2007**, *6*, 198–201. [CrossRef] [PubMed]

49. Walker, B.G.; Molteni, C.; Marzari, N. Ab initio molecular dynamics of metal surfaces. *J. Phys.* **2004**, *16*, S2575–S2596. [CrossRef]

50. Rissanou, A.N.; Power, A.J.; Harmandaris, V. Structural and dynamical properties of polyethylene/graphene nanocomposites through molecular dynamics simulations. *Polymers* **2015**, *7*, 390–417. [CrossRef]

51. Car, R.; Parrinello, M. Unified approach for molecular dynamics and density-functional theory. *Phys. Rev. Lett.* **1985**, *55*, 2471–2474. [CrossRef] [PubMed]

52. Hageman, J.; Meier, R.J.; Heinemann, M.; de Groot, R.A. Young modulus of crystalline polyethylene from ab initio molecular dynamics. *Macromolecules* **1997**, *30*, 5953–5957. [CrossRef]

53. Serra, S.; Iarlori, S.; Tosatti, E.; Scandolo, S.; Santoro, G. Dynamical and thermal properties of polyethylene by ab initio simulation. *Chem. Phys. Lett.* **2000**, *331*, 339–345. [CrossRef]

54. Saitta, A.M.; Klein, M.L. First-principles molecular dynamics study of the rupture processes of a bulklike polyethylene knot. *J. Phys. Chem. B* **2001**, *105*, 6495–6499. [CrossRef]

55. Cavazzoni, C.; Colle, R.; Farchioni, R.; Grosso, G. Car-Parrinello molecular dynamics study of electronic and structural properties of neutral polyanilines. *Phys. Rev. B* **2002**, *66*, 165110. [CrossRef]

56. Wallace, D.S.; Stoneham, A.M.; Hayes, W.; Fisher, A.J.; Harker, A.H. Theory of defects in conducting polymers. I. Theoretical principles and simple applications. *J. Phys.* **1991**, *3*, 3879–3903. [CrossRef]

57. Wallace, D.S.; Stoneham, A.M.; Hayes, W.; Fisher, A.J.; Testa, A. Theory of defects in conducting polymers. II. Application to polyacetylene. *J. Phys.* **1991**, *3*, 3905–3920. [CrossRef]

58. Röthlisberger, U.; Sprik, M.; Klein, M.L. Living polymers: Ab initio molecular dynamics study of the initiation step in the polymerization of isoprene induced by ethyl lithium. *J. Chem. Soc. Faraday Trans.* **1998**, *94*, 501–508. [CrossRef]

59. Bernasconi, M.; Chiarotti, G.L.; Focher, P.; Parrinello, M.; Tosatti, E. Solid-state polymerization of acetylene under pressure: Ab Initio simulation. *Phys. Rev. Lett.* **1997**, *78*, 2008–2011. [CrossRef]

60. Quarti, C.; Milani, A.; Castiglioni, C. Ab initio calculation of the IR spectrum of PTFE: Helical symmetry and defects. *J. Phys. Chem. B* **2013**, *117*, 706–718. [CrossRef] [PubMed]

61. D'Amore, M.; Talarico, G.; Barone, V. Periodic and high-temperature disordered conformations of polytetrafluoroethylene chains: An ab initio modeling. *J. Am. Chem. Soc.* **2006**, *128*, 1099–1108.

62. Dai, L.; Yang, S.-W.; Chen, X.-T.; Wu, P.; Tan, V. Investigation of metal diffusion into polymers by ab initio molecular dynamics. *Appl. Phys. Lett.* **2005**, *87*. [CrossRef]

63. Piscitelli, F.; Posocco, P.; Toth, R.; Fermeglia, M.; Pricl, S.; Mensitieri, G.; Lavorgna, M. Sodium montmorillonite silylation: Unexpected effect of the aminosilane chain length. *J. Colloid Interface Sci.* **2010**, *351*, 108–115. [CrossRef] [PubMed]

64. Farquhar, I.E. *Ergodic Theory in Statistical Mechanics*; Interscience Publishers: New York, NY, USA, 1964.

65. Baumgärtner, A.; Burkitt, A.N.; Ceperley, D.M.; de Raedt, H.; Heermann, D.W.; Herrmann, H.J; Landau, D.P; Levesque, D.; von der Linden, W. *The Monte Carlo Method in Condensed Matter Physics*; Springer: Berlin, Germany, 2012.

66. Brin, M.; Stuck, G. *Introduction to Dynamical Systems*; Cambridge University Press: New York, NY, USA, 2002.

67. Metropolis, N.; Rosenbluth, A.W.; Rosenbluth, M.N.; Teller, A.H.; Teller, E. Equation of state calculations by fast computing machines. *J. Chem. Phys.* **1953**, *21*, 1087–1092. [CrossRef]

68. Potts, R.B. Some generalized order-disorder transformations. *Math. Proc. Camb. Philos. Soc.* **1952**, *48*, 106–109. [CrossRef]

69. Bortz, A.B.; Kalos, M.H.; Lebowitz, J.L. A new algorithm for Monte Carlo simulation of Ising spin systems. *J. Comput. Phys.* **1975**, *17*, 10–18. [CrossRef]

70. Gillespie, D.T. Exact stochastic simulation of coupled chemical reactions. *J. Phys. Chem.* **1977**, *81*, 2340–2361. [CrossRef]

71. Makki, H.; Adema, K.N.S.; Peters, E.A.J.F.; Laven, J.; Van Der Ven, L.G.J.; Van Benthem, R.A.T.M.; de With, G. A simulation approach to study photo-degradation processes of polymeric coatings. *Polym. Degrad. Stab.* **2014**, *105*, 68–79. [CrossRef]

72. Mermigkis, P.G.; Tsalikis, D.G.; Mavrantzas, V.G. Determination of the effective diffusivity of water in a poly (methyl methacrylate) membrane containing carbon nanotubes using kinetic Monte Carlo simulations. *J. Chem. Phys.* **2015**, *143*. [CrossRef] [PubMed]

73. Adema, K.N.S.; Makki, H.; Peters, E.A.J.F.; Laven, J.; Van Der Ven, L.G.J.; Van Benthem, R.A.T.M.; de With, G. Kinetic Monte Carlo simulation of the photodegradation process of polyester-urethane coatings. *Phys. Chem. Chem. Phys.* **2015**, *17*, 19962–19976. [CrossRef] [PubMed]

74. Kunz, L.; Kuhn, F.M.; Deutschmann, O. Kinetic Monte Carlo simulations of surface reactions on supported nanoparticles: A novel approach and computer code. *J. Chem. Phys.* **2015**, *143*. [CrossRef] [PubMed]

75. Zepeda-Ruiz, L.A.; Gilmer, G.H.; Walton, C.C.; Hamza, A.V.; Chason, E. Surface morphology evolution during sputter deposition of thin films—Lattice Monte Carlo simulations. *J. Cryst. Growth* **2010**, *312*, 1183–1187. [CrossRef]

76. Rysz, J. Monte Carlo simulations of phase separation in thin polymer blend films: Scaling properties of morphological measures. *Polymer* **2005**, *46*, 977–982. [CrossRef]

77. Galuschko, A.; Lang, M.; Kreer, T.; Sommer, J.-U. Monte carlo simulation of thin film polymer melts. *Soft Matter* **2014**, *12*, S49–S55. [CrossRef]

78. Ivanov, V.A.; Rodionova, A.S.; An, E.A.; Martemyanova, J.A.; Stukan, M.R.; Müller, M.; Paul, W.; Binder, K. Orientational ordering transitions of semiflexible polymers in thin films: A Monte Carlo simulation. *Phys. Rev. E* **2011**, *84*. [CrossRef] [PubMed]

79. Müller, M. Chain conformations and correlations in thin polymer films: A Monte Carlo study. *J. Chem. Phys.* **2002**, *116*, 9930–9938. [CrossRef]

80. Werner, A.; Schmid, F.; Müller, M.; Binder, K. Anomalous size-dependence of interfacial profiles between coexisting phases of polymer mixtures in thin-film geometry: A Monte Carlo simulation. *J. Chem. Phys.* **1997**, *107*, 8175–8188. [CrossRef]

81. Zykova-Timan, T.; Horbach, J.; Binder, K. Monte Carlo simulations of the solid-liquid transition in hard spheres and colloid-polymer mixtures. *J. Chem. Phys.* **2010**, *133*. [CrossRef] [PubMed]

82. Binder, K. Monte Carlo simulation of polymers at interfaces. *Phys. A Stat. Mech. Appl.* **1993**, *200*, 722–729. [CrossRef]

83. Bitsanis, I.A.; Brinke, G.T. A lattice Monte Carlo study of long chain conformations at solid-polymer melt interfaces. *J. Chem. Phys.* **1993**, *99*, 3100–3111. [CrossRef]

84. Jiang, J.; Liu, H.; Hu, Y. Lattice Monte Carlo simulation of polymer adsorption at an interface, 1: Monodisperse polymer. *Macromol. Theory Simul.* **1998**, *7*, 105–111. [CrossRef]

85. Jiang, J.; Liu, H.; Hu, Y. Lattice Monte Carlo simulation of polymer adsorption at an interface, 2: Polydisperse polymer. *Macromol. Theory Simul.* **1998**, *7*, 113–117.

86. John, A.; Nagel, J.; Heinrich, G. Monte Carlo simulation of polymer reactions at interfaces. *Macromol. Theory Simul.* **2007**, *16*, 430–440. [CrossRef]

87. Madden, W.G. Monte Carlo studies of the melt-vacuum interface of a lattice polymer. *J. Chem. Phys.* **1987**, *87*, 1405–1422. [CrossRef]

88. Müller, M. Reactions at polymer interfaces: A Monte Carlo simulation. *Macromolecules* **1997**, *30*, 6353–6357. [CrossRef]

89. Müller, M.; Binder, K.; Oed, W. Structural and thermodynamic properties of interfaces between coexisting phases in polymer blends: A Monte Carlo simulation. *J. Chem. Soc. Faraday Trans.* **1995**, *91*, 2369–2379. [CrossRef]

90. Müller, M.; MacDowell, L.G. Interface and surface properties of short polymers in solution: Monte Carlo simulations and self-consistent field theory. *Macromolecules* **2000**, *33*, 3902–3923. [CrossRef]

91. Müller, M.; Werner, A. Interfaces between highly incompatible polymers of different stiffness: Monte Carlo simulations and self-consistent field calculations. *J. Chem. Phys.* **1997**, *107*, 10764–10776. [CrossRef]

92. Reiter, J.; Zifferer, G.; Olaj, O.F. Monte Carlo studies of the interface between two polymer melts. *Macromolecules* **1990**, *23*, 224–228. [CrossRef]

93. Toral, R.; Chakrabarti, A. Monte Carlo study of polymer chains end-grafted onto a spherical interface. *Phys. Rev. E* **1993**, *47*, 4240–4246. [CrossRef]

94. Pandey, Y.N.; Doxastakis, M. Detailed atomistic Monte Carlo simulations of a polymer melt on a solid surface and around a nanoparticle. *J. Chem. Phys.* **2012**, *136*, 94901. [CrossRef] [PubMed]

95. Shu, R.; Zha, L.; Eman, A.A.; Hu, W. Fibril crystal growth in diblock copolymer solutions studied by dynamic monte carlo simulations. *J. Phys. Chem. B* **2015**, *119*, 5926–5932. [CrossRef] [PubMed]

96. Ren, Y.; Ma, A.; Li, J.; Jiang, X.; Ma, Y.; Toda, A.; Hu, W. Melting of polymer single crystals studied by dynamic Monte Carlo simulations. *Eur. Phys. J. E* **2010**, *33*, 189–202. [CrossRef] [PubMed]

97. Doye, J.; Frenkel, D. Kinetic Monte Carlo simulations of the growth of polymer crystals. *J. Chem. Phys.* **1999**, *110*, 2692–2702. [CrossRef]

98. Zhang, J.; Muthukumar, M. Monte Carlo simulations of single crystals from polymer solutions. *J. Chem. Phys.* **2007**, *126*. [CrossRef] [PubMed]

99. Aoki, K. Monte Carlo simulation of two-dimensional growth of conductive zones in interconversion of conducting polymer films involving random morphology. *J. Electroanal. Chem.* **1990**, *292*, 63–72. [CrossRef]

100. Balmer, J.A.; Mykhaylyk, O.O.; Schmid, A.; Armes, S.P.; Fairclough, J.P.A.; Ryan, A.J. Characterization of polymer-silica nanocomposite particles with core-shell morphologies using monte carlo simulations and small angle X-ray scattering. *Langmuir* **2011**, *27*, 8075–8089. [CrossRef] [PubMed]

101. Ruan, C.; Liu, C.; Zheng, G. Monte Carlo Simulation for the Morphology and Kinetics of Spherulites and Shish-Kebabs in Isothermal Polymer Crystallization. *Math. Probl. Eng.* **2015**, *2015*. [CrossRef]

102. Duda, Y.; Vázquez, F. Modeling of composite latex particle morphology by off-lattice Monte Carlo simulation. *Langmuir* **2005**, *21*, 1096–1102. [CrossRef] [PubMed]

103. He, X.; Liang, H.; Pan, C. Monte Carlo simulation of morphologies of self-assembled amphiphilic diblock copolymers in solution. *Phys. Rev. E* **2001**, *63*, 318041–318044. [CrossRef] [PubMed]

104. Nagpal, U.; Detcheverry, F.A.; Nealey, P.F.; De Pablo, J.J. Morphologies of linear triblock copolymers from Monte Carlo simulations. *Macromolecules* **2011**, *44*, 5490–5497. [CrossRef]

105. Raj Mohan, S.; Joshi, M.P.; Singh, M.P. Charge transport in disordered organic solids: A Monte Carlo simulation study on the effects of film morphology. *Org. Electron.* **2008**, *9*, 355–368. [CrossRef]

106. Narambuena, C.F.; Leiva, E.P.M.; Chávez-Páez, M.; Pérez, E. Effect of chain stiffness on the morphology of polyelectrolyte complexes. A Monte Carlo simulation study. *Polymer* **2010**, *51*, 3293–3302. [CrossRef]

107. Wang, X.; Chiang, M.; Snyder, C.R. Monte-Carlo simulation for the fracture process and energy release rate of unidirectional carbon fiber-reinforced polymers at different temperatures. *Compos. Part A* **2004**, *35*, 1277–1284. [CrossRef]

108. Li, J.; Ma, Y.; Hu, W. Dynamic Monte Carlo simulation of non-equilibrium Brownian diffusion of single-chain macromolecules. *Mol. Simul.* **2016**, *42*, 321–327. [CrossRef]

109. Neyertz, S.; Brown, D. A trajectory-extending kinetic Monte Carlo (TEKMC) method for estimating penetrant diffusion coefficients in molecular dynamics simulations of glassy polymers. *Macromolecules* **2010**, *43*, 9210–9214. [CrossRef]

110. Sikorski, A.; Adamczyk, P. Diffusion of polymer chains in porous media. A Monte Carlo study. *Polymer* **2010**, *51*, 581–586. [CrossRef]

111. Tüzel, E.; Kisacikoğlu, K.B.; Pekcan, Ö. Monitoring diffusion of reptating polymer chains by a direct energy transfer method: A Monte Carlo simulation. *Macromol. Theory Simul.* **2002**, *11*, 678–686. [CrossRef]

112. Mavrantzas, V.G.; Theodorou, D.N. Atomistic simulation of polymer melt elasticity. *Macromolecules* **1998**, *31*, 6310–6332. [CrossRef]

113. Baig, C.; Mavrantzas, V.G. Multiscale simulation of polymer melt viscoelasticity. *Phys. Rev. B* **2009**, *79*. [CrossRef]

114. Brindle, D.; Care, C.M. Phase diagram for the lattice model of amphiphile and solvent mixtures by Monte Carlo simulation. *J. Chem. Soc., Faraday Trans.* **1992**, *88*, 2163–2166. [CrossRef]

115. Ivanov, V.A.; Stukan, M.R.; Müller, M.; Paul, W.; Binder, K. Phase diagram of solutions of stiff-chain macromolecules: A Monte Carlo simulation. *J. Chem. Phys.* **2003**, *118*, 10333–10342. [CrossRef]

116. Guevara-Carrion, G.; Hasse, H.; Vrabec, J. Thermodynamic properties for applications in chemical industry via classical force fields. *Top. Curr. Chem.* **2012**, *307*, 201–250. [PubMed]

117. Verlet, L. Computer "experiments" on classical fluids. I. Thermodynamical properties of Lennard-Jones molecules. *Phys. Rev.* **1967**, *159*, 98–103. [CrossRef]

118. Verlet, L. Computer "experiments" on classical fluids. II. Equilibrium correlation functions. *Phys. Rev.* **1968**, *165*, 201–214. [CrossRef]

119. Kremer, K.; Grest, G.S. Dynamics of entangled linear polymer melts: A molecular-dynamics simulation. *J. Chem. Phys.* **1990**, *92*, 5057–5086. [CrossRef]

120. Aoyagi, T.; Doi, M. Molecular dynamics simulation of entangled polymers in shear flow. *Comput. Theor. Polym. Sci.* **2000**, *10*, 317–321. [CrossRef]

121. Durand, M.; Meyer, H.; Benzerara, O.; Baschnagel, J.; Vitrac, O. Molecular dynamics simulations of the chain dynamics in monodisperse oligomer melts and of the oligomer tracer diffusion in an entangled polymer matrix. *J. Chem. Phys.* **2010**, *132*. [CrossRef] [PubMed]

122. Harmandaris, V.A.; Mavrantzas, V.G.; Theodorou, D.N.; Kröger, M.; Ramírez, J.; Ottinger, H.C.; Vlassopoulos, D. Crossover from the rouse to the entangled polymer melt regime: Signals from long, detailed atomistic molecular dynamics simulations, supported by rheological experiments. *Macromolecules* **2003**, *36*, 1376–1387. [CrossRef]

123. Likhtman, A.E.; Sukumaran, S.K.; Ramirez, J. Linear viscoelasticity from molecular dynamics simulation of entangled polymers. *Macromolecules* **2007**, *40*, 6748–6757. [CrossRef]

124. Wang, Z.; Larson, R.G. Constraint release in entangled binary blends of linear polymers: A molecular dynamics study. *Macromolecules* **2008**, *41*, 4945–4960. [CrossRef]

125. Harmandaris, V.A.; Daoulas, K.; Mavrantzas, V.G. Molecular dynamics simulation of a polymer melt/solid interface: Local dynamics and chain mobility in a thin film of polyethylene melt adsorbed on graphite. *Macromolecules* **2005**, *38*, 5796–5809. [CrossRef]

126. Milano, G.; Santangelo, G.; Ragone, F.; Cavallo, L.; Di Matteo, A. Gold nanoparticle/polymer interfaces: All atom structures from molecular dynamics simulations. *J. Phys. Chem. C* **2011**, *115*, 15154–15163. [CrossRef]

127. Luo, T.; Lloyd, J.R. Enhancement of thermal energy transport across graphene/graphite and polymer interfaces: A molecular dynamics study. *Adv. Funct. Mater.* **2012**, *22*, 2495–2502. [CrossRef]

128. Neyertz, S.; Brown, D. Molecular dynamics study of carbon dioxide sorption and plasticization at the interface of a glassy polymer membrane. *Macromolecules* **2013**, *46*, 2433–2449. [CrossRef]

129. Lamas, E.J.; Balbuena, P.B. Molecular dynamics studies of a model polymer-catalyst-carbon interface. *Electrochim. Acta* **2006**, *51*, 5904–5911. [CrossRef]

130. Song, Y.; Feng, W.; Liu, K.; Yang, P.; Zhang, W.; Zhang, X. Exploring the folding pattern of a polymer chain in a single crystal by combining single-molecule force spectroscopy and steered molecular dynamics simulations. *Langmuir* **2013**, *29*, 3853–3857. [CrossRef] [PubMed]

131. Yamamoto, T. Molecular dynamics simulations of steady-state crystal growth and homogeneous nucleation in polyethylene-like polymer. *J. Chem. Phys.* **2008**, *129*. [CrossRef] [PubMed]

132. Yamamoto, T. Molecular dynamics of reversible and irreversible melting in chain-folded crystals of short polyethylene-like polymer. *Macromolecules* **2010**, *43*, 9384–9393. [CrossRef]

133. Hegde, G.A.; Chang, J.-F.; Chen, Y.-L.; Khare, R. Conformation and diffusion behavior of ring polymers in solution: A comparison between molecular dynamics, multiparticle collision dynamics, and lattice Boltzmann simulations. *J. Chem. Phys.* **2011**, *135*. [CrossRef] [PubMed]

134. Bahlakeh, G.; Nikazar, M.; Hafezi, M.-J.; Dashtimoghadam, E.; Hasani-Sadrabadi, M.M. Molecular dynamics simulation study of proton diffusion in polymer electrolyte membranes based on sulfonated poly (ether ether ketone). *Int. J. Hydrog. Energy* **2012**, *37*, 10256–10264. [CrossRef]

135. Liu, J.; Cao, D.; Zhang, L. Molecular dynamics study on nanoparticle diffusion in polymer melts: A test of the stokes-einstein law. *J. Phys. Chem. C* **2008**, *112*, 6653–6661. [CrossRef]

136. Zhao, X.-T.; Yang, H.; Sheng, Y.-Z.; Li, J.-Y.; Sun, M. Molecular dynamics simulation on the effect of the distance between SWCNTs for short polymers diffusion among single wall carbon nanotubes. *Comput. Mater. Sci.* **2014**, *95*, 446–450. [CrossRef]

137. Jang, S.S.; Molinero, V.; Çağin, T.; Goddard, W.A., III. Nanophase-Segregation and Transport in Nafion 117 from Molecular Dynamics Simulations: Effect of Monomeric Sequence. *J. Phys. Chem. B* **2004**, *108*, 3149–3157. [CrossRef]

138. Błoński, S.; Brostow, W. Molecular dynamics simulations of chain relaxation and crack propagation in polymer liquid crystals. *J. Chem. Phys.* **1991**, *95*, 2890–2896.

139. Brostow, W.; Cunha, A.M.; Quintanilla, J.; Simões, R. Crack formation and propagation in molecular dynamics simulations of polymer liquid crystals. *Macromol. Theory Simul.* **2002**, *11*, 308–314. [CrossRef]

140. Brostow, W.; Hinze, J.A.; Simões, R. Tribological behavior of polymers simulated by molecular dynamics. *J. Mater. Res.* **2004**, *19*, 851–856. [CrossRef]

141. Shagolsem, L.S.; Sommer, J.-U. Order and phase behavior of thin film of diblock copolymer-selective nanoparticle mixtures: A molecular dynamics simulation study. *Macromolecules* **2014**, *47*, 830–839. [CrossRef]

142. Hartmann, L.; Gorbatschow, W.; Hauwede, J.; Kremer, F. Molecular dynamics in thin films of isotactic poly(methyl methacrylate). *Eur. Phys. J. E* **2002**, *8*, 145–154. [CrossRef] [PubMed]

143. Chen, J.; Li, L.; Zhou, D.; Xu, J.; Xue, G. Effect of molecular chain architecture on dynamics of polymer thin films measured by the ac-chip calorimeter. *Macromolecules* **2014**, *47*, 3497–3501. [CrossRef]

144. Gooneie, A.; Gonzalez-Gutierrez, J.; Holzer, C. Atomistic Modelling of Confined Polypropylene Chains between Ferric Oxide Substrates at Melt Temperature. *Polymers* **2016**, *8*, 361. [CrossRef]

145. Egorov, E.A.; Zhizhenkov, V.V. Molecular dynamics and strengthening of liquid-crystal polymers. *Phys. Solid State* **2005**, *47*, 942–948. [CrossRef]

146. Stimson, L.M.; Wilson, M.R. Molecular dynamics simulations of side chain liquid crystal polymer molecules in isotropic and liquid-crystalline melts. *J. Chem. Phys.* **2005**, *123*. [CrossRef] [PubMed]

147. Daivis, P.J.; Matin, M.L.; Todd, B.D. Nonlinear shear and elongational rheology of model polymer melts by non-equilibrium molecular dynamics. *J. Non-Newton. Fluid Mech.* **2003**, *111*, 1–18. [CrossRef]

148. Hajizadeh, E.; Todd, B.D.; Daivis, P.J. A molecular dynamics investigation of the planar elongational rheology of chemically identical dendrimer-linear polymer blends. *J. Chem. Phys.* **2015**, *142*. [CrossRef] [PubMed]

149. Kairn, T.; Daivis, P.J.; Ivanov, I.; Bhattacharya, S.N. Molecular-dynamics simulation of model polymer nanocomposite rheology and comparison with experiment. *J. Chem. Phys.* **2005**, *123*. [CrossRef] [PubMed]

150. Jeng, Y.-R.; Chen, C.-C.; Shyu, S.-H. A molecular dynamics study of lubrication rheology of polymer fluids. *Tribol. Lett.* **2003**, *15*, 293–300. [CrossRef]

151. Todd, B.D.; Daivis, P.J. Nonequilibrium molecular dynamics simulations of planar elongational flow with spatially and temporally periodic boundary conditions. *Phys. Rev. Lett.* **1998**, *81*, 1118–1121. [CrossRef]

152. Baig, C.; Edwards, B.J.; Keffer, D.J.; Cochran, H.D.; Harmandaris, V.A. Rheological and structural studies of linear polyethylene melts under planar elongational flow using nonequilibrium molecular dynamics simulations. *J. Chem. Phys.* **2006**, *124*, 84902. [CrossRef] [PubMed]

153. Chenoweth, K.; Cheung, S.; van Duin, A.; Goddard, W.A., III; Kober, E.M. Simulations on the thermal decomposition of a poly(dimethylsiloxane) polymer using the ReaxFF reactive force field. *J. Am. Chem. Soc.* **2005**, *127*, 7192–7202. [CrossRef] [PubMed]

154. Chenoweth, K.; van Duin, A.; Goddard, W.A., III. ReaxFF reactive force field for molecular dynamics simulations of hydrocarbon oxidation. *J. Phys. Chem. A* **2008**, *112*, 1040–1053. [CrossRef] [PubMed]

155. Van Duin, A.; Dasgupta, S.; Lorant, F.; Goddard, W.A., III. ReaxFF: A reactive force field for hydrocarbons. *J. Phys. Chem. A* **2001**, *105*, 9396–9409. [CrossRef]

156. Odegard, G.M.; Jensen, B.D.; Gowtham, S.; Wu, J.; He, J.; Zhang, Z. Predicting mechanical response of crosslinked epoxy using ReaxFF. *Chem. Phys. Lett.* **2014**, *591*, 175–178. [CrossRef]

157. Tieleman, D.P.; Marrink, S.J.; Berendsen, H. A computer perspective of membranes: Molecular dynamics studies of lipid bilayer systems. *Biochim. Biophys. Acta Rev. Biomembr.* **1997**, *1331*, 235–270. [CrossRef]

158. Heller, H.; Schaefer, M.; Schulten, K. Molecular dynamics simulation of a bilayer of 200 lipids in the gel and in the liquid-crystal phases. *J. Phys. Chem.* **1993**, *97*, 8343–8360. [CrossRef]

159. Lipowsky, R.; Grotehans, S. Hydration vs. Protrusion Forces Between Lipid Bilayers. *Europhys. Lett.* **1993**, *23*, 599. [CrossRef]

160. Lindahl, E.; Edholm, O. Mesoscopic undulations and thickness fluctuations in lipid bilayers from molecular dynamics simulations. *Biophys. J.* **2000**, *79*, 426–433. [CrossRef]

161. Gao, L.; Shillcock, J.; Lipowsky, R. Improved dissipative particle dynamics simulations of lipid bilayers. *J. Chem. Phys.* **2007**, *126*. [CrossRef] [PubMed]

162. Malevanets, A.; Kapral, R. Mesoscopic model for solvent dynamics. *J. Chem. Phys.* **1999**, *110*, 8605. [CrossRef]

163. Alekseeva, U.; Winkler, R.G.; Sutmann, G. Hydrodynamics in adaptive resolution particle simulations: Multiparticle collision dynamics. *J. Comput. Phys.* **2016**, *314*, 14–34. [CrossRef]

164. Satoh, A. *Introduction to Molecular-Microsimulation for Colloidal Dispersions*, 1st ed.; Elsevier: Amsterdam, The Netherlands, 2003.

165. Satoh, A. *Introduction to Practice of Molecular Simulation*; Elsevier Inc.: Burlington, MA, USA, 2011.

166. Pagonabarraga, I. Lattice boltzmann modeling of complex fluids: Colloidal suspensions and fluid mixtures. In *Novel Methods in Soft Matter Simulations*; Karttunen, M., Vattulainen, I., Lukkarinen, A., Eds.; Springer: Berlin, Germany, 2004; pp. 279–309.

167. Sukop, M.; Throne, D.T. *Lattice Boltzmann Modeling: An Introduction for Geoscientists and Engineers*, 1st ed.; Springer: New York, NY, USA, 2006.

168. Ermak, D.L.; McCammon, J.A. Brownian dynamics with hydrodynamic interactions. *J. Chem. Phys.* **1978**, *69*, 1352–1360. [CrossRef]

169. Ando, T.; Chow, E.; Saad, Y.; Skolnick, J. Krylov subspace methods for computing hydrodynamic interactions in Brownian dynamics simulations. *J. Chem. Phys.* **2012**, *137*. [CrossRef] [PubMed]

170. Cerbelaud, M.; Lestriez, B.; Guyomard, D.; Videcoq, A.; Ferrando, R. Brownian dynamics simulations of colloidal suspensions containing polymers as precursors of composite electrodes for lithium batteries. *Langmuir* **2012**, *28*, 10713–10724. [CrossRef] [PubMed]

171. Patti, A.; Cuetos, A. Brownian dynamics and dynamic Monte Carlo simulations of isotropic and liquid crystal phases of anisotropic colloidal particles: A comparative study. *Phys. Rev. E* **2012**, *86*. [CrossRef] [PubMed]

172. Gu, L.; Xu, S.; Sun, Z.; Wang, J.T. Brownian dynamics simulation of the crystallization dynamics of charged colloidal particles. *J. Colloid Interface Sci.* **2010**, *350*, 409–416. [CrossRef] [PubMed]

173. Santos, P.; Campanella, O.H.; Carignano, M.A. Brownian dynamics study of gel-forming colloidal particles. *J. Phys. Chem. B* **2010**, *114*, 13052–13058. [CrossRef] [PubMed]

174. Saveyn, H.; de Baets, B.; Thas, O.; Hole, P.; Smith, J.; van der Meeren, P. Accurate particle size distribution determination by nanoparticle tracking analysis based on 2-D Brownian dynamics simulation. *J. Colloid Interface Sci.* **2010**, *352*, 593–600. [CrossRef] [PubMed]

175. Li, Y.; Zhu, Y.-L.; Li, Y.-C.; Qian, H.-J.; Sun, C.-C. Self-assembly of two-patch particles in solution: A Brownian dynamics simulation study. *Mol. Simul.* **2014**, *40*, 449–457. [CrossRef]

176. Mendes, M.J.; Schmidt, H.K.; Pasquali, M. Brownian dynamics simulations of single-wall carbon nanotube separation by type using dielectrophoresis. *J. Phys. Chem. B* **2008**, *112*, 7467–7477. [CrossRef] [PubMed]

177. Van Den Noort, A.; Briels, W.J. Brownian dynamics simulations of concentration coupled shear banding. *J. Non-Newton. Fluid Mech.* **2008**, *152*, 148–155. [CrossRef]

178. Jain, A.; Sunthar, P.; Dünweg, B.; Prakash, J.R. Optimization of a Brownian-dynamics algorithm for semidilute polymer solutions. *Phys. Rev. E* **2012**, *85*. [CrossRef] [PubMed]

179. Li, B.; Zhu, Y.-L.; Liu, H.; Lu, Z.-Y. Brownian dynamics simulation study on the self-assembly of incompatible star-like block copolymers in dilute solution. *Phys. Chem. Chem. Phys.* **2012**, *14*, 4964–4970. [CrossRef] [PubMed]

180. Zhang, Y.; de Pablo, J.J.; Graham, M.D. An immersed boundary method for Brownian dynamics simulation of polymers in complex geometries: Application to DNA flowing through a nanoslit with embedded nanopits. *J. Chem. Phys.* **2012**, *136*. [CrossRef] [PubMed]

181. Pham, T.T.; Bajaj, M.; Prakash, J.R. Brownian dynamics simulation of polymer collapse in a poor solvent: Influence of implicit hydrodynamic interactions. *Soft Matter* **2008**, *4*, 1196–1207. [CrossRef]

182. Delong, S.; Usabiaga, F.B.; Delgado-Buscalioni, R.; Griffith, B.E.; Donev, A. Brownian dynamics without Green's functions. *J. Chem. Phys.* **2014**, *140*. [CrossRef] [PubMed]

183. Iliafar, S.; Vezenov, D.; Jagota, A. Brownian dynamics simulation of peeling a strongly-Adsorbed polymer molecule from a frictionless substrate. *Langmuir* **2013**, *29*, 1435–1445. [CrossRef] [PubMed]

184. Lee, P.-H.; Helms, V.; Geyer, T. Coarse-grained Brownian dynamics simulations of protein translocation through nanopores. *J. Chem. Phys.* **2012**, *137*. [CrossRef] [PubMed]

185. Adhikari, R.; Bhattacharya, A. Driven translocation of a semi-flexible chain through a nanopore: A Brownian dynamics simulation study in two dimensions. *J. Chem. Phys.* **2013**, *138*. [CrossRef] [PubMed]

186. Hoogerbrugge, P.J.; Koelman, J.M.V.A. Simulating Microscopic Hydrodynamic Phenomena with Dissipative Particle Dynamics. *Europhys. Lett.* **1992**, *19*, 155. [CrossRef]

187. Groot, R.D.; Warren, P.B. Dissipative particle dynamics: Bridging the gap between atomistic and mesoscopic simulation. *J. Chem. Phys.* **1997**, *107*, 4423–4435. [CrossRef]

188. Gooneie, A.; Mattausch, H.; Witschnigg, A.; Schuschnigg, S.; Holzer, C. Multiscale simulation of polymer nanocomposites in processing: Challenges and outlooks. *Key Eng. Mater.* **2015**, *651*, 533–538. [CrossRef]

189. Español, P.; Warren, P. Statistical mechanics of dissipative particle dynamics. *Europhys. Lett.* **1995**, *30*, 191. [CrossRef]

190. Groot, R.D. Applications of Dissipative Particle Dynamics. In *Novel Methods in Soft Matter Simulations*; Karttunen, M., Vattulainen, I., Lukkarinen, A., Eds.; Springer: Berlin, Germany, 2004; pp. 5–38.

191. Groot, R.D.; Madden, T.J. Dynamic simulation of diblock copolymer microphase separation. *J. Chem. Phys.* **1998**, *108*, 8713–8724. [CrossRef]

192. Den Otter, W.K.; Clarke, J. The temperature in dissipative particle dynamics. *Int. J. Mod. Phys. C* **2000**, *11*, 1179–1193. [CrossRef]

193. Pan, W.; Caswell, B.; Karniadakis, G.E. Rheology, microstructure and migration in brownian colloidal suspensions. *Langmuir* **2010**, *26*, 133–142. [CrossRef] [PubMed]

194. Yamanoi, M.; Pozo, O.; Maia, J.M. Linear and non-linear dynamics of entangled linear polymer melts by modified tunable coarse-grained level Dissipative Particle Dynamics. *J. Chem. Phys.* **2011**, *135*, 44904. [CrossRef] [PubMed]

195. Gooneie, A.; Schuschnigg, S.; Holzer, C. Orientation of anisometric layered silicate particles in uncompatibilized and compatibilized polymer melts under shear flow: A dissipative particle dynamics study. *Macromol. Theory Simul.* **2016**, *25*, 85–98. [CrossRef]

196. Gooneie, A.; Schuschnigg, S.; Holzer, C. Dissipative particle dynamics models of orientation of weakly-interacting anisometric silicate particles in polymer melts under shear flow: Comparison with the standard orientation models. *Macromol. Theory Simul.* **2016**, *25*, 287–302. [CrossRef]

197. Fedosov, D.A.; Noguchi, H.; Gompper, G. Multiscale modeling of blood flow: From single cells to blood rheology. *Biomech. Model. Mechanobiol.* **2014**, *13*, 239–258. [CrossRef] [PubMed]

198. Zhang, P.; Zhang, N.; Deng, Y.; Bluestein, D. A multiple time stepping algorithm for efficient multiscale modeling of platelets flowing in blood plasma. *J. Comput. Phys.* **2015**, *284*, 668–686. [CrossRef] [PubMed]

199. Gooneie, A.; Schuschnigg, S.; Holzer, C. Dissipative particle dynamics simulations of orientation of layered silicate particles embedded in polymer melts under shear flows. *AIP Conf. Proc.* **2016**, *1779*, 50010.

200. Gai, J.-G.; Hu, G.-H.; Li, H.-L.; Zhu, S.-P.; Hoppe, S. Dissipative particle dynamics and flory-huggins theories for predicting the rheological behavior of ultrahigh molecular weight polyethylene blends. *Ind. Eng. Chem. Res.* **2010**, *49*, 11369–11379. [CrossRef]

201. Goicochea, A.G. Adsorption and disjoining pressure isotherms of confined polymers using dissipative particle dynamics. *Langmuir* **2007**, *23*, 11656–11663. [CrossRef] [PubMed]

202. Kacar, G.; Peters, E.; de With, G. Mesoscopic simulations for the molecular and network structure of a thermoset polymer. *Soft Matter* **2013**, *9*, 5785–5793. [CrossRef]

203. Kacar, G.; Peters, E.; de With, G. Structure of a thermoset polymer near an alumina substrate as studied by dissipative particle dynamics. *J. Phys. Chem. C* **2013**, *117*, 19038–19047. [CrossRef]

204. Kauzlari, D.; Meier, J.T.; Español, P.; Succi, S.; Greiner, A.; Korvink, J.G. Bottom-up coarse-graining of a simple graphene model: The blob picture. *J. Chem. Phys.* **2011**, *134*. [CrossRef] [PubMed]

205. Lee, M.-T.; Mao, R.; Vishnyakov, A.; Neimark, A.V. Parametrization of chain molecules in dissipative particle dynamics. *J. Phys. Chem. B* **2016**. [CrossRef] [PubMed]

206. Maly, M.; Posocco, P.; Pricl, S.; Fermeglia, M. Self-assembly of nanoparticle mixtures in diblock copolymers: Multiscale molecular modeling. *Ind. Eng. Chem. Res.* **2008**, *47*, 5023–5038. [CrossRef]

207. Posocco, P.; Posel, Z.; Fermeglia, M.; Lísal, M.; Pricl, S. A molecular simulation approach to the prediction of the morphology of self-assembled nanoparticles in diblock copolymers. *J. Mater. Chem.* **2010**, *20*, 10511–10520. [CrossRef]

208. Esteves, A.C.C.; Lyakhova, K.; Van Der Ven, L.G.J.; Van Benthem, R.A.T.M.; de With, G. Surface segregation of low surface energy polymeric dangling chains in a cross-linked polymer network investigated by a combined experimental-simulation Approach. *Macromolecules* **2013**, *46*, 1993–2002. [CrossRef]

209. Esteves, A.C.C.; Lyakhova, K.; van Riel, J.M.; Van Der Ven, L.G.J.; Van Benthem, R.A.T.M.; de With, G. Self-replenishing ability of cross-linked low surface energy polymer films investigated by a complementary experimental-simulation approach. *J. Chem. Phys.* **2014**, *140*, 124902. [CrossRef] [PubMed]

210. Lyakhova, K.; Esteves, A.C.C.; van de Put, M.W.P.; van der Ven, L.G.J.; van Benthem, R.A.T.M.; de With, G. Simulation-Experimental Approach to Investigate the Role of Interfaces in Self-Replenishing Composite Coatings. *Adv. Mater. Interfaces* **2014**, *1*, 1400053. [CrossRef]

211. Rahatekar, S.S.; Hamm, M.; Shaffer, M.; Elliott, J.A. Mesoscale modeling of electrical percolation in fiber-filled systems. *J. Chem. Phys.* **2005**, *123*. [CrossRef] [PubMed]

212. Frisch, U.; Hasslacher, B.; Pomeau, Y. Lattice-gas automata for the Navier-Stokes equation. *Phys. Rev. Lett.* **1986**, *56*, 1505–1508. [CrossRef] [PubMed]

213. Benzi, R.; Succi, S.; Vergassola, M. The lattice Boltzmann equation: Theory and applications. *Phys. Rep.* **1992**, *222*, 145–197. [CrossRef]

214. Higuera, F.J.; Jiménez, J. Boltzmann approach to lattice gas simulations. *Europhys. Lett.* **1989**, *9*, 663–668. [CrossRef]

215. Higuera, F.J.; Succi, S.; Benzi, R. Lattice gas dynamics with enhanced collisions. *Europhys. Lett.* **1989**, *9*, 345–349. [CrossRef]

216. Bhatnagar, P.L.; Gross, E.P.; Krook, M. A model for collision processes in gases. I. Small amplitude processes in charged and neutral one-component systems. *Phys. Rev.* **1954**, *94*, 511–525. [CrossRef]

217. Qian, Y.H.; D'Humières, D.; Lallemand, P. Lattice bgk models for navier-stokes equation. *Europhys. Lett.* **1992**, *17*, 479–484. [CrossRef]

218. Dünweg, B.; Ladd, A. Lattice Boltzmann Simulations of Soft Matter Systems. *arXiv*, **2009**, arXiv:0803.2826.

219. Usta, O.B.; Ladd, A.; Butler, J.E. Lattice-Boltzmann simulations of the dynamics of polymer solutions in periodic and confined geometries. *J. Chem. Phys.* **2005**, *122*. [CrossRef]

220. Ahlrichs, P.; Dünweg, B. Lattice-boltzmann simulation of polymer-solvent systems. *Int. J. Mod. Phys. C* **1998**, *9*, 1429–1438. [CrossRef]

221. Aidun, C.K.; Clausen, J.R. Lattice-boltzmann method for complex flows. *Annu. Rev. Fluid Mech.* **2010**, *42*, 439–472. [CrossRef]

222. Spaid, M.; Phelan, F.R., Jr. Lattice Boltzmann methods for modeling microscale flow in fibrous porous media. *Phys. Fluids* **1997**, *9*, 2468–2474. [CrossRef]

223. Sinha, P.K.; Mukherjee, P.P.; Wang, C.-Y. Impact of GDL structure and wettability on water management in polymer electrolyte fuel cells. *J. Mater. Chem.* **2007**, *17*, 3089–3103. [CrossRef]

224. Care, C.M.; Cleaver, D.J. Computer simulation of liquid crystals. *Rep. Prog. Phys.* **2005**, *68*, 2665–2700. [CrossRef]

225. Denniston, C.; Orlandini, E.; Yeomans, J.M. Lattice Boltzmann simulations of liquid crystal hydrodynamics. *Phys. Rev. E* **2001**, *63*, 056702. [CrossRef] [PubMed]

226. Marenduzzo, D.; Orlandini, E.; Cates, M.E.; Yeomans, J.M. Steady-state hydrodynamic instabilities of active liquid crystals: Hybrid lattice Boltzmann simulations. *Phys. Rev. E Stat., Nonlinear Soft Matter Phys.* **2007**, *76*. [CrossRef] [PubMed]

227. Usta, O.B.; Perchak, D.; Clarke, A.; Yeomans, J.M.; Balazs, A.C. Shear and extensional deformation of droplets containing polymers and nanoparticles. *J. Chem. Phys.* **2009**, *130*. [CrossRef] [PubMed]

228. Nabovati, A.; Llewellin, E.W.; Sousa, A. A general model for the permeability of fibrous porous media based on fluid flow simulations using the lattice Boltzmann method. *Compos. Part A* **2009**, *40*, 860–869. [CrossRef]

229. Wang, M.; He, J.; Yu, J.; Pan, N. Lattice Boltzmann modeling of the effective thermal conductivity for fibrous materials. *Int. J. Therm. Sci.* **2007**, *46*, 848–855. [CrossRef]

230. Bird, R.B.; Armstrong, R.C.; Hassager, O. *Dynamics of Polymeric Liquids*; John Wiley & Sons Inc.: Hoboken, NJ, USA, 1987.

231. Rappaz, M.; Bellet, M.; Deville, M. *Numerical Modeling in Materials Science and Engineering*; Springer: Leutershausen, Germany, 2003.

232. Ellero, M.; Español, P.; Flekkøy, E.G. Thermodynamically consistent fluid particle model for viscoelastic flows. *Phys. Rev. E* **2003**, *68*, 041504. [CrossRef] [PubMed]

233. Vázquez-Quesada, A.; Ellero, M.; Español, P. Smoothed particle hydrodynamic model for viscoelastic fluids with thermal fluctuations. *Phys. Rev. E* **2009**, *79*. [CrossRef] [PubMed]

234. Bian, X.; Litvinov, S.; Qian, R.; Ellero, M.; Adams, N.A. Multiscale modeling of particle in suspension with smoothed dissipative particle dynamics. *Phys. Fluids* **2012**, *24*. [CrossRef]

235. Vázquez-Quesada, A.; Ellero, M.; Español, P. Consistent scaling of thermal fluctuations in smoothed dissipative particle dynamics. *J. Chem. Phys.* **2009**, *130*. [CrossRef] [PubMed]

236. Petsev, N.D.; Leal, L.G.; Shell, M.S. Multiscale simulation of ideal mixtures using smoothed dissipative particle dynamics. *J. Chem. Phys.* **2016**, *144*. [CrossRef] [PubMed]

237. Pirondi, A.; Giuliese, G.; Moroni, F. Fatigue debonding three-dimensional simulation with cohesive zone. *J. Adhes.* **2016**, *92*, 553–571. [CrossRef]

238. Schiel, M.; Reh, S.; Schwienhorst, M.; Welters, T.; Stammen, E.; Dilger, K. Finite element modelling of cure-dependent mechanical properties by model-free kinetic analysis using a cohesive zone approach. *J. Adhes.* **2016**, *92*, 572–585. [CrossRef]

239. Heydari-Meybodi, M.; Saber-Samandari, S.; Sadighi, M. 3D multiscale modeling to predict the elastic modulus of polymer/nanoclay composites considering realistic interphase property. *Compos. Interfaces* **2016**, *23*, 641–661. [CrossRef]

240. Sun, M.-K.; Shieh, J.; Chen, C.-S.; Chiang, H.; Huang, C.-W.; Chen, W.-S. Effects of an implant on temperature distribution in tissue during ultrasound diathermy. *Ultrason. Sonochem.* **2016**, *32*, 44–53. [CrossRef] [PubMed]

241. Gooneie, A.; Schuschnigg, S.; Duretek, I.; Holzer, C. Numerical simulations of the flow of wood polypropylene composites with wall slipping in a profile die: The significance of material data. *Arch. Iran. Med.* **2015**, *1664*, 50014.

242. Duretek, I.; Schuschnigg, S.; Gooneie, A.; Langecker, G.R.; Holzer, C.; Gomze, L.A. Rheological properties of wood polymer composites and their role in extrusion. *J. Phys. Conf. Ser.* **2015**, *602*, 12014. [CrossRef]

243. Chen, K.; Zhang, D.; Yang, X.; Cui, X.; Zhang, X.; Wang, Q. Research on torsional friction behavior and fluid load support of PVA/HA composite hydrogel. *J. Mech. Behav. Biomed. Mater.* **2016**, *62*, 182–194. [CrossRef] [PubMed]

244. Ehrenhofer, A.; Bingel, G.; Paschew, G.; Tietze, M.; Schröder, R.; Richter, A.; Wallmersperger, T. Permeation control in hydrogel-layered patterned PET membranes with defined switchable pore geometry—Experiments and numerical simulation. *Sens. Actuators B* **2016**, *232*, 499–505. [CrossRef]

245. Baaijens, F. Mixed finite element methods for viscoelastic flow analysis: A review. *J. Non-Newton. Fluid Mech.* **1998**, *79*, 361–385. [CrossRef]

246. Verbeeten, W.; Peters, G.; Baaijens, F. Differential constitutive equations for polymer melts: The extended Pom-Pom model. *J. Rheol.* **2001**, *45*, 823–843. [CrossRef]

247. Yue, P.; Zhou, C.; Feng, J.J.; Ollivier-Gooch, C.F.; Hu, H.H. Phase-field simulations of interfacial dynamics in viscoelastic fluids using finite elements with adaptive meshing. *J. Comput. Phys.* **2006**, *219*, 47–67. [CrossRef]

248. Wilkes, E.D.; Phillips, S.D.; Basaran, O.A. Computational and experimental analysis of dynamics of drop formation. *Phys. Fluids* **1999**, *11*, 3577–3598. [CrossRef]

249. Patera, A.T. A spectral element method for fluid dynamics. *J. Comput. Phys.* **1984**, *54*, 468–488. [CrossRef]

250. Pozrikidis, C. *Introduction to Finite and Spectral Element Methods Using MATLAB*, 2nd ed.; CRC Press: Boca Raton, FL, USA, 2014.

251. Van Os, R.; Phillips, T.N. The prediction of complex flows of polymer melts using spectral elements. *J. Non-Newton. Fluid Mech.* **2004**, *122*, 287–301. [CrossRef]

252. Fiétier, N.; Deville, M.O. Time-dependent algorithms for the simulation of viscoelastic flows with spectral element methods. *J. Comput. Phys.* **2003**, *186*, 93–121. [CrossRef]

253. Li, R.; Chen, Z.; Wu, W. *Generalized Difference Methods for Differential Equations: Numerical Analysis of Finite Volume Methods*; Marcel Dekker: New York, NY, USA, 2000.

254. Hughes, T.; Brooks, A. Multi-dimensional upwind scheme with no crosswind diffusion. *Am. Soc. Mech. Eng.* **1979**, *34*, 19–35.

255. Hughes, T.; Mallet, M.; Akira, M. A new finite element formulation for computational fluid dynamics: II. Beyond SUPG. *Comput. Methods Appl. Mech. Eng.* **1986**, *54*, 341–355. [CrossRef]

256. Jiang, B.; Liao, G. The Least-Squares Meshfree Finite Element Method. In Proceedings of the Computational Mechanics: International Symposium on Computational Mechanic, Beijing, China, 30 July–1 August 2009; p. 341.

257. Kumar, R.; Dennis, B.H. A Least-Squares Galerkin Split Finite Element Method for Compressible Navier-Stokes Equations. In Proceedings of the 29th Computers and Information in Engineering Conference, San Diego, CA, USA, 30 August 30–2 September 2009.

258. Baliga, B.R.; Patankar, S.V. A control volume finite-element method for two-dimensional fluid flow and heat transfer. *Numer. Heat Transf.* **1983**, *6*, 245–261. [CrossRef]

259. Patankar, S.V. A calculation procedure for two-dimensional elliptic situations. *Numer. Heat Transf.* **1981**, *4*, 409–425. [CrossRef]

260. Prakash, C.; Patankar, S.V. A control volume-based finite-element method for solving the navier-stokes equations using equal-order velocity-pressure interpolation. *Numer. Heat Transf.* **1985**, *8*, 259–280. [CrossRef]

261. Balsara, D.S. Divergence-free reconstruction of magnetic fields and WENO schemes for magnetohydrodynamics. *J. Comput. Phys.* **2009**, *228*, 5040–5056. [CrossRef]

262. Powell, K.G.; Roe, P.L.; Linde, T.J.; Gombosi, T.I.; de Zeeuw, D.L. A Solution-Adaptive Upwind Scheme for Ideal Magnetohydrodynamics. *J. Comput. Phys.* **1999**, *154*, 284–309. [CrossRef]

263. Tóth, G. The $\bigtriangledown \cdot B = 0$ Constraint in Shock-Capturing Magnetohydrodynamics Codes. *J. Comput. Phys.* **2000**, *161*, 605–652. [CrossRef]

264. Liu, F.; Cai, J.; Zhu, Y.; Tsai, H.M.; Wong, A. Calculation of wing flutter by a coupled fluid-structure method. *J. Aircr.* **2001**, *38*, 334–342. [CrossRef]

265. Makhijani, V.B.; Yang, H.Q.; Dionne, P.J.; Thubrikar, M.J. Three-dimensional coupled fluid-structure simulation of pericardial bioprosthetic aortic valve function. *ASAIO J.* **1997**, *43*, M387–M392. [CrossRef] [PubMed]

266. Narumanchi, S.; Murthy, J.Y.; Amon, C.H. Submicron heat transport model in silicon accounting for phonon dispersion and polarization. *J. Heat Transf.* **2004**, *126*, 946–955. [CrossRef]

267. Voicolescu, I.; Andrew McGill, R.; Zaghloul, M.E.; Mott, D.; Stepnowski, J.; Stepnowski, S.; Summers, H.; Nguyen, V.; Ross, S.; Walsh, K.; et al. Micropreconcentrator for enhanced trace detection of explosives and chemical agents. *IEEE Sens. J.* **2006**, *6*, 1094–1103. [CrossRef]

268. Moukalled, F.; Mangani, L.; Darwish, M. *The Finite Volume Method in Computational Fluid Dynamics: An Advanced Introduction with OpenFOAM® and Matlab®*; Springer: Cham, Switzerland, 2016.

269. Patankar, S.V. *Numerical Heat Transfer and Fluid Flow*; Hemisphere Publishing: Washington, DC, USA, 1980.

270. Leonard, B.P. A stable and accurate convective modelling procedure based on quadratic upstream interpolation. *Comput. Methods Appl. Mech. Eng.* **1979**, *19*, 59–98. [CrossRef]

271. Weller, H.G.; Tabor, G.; Jasak, H.; Fureby, C. A tensorial approach to computational continuum mechanics using object-oriented techniques. *Comput. Phys.* **1998**, *12*, 620–631. [CrossRef]

272. Jasak, H. OpenFOAM: Open source CFD in research and industry. *Int. J. Nav. Archit. Ocean Eng.* **2009**, *1*, 89–94.

273. Favero, J.L.; Secchi, A.R.; Cardozo, N.; Jasak, H. Viscoelastic flow analysis using the software OpenFOAM and differential constitutive equations. *J. Non-Newton. Fluid Mech.* **2010**, *165*, 1625–1636. [CrossRef]

274. Favero, J.L.; Secchi, A.R.; Cardozo, N.; Jasak, H. Viscoelastic flow simulation: Development of a methodology of analysis using the software OpenFOAM and differential constitutive equations. *Comput. Aided Chem. Eng.* **2009**, *27*, 915–920.

275. Favero, J.L.; Secchi, A.R.; Cardozo, N.; Jasak, H. Viscoelastic fluid analysis in internal and in free surface flows using the software OpenFOAM. *Comput. Chem. Eng.* **2010**, *34*, 1984–1993. [CrossRef]

276. Holmes, L.; Favero, J.; Osswald, T. Numerical simulation of three-dimensional viscoelastic planar contraction flow using the software OpenFOAM. *Comput. Chem. Eng.* **2012**, *37*, 64–73. [CrossRef]

277. Yang, W.-J.; Yi, W.; Ren, X.-G.; Xu, L.-Y.; Xu, X.-H.; Yuan, X.-F. Toward large scale parallel computer simulation of viscoelastic fluid flow: A study of benchmark flow problems. *J. Non-Newton. Fluid Mech.* **2015**, *222*, 82–95. [CrossRef]

278. Lima, N.C.; D'ávila, M.A. Numerical simulation of electrohydrodynamic flows of Newtonian and viscoelastic droplets. *J. Non-Newton. Fluid Mech.* **2014**, *213*, 1–14. [CrossRef]

279. Cao, Y.; Ren, X.-G.; Guo, X.-W.; Wang, M.; Wang, Q.; Xu, X.-H.; Yang, X.-J. A new method to simulate free surface flows for Viscoelastic fluid. *Adv. Mater. Sci. Eng.* **2015**, *2015*. [CrossRef]

280. Habla, F.; Marschall, H.; Hinrichsen, O.; Dietsche, L.; Jasak, H.; Favero, J.L. Numerical simulation of viscoelastic two-phase flows using openFOAM®. *Chem. Eng. Sci.* **2011**, *66*, 5487–5496. [CrossRef]

281. Zhang, K.; Kuang, T.; Liu, H.; Zeng, X.; Deng, Y.; Jasak, H. Simulation and analysis of mold filling in water-assisted injection molding of viscoelastic polymers. *Gaofenzi Cailiao Kexue Yu Gongcheng* **2014**, *30*, 93–96.

282. Haddadi Sisakht, B.; Jordan, C.; Schretter, P.; Lassmann, T.; Harasek, M. Designing Better Membrane Modules Using CFD. *Chem. Prod. Process Model.* **2016**, *11*, 57–66. [CrossRef]

283. Wu, W.-T.; Yang, F.; Antaki, J.F.; Aubry, N.; Massoudi, M. Study of blood flow in several benchmark micro-channels using a two-fluid approach. *Int. J. Eng. Sci.* **2015**, *95*, 49–59. [CrossRef] [PubMed]

284. Carolan, D.; Chong, H.M.; Ivankovic, A.; Kinloch, A.J.; Taylor, A.C. Co-continuous polymer systems: A numerical investigation. *Comput. Mater. Sci.* **2015**, *98*, 24–33. [CrossRef]

285. Shou, Z.; Buxton, G.A.; Balazs, A.C. Predicting the self-assembled morphology and mechanical properties of mixtures of diblocks and rod-like nanoparticles. *Compos. Interfaces* **2003**, *10*, 343–368. [CrossRef]

286. Travasso, R.; Buxton, G.A.; Kuksenok, O.; Good, K.; Balazs, A.C. Modeling the morphology and mechanical properties of sheared ternary mixtures. *J. Chem. Phys.* **2005**, *122*, 194906. [CrossRef] [PubMed]

287. Zhao, X.; Deng, S.; Huang, Y.; Liu, H.; Hu, Y. Simulation of morphologies and mechanical properties of A/B polymer blend film. *Chin. J. Chem. Eng.* **2011**, *19*, 549–557. [CrossRef]

288. Smith, K.A.; Tyagi, S.; Balazs, A.C. Healing surface defects with nanoparticle-filled polymer coatings: Effect of particle geometry. *Macromolecules* **2005**, *38*, 10138–10147. [CrossRef]

289. Tyagi, S.; Lee, J.Y.; Buxton, G.A.; Balazs, A.C. Using nanocomposite coatings to heal surface defects. *Macromolecules* **2004**, *37*, 9160–9168. [CrossRef]

290. Brown, J.R.; Seo, Y.; Maula, T.; Hall, L.M. Fluids density functional theory and initializing molecular dynamics simulations of block copolymers. *J. Chem. Phys.* **2016**, *144*. [CrossRef] [PubMed]

291. Buxton, G.A.; Balazs, A.C. Predicting the mechanical and electrical properties of nanocomposites formed from polymer blends and nanorods. *Mol. Simul.* **2004**, *30*, 249–257. [CrossRef]

292. Buxton, G.A.; Balazs, A.C. Simulating the morphology and mechanical properties of filled diblock copolymers. *Phys. Rev. E Stat. Nonlinear Soft Matter Phys.* **2003**, *67*, 31802. [CrossRef] [PubMed]

293. Suter, J.L.; Groen, D.; Coveney, P.V. Chemically specifi C multiscale modeling of clay-polymer nanocomposites reveals intercalation dynamics, tactoid self-assembly and emergent materials properties. *Adv. Mater.* **2015**, *27*, 966–984. [CrossRef] [PubMed]

294. Scocchi, G.; Posocco, P.; Fermeglia, M.; Pricl, S. Polymer—Clay nanocomposites: A multiscale molecular modeling approach. *J. Phys. Chem. B* **2007**, *111*, 2143–2151. [CrossRef] [PubMed]

295. Scocchi, G.; Posocco, P.; Handgraaf, J.-W.; Fraaije, J.G.E.M.; Fermeglia, M.; Pricl, S. A complete multiscale modelling approach for polymer-clay nanocomposites. *Chem. Eur. J.* **2009**, *15*, 7586–7592. [CrossRef] [PubMed]

296. Pereira, S.P.; Scocchi, G.; Toth, R.; Posocco, P.; Nieto, D.R.; Pricl, S.; Fermeglia, M. Multiscale Modeling of Polymer/Clay Nanocomposites. *J. Multiscale Model.* **2011**, *3*, 151–176. [CrossRef]

297. Kalligiannaki, E.; Chazirakis, A.; Tsourtis, A.; Katsoulakis, M.A.; Plecháč, P.; Harmandaris, V. Parametrizing coarse grained models for molecular systems at equilibrium. *Eur. Phys. J. Spec. Top.* **2016**, *225*, 1347–1372. [CrossRef]

298. Harmandaris, V.; Kalligiannaki, E.; Katsoulakis, M.; Plecháč, P. Path-space variational inference for non-equilibrium coarse-grained systems. *J. Comput. Phys.* **2016**, *314*, 355–383. [CrossRef]

299. Li, Y.; Abberton, B.C.; Kröger, M.; Liu, W.K. Challenges in multiscale modeling of polymer dynamics. *Polymers* **2013**, *5*, 751–832. [CrossRef]

300. Brini, E.; Algaer, E.A.; Ganguly, P.; Li, C.; Rodríguez-Ropero, F.; van der Vegt, N. Systematic coarse-graining methods for soft matter simulations-a review. *Soft Matter* **2013**, *9*, 2108–2119. [CrossRef]

301. Hess, B.; Holm, C.; van der Vegt, N. Modeling multibody effects in ionic solutions with a concentration dependent dielectric permittivity. *Phys. Rev. Lett.* **2006**, *96*. [CrossRef] [PubMed]

302. Shen, J.-W.; Li, C.; van der Vegt, N.; Peter, C. Transferability of coarse grained potentials: Implicit solvent models for hydrated ions. *J. Chem. Theory Comput.* **2011**, *7*, 1916–1927. [CrossRef] [PubMed]

303. Wang, Y.; Noid, W.G.; Liu, P.; Voth, G.A. Effective force coarse-graining. *Phys. Chem. Chem. Phys.* **2009**, *11*, 2002–2015. [CrossRef] [PubMed]

304. Brini, E.; Marcon, V.; van der Vegt, N. Conditional reversible work method for molecular coarse graining applications. *Phys. Chem. Chem. Phys.* **2011**, *13*, 10468–10474. [CrossRef] [PubMed]

305. Brini, E.; van der Vegt, N. Chemically transferable coarse-grained potentials from conditional reversible work calculations. *J. Chem. Phys.* **2012**, *137*. [CrossRef] [PubMed]

306. Villa, A.; Peter, C.; van der Vegt, N. Self-assembling dipeptides: Conformational sampling in solvent-free coarse-grained simulation. *Phys. Chem. Chem. Phys.* **2009**, *11*, 2077–2086. [CrossRef] [PubMed]

307. Li, C.; Shen, J.; Peter, C.; van der Vegt, N. A chemically accurate implicit-solvent coarse-grained model for polystyrenesulfonate solutions. *Macromolecules* **2012**, *45*, 2551–2561. [CrossRef]

308. Tschöp, W.; Kremer, K.; Hahn, O.; Batoulis, J.; Bürger, T. Simulation of polymer melts. I. coarse-graining procedure for polycarbonates. *Acta Polym.* **1998**, *49*, 61–74. [CrossRef]

309. Lyubartsev, A.P.; Laaksonen, A. Calculation of effective interaction potentials from radial distribution functions: A reverse Monte Carlo approach. *Phys. Rev. E* **1995**, *52*, 3730–3737. [CrossRef]

310. Lyubartsev, A.P.; Laaksonen, A. Osmotic and activity coefficients from effective potentials for hydrated ions. *Phys. Rev. E* **1997**, *55*, 5689–5696. [CrossRef]

311. Reith, D.; Pütz, M.; Müller-Plathe, F. Deriving effective mesoscale potentials from atomistic simulations. *J. Comput. Chem.* **2003**, *24*, 1624–1636. [CrossRef] [PubMed]

312. Peter, C.; Delle Site, L.; Kremer, K. Classical simulations from the atomistic to the mesoscale and back: Coarse graining an azobenzene liquid crystal. *Soft Matter* **2008**, *4*, 859–869. [CrossRef]

313. Murtola, T.; Karttunen, M.; Vattulainen, I. Systematic coarse graining from structure using internal states: Application to phospholipid/cholesterol bilayer. *J. Chem. Phys.* **2009**, *131*. [CrossRef] [PubMed]

314. Savelyev, A.; Papoian, G.A. Molecular renormalization group coarse-graining of electrolyte solutions: Application to aqueous NaCl and KCl. *J. Phys. Chem. B* **2009**, *113*, 7785–7793. [CrossRef] [PubMed]

315. Savelyev, A.; Papoian, G.A. Molecular renormalization group coarse-graining of polymer chains: Application to double-stranded DNA. *Biophys. J.* **2009**, *96*, 4044–4052. [CrossRef] [PubMed]

316. Savelyev, A.; Papoian, G.A. Chemically accurate coarse graining of double-stranded DNA. *Proc. Natl. Acad. Sci. USA* **2010**, *107*, 20340–20345. [CrossRef] [PubMed]

317. Megariotis, G.; Vyrkou, A.; Leygue, A.; Theodorou, D.N. Systematic coarse graining of 4-Cyano-4′-pentylbiphenyl. *Ind. Eng. Chem. Res.* **2011**, *50*, 546–556. [CrossRef]

318. Mukherjee, B.; Delle Site, L.; Kremer, K.; Peter, C. Derivation of coarse grained models for multiscale simulation of liquid crystalline phase transitions. *J. Phys. Chem. B* **2012**, *116*, 8474–8484. [CrossRef] [PubMed]

319. Meyer, H.; Biermann, O.; Faller, R.; Reith, D.; Müller-Plathe, F. Coarse graining of nonbonded inter-particle potentials using automatic simplex optimization to fit structural properties. *J. Chem. Phys.* **2000**, *113*, 6264–6275. [CrossRef]

320. Ganguly, P.; Mukherji, D.; Junghans, C.; van der Vegt, N. Kirkwood-buff coarse-grained force fields for aqueous solutions. *J. Chem. Theory Comput.* **2012**, *8*, 1802–1807. [CrossRef] [PubMed]

321. Shell, M.S. The relative entropy is fundamental to multiscale and inverse thermodynamic problems. *J. Chem. Phys.* **2008**, *129*. [CrossRef] [PubMed]

322. Chaimovich, A.; Shell, M.S. Relative entropy as a universal metric for multiscale errors. *Phys. Rev. E* **2010**, *81*. [CrossRef] [PubMed]

323. Chaimovich, A.; Shell, M.S. Coarse-graining errors and numerical optimization using a relative entropy framework. *J. Chem. Phys.* **2011**, *134*. [CrossRef] [PubMed]

324. Chaimovich, A.; Shell, M.S. Anomalous waterlike behavior in spherically-symmetric water models optimized with the relative entropy. *Phys. Chem. Chem. Phys.* **2009**, *11*, 1901–1915. [CrossRef] [PubMed]

325. Mullinax, J.W.; Noid, W.G. Reference state for the generalized Yvon-Born-Green theory: Application for coarse-grained model of hydrophobic hydration. *J. Chem. Phys.* **2010**, *133*. [CrossRef] [PubMed]

326. Ercolesi, F.; Adams, J.B. Interatomic potentials from first-principles calculations: The force-matching method. *Europhys. Lett.* **1994**, *26*, 583–588. [CrossRef]
327. Rühle, V.; Junghans, C.; Lukyanov, A.; Kremer, K.; Andrienko, D. Versatile object-oriented toolkit for coarse-graining applications. *J. Chem. Theory Comput.* **2009**, *5*, 3211–3223. [CrossRef] [PubMed]
328. Izvekov, S.; Voth, G.A. A multiscale coarse-graining method for biomolecular systems. *J. Phys. Chem. B* **2005**, *109*, 2469–2473. [CrossRef] [PubMed]
329. Izvekov, S.; Chung, P.W.; Rice, B.M. The multiscale coarse-graining method: Assessing its accuracy and introducing density dependent coarse-grain potentials. *J. Chem. Phys.* **2010**, *133*. [CrossRef] [PubMed]
330. Zhou, J.; Thorpe, I.F.; Izvekov, S.; Voth, G.A. Coarse-grained peptide modeling using a systematic multiscale approach. *Biophys. J.* **2007**, *92*, 4289–4303. [CrossRef] [PubMed]
331. Hills, R.D., Jr.; Lu, L.; Voth, G.A. Multiscale coarse-graining of the protein energy landscape. *PLoS Comput. Biol.* **2010**, *6*, 1–15. [CrossRef] [PubMed]
332. Izvekov, S.; Voth, G.A. Multiscale coarse graining of liquid-state systems. *J. Chem. Phys.* **2005**, *123*. [CrossRef] [PubMed]
333. Noid, W.G.; Chu, J.-W.; Ayton, G.S.; Krishna, V.; Izvekov, S.; Voth, G.A.; Das, A.; Andersen, H.C. The multiscale coarse-graining method. I. A rigorous bridge between atomistic and coarse-grained models. *J. Chem. Phys.* **2008**, *128*, 244114. [CrossRef] [PubMed]
334. Noid, W.G.; Chu, J.-W.; Ayton, G.S.; Voth, G.A. Multiscale coarse-graining and structural correlations: Connections to liquid-state theory. *J. Phys. Chem. B* **2007**, *111*, 4116–4127. [CrossRef] [PubMed]
335. Noid, W.G.; Liu, P.; Wang, Y.; Chu, J.-W.; Ayton, G.S.; Izvekov, S.; Andersen, H.C.; Voth, G.A. The multiscale coarse-graining method. II. Numerical implementation for coarse-grained molecular models. *J. Chem. Phys.* **2008**, *128*, 244115. [CrossRef] [PubMed]
336. Wu, C. Phase morphologies of binary polymer blends predicted by systematically coarse-grained models. *Macromol. Theory Simul.* **2016**. [CrossRef]
337. Potestio, R.; Peter, C.; Kremer, K. Computer simulations of soft matter: Linking the scales. *Entropy* **2014**, *16*, 4199–4245. [CrossRef]
338. Rzepiela, A.J.; Louhivuori, M.; Peter, C.; Marrink, S.J. Hybrid simulations: Combining atomistic and coarse-grained force fields using virtual sites. *Phys. Chem. Chem. Phys.* **2011**, *13*, 10437–10448. [CrossRef] [PubMed]
339. Li, Y.; Tang, S.; Abberton, B.C.; Kröger, M.; Burkhart, C.; Jiang, B.; Papakonstantopoulos, G.J.; Poldneff, M.; Liu, W.K. A predictive multiscale computational framework for viscoelastic properties of linear polymers. *Polymer* **2012**, *53*, 5935–5952. [CrossRef]
340. Noid, W.G. Perspective: Coarse-grained models for biomolecular systems. *J. Chem. Phys.* **2013**, *139*. [CrossRef] [PubMed]
341. Rudzinski, J.F.; Noid, W.G. Investigation of coarse-grained mappings via an iterative generalized Yvon-Born-Green method. *J. Phys. Chem. B* **2014**, *118*, 8295–8312. [CrossRef] [PubMed]
342. Torrie, G.M.; Valleau, J.P. Nonphysical sampling distributions in Monte Carlo free-energy estimation: Umbrella sampling. *J. Comput. Phys.* **1977**, *23*, 187–199. [CrossRef]
343. Den Otter, W.K.; Briels, W.J. The calculation of free-energy differences by constrained molecular-dynamics simulations. *J. Chem. Phys.* **1998**, *109*, 4139–4146. [CrossRef]
344. Villa, A.; Peter, C.; van der Vegt, N. Transferability of nonbonded interaction potentials for coarse-grained simulations: Benzene in water. *J. Chem. Theory Comput.* **2010**, *6*, 2434–2444. [CrossRef] [PubMed]
345. Hahn, O.; Site, L.D.; Kremer, K. Simulation of polymer melts: From spherical to ellipsoidal beads. *Macromol. Theory Simul.* **2001**, *10*, 288–303. [CrossRef]
346. Xie, G.-L.; Zhang, Y.-H.; Huang, S.-P. Glass formation of n-butanol: Coarse-grained molecular dynamics simulations using gay-berne potential model. *Chin. J. Chem. Phys.* **2012**, *25*, 177–185. [CrossRef]
347. Müller-Plathe, F. Local structure and dynamics in solvent-swollen polymers. *Macromolecules* **1996**, *29*, 4782–4791. [CrossRef]
348. Milano, G.; Müller-Plathe, F. Mapping atomistic simulations to mesoscopic models: A systematic coarse-graining procedure for vinyl polymer chains. *J. Phys. Chem. B* **2005**, *109*, 18609–18619. [CrossRef] [PubMed]

349. Milano, G.; Goudeau, S.; Müller-Plathe, F. Multicentered Gaussian-based potentials for coarse-grained polymer simulations: Linking atomistic and mesoscopic scales. *J. Polym. Sci. Part B* **2005**, *43*, 871–885. [CrossRef]

350. Spyriouni, T.; Tzoumanekas, C.; Theodorou, D.; Müller-Plathe, F.; Milano, G. Coarse-grained and reverse-mapped united-atom simulations of long-chain atactic polystyrene melts: Structure, thermodynamic properties, chain conformation, and entanglements. *Macromolecules* **2007**, *40*, 3876–3885. [CrossRef]

351. Sun, Q.; Faller, R. Systematic coarse-graining of atomistic models for simulation of polymeric systems. *Comput. Chem. Eng.* **2005**, *29*, 2380–2385. [CrossRef]

352. Sun, Q.; Faller, R. Crossover from unentangled to entangled dynamics in a systematically coarse-grained polystyrene melt. *Macromolecules* **2006**, *39*, 812–820. [CrossRef]

353. Qian, H.-J.; Carbone, P.; Xiaoyu, C.; Karimi-Varzaneh, H.A.; Liew, C.C.; Müller-Plathe, F. Temperature-Transferable Coarse-Grained potentials for ethylbenzene, polystyrene, and their mixtures. *Macromolecules* **2008**, *41*, 9919–9929. [CrossRef]

354. Harmandaris, V.A.; Adhikari, N.P.; van der Vegt, N.; Kremer, K. Hierarchical modeling of polystyrene: From atomistic to coarse-grained simulations. *Macromolecules* **2006**, *39*, 6708–6719. [CrossRef]

355. Harmandaris, V.A.; Reith, D.; van der Vegt, N.; Kremer, K. Comparison between coarse-graining models for polymer systems: Two mapping schemes for polystyrene. *Macromol. Chem. Phys.* **2007**, *208*, 2109–2120. [CrossRef]

356. Fritz, D.; Harmandaris, V.A.; Kremer, K.; van der Vegt, N. Coarse-grained polymer melts based on isolated atomistic chains: Simulation of polystyrene of different tacticities. *Macromolecules* **2009**, *42*, 7579–7588. [CrossRef]

357. Mulder, T.; Harmandaris, V.A.; Lyulin, A.V.; van der Vegt, N.; Vorselaars, B.; Michels, M. Equilibration and deformation of amorphous polystyrene: Scale-jumping simulational approach. *Macromol. Theory Simul.* **2008**, *17*, 290–300. [CrossRef]

358. Mulder, T.; Harmandaris, V.A.; Lyulin, A.V.; van der Vegt, N.; Kremer, K.; Michels, M. Structural properties of atactic polystyrene of different thermal history obtained from a multiscale simulation. *Macromolecules* **2009**, *42*, 384–391. [CrossRef]

359. Harmandaris, V.A.; Kremer, K. Predicting polymer dynamics at multiple length and time scales. *Soft Matter* **2009**, *5*, 3920–3926. [CrossRef]

360. Harmandaris, V.A.; Kremer, K. Dynamics of polystyrene melts through hierarchical multiscale simulations. *Macromolecules* **2009**, *42*, 791–802. [CrossRef]

361. Karimi-Varzaneh, H.A.; van der Vegt, N.; Müller-Plathe, F.; Carbone, P. How good are coarse-grained polymer models? A comparison for atactic polystyrene. *ChemPhysChem* **2012**, *13*, 3428–3439. [CrossRef] [PubMed]

362. Batchelor, G.K. *An Introduction to Fluid Dynamics*; Cambridge University Press: New York, NY, USA, 2000.

363. Lyubimov, I.; Guenza, M.G. First-principle approach to rescale the dynamics of simulated coarse-grained macromolecular liquids. *Phys. Rev. E* **2011**, *84*. [CrossRef] [PubMed]

364. Lyubimov, I.Y.; McCarty, J.; Clark, A.; Guenza, M.G. Analytical rescaling of polymer dynamics from mesoscale simulations. *J. Chem. Phys.* **2010**, *132*. [CrossRef] [PubMed]

365. Lyubimov, I.Y.; Guenza, M.G. Theoretical reconstruction of realistic dynamics of highly coarse-grained cis-1,4-polybutadiene melts. *J. Chem. Phys.* **2013**, *138*. [CrossRef] [PubMed]

366. Fritz, D.; Koschke, K.; Harmandaris, V.A.; van der Vegt, N.; Kremer, K. Multiscale modeling of soft matter: Scaling of dynamics. *Phys. Chem. Chem. Phys.* **2011**, *13*, 10412–10420. [CrossRef] [PubMed]

367. Colmenero, J.; Arbe, A. Segmental dynamics in miscible polymer blends: Recent results and open questions. *Soft Matter* **2007**, *3*, 1474–1485. [CrossRef]

368. Roland, C.M.; Ngai, K.L. Dynamical heterogeneity in a miscible polymer blend. *Macromolecules* **1991**, *24*, 2261–2265. [CrossRef]

369. Harmandaris, V.A.; Kremer, K.; Floudas, G. Dynamic heterogeneity in fully miscible blends of polystyrene with oligostyrene. *Phys. Rev. Lett.* **2013**, *110*. [CrossRef] [PubMed]

370. Louis, A.A. Beware of density dependent pair potentials. *J. Phys.* **2002**, *14*, 9187–9206. [CrossRef]

371. Eslami, H.; Karimi-Varzaneh, H.A.; Müller-Plathe, F. Coarse-grained computer simulation of nanoconfined polyamide-6,6. *Macromolecules* **2011**, *44*, 3117–3128. [CrossRef]

372. Bayramoglu, B.; Faller, R. Coarse-grained modeling of polystyrene in various environments by iterative Boltzmann inversion. *Macromolecules* **2012**, *45*, 9205–9219. [CrossRef]

373. Fukunaga, H.; Takimoto, J.-I.; Doi, M. A coarse-graining procedure for flexible polymer chains with bonded and nonbonded interactions. *J. Chem. Phys.* **2002**, *116*, 8183–8190. [CrossRef]

374. Carbone, P.; Varzaneh, H.; Chen, X.; Müller-Plathe, F. Transferability of coarse-grained force fields: The polymer case. *J. Chem. Phys.* **2008**, *128*. [CrossRef] [PubMed]

375. Harmandaris, V.A.; Floudas, G.; Kremer, K. Temperature and pressure dependence of polystyrene dynamics through molecular dynamics simulations and experiments. *Macromolecules* **2011**, *44*, 393–402. [CrossRef]

376. Strauch, T.; Yelash, L.; Paul, W. A coarse-graining procedure for polymer melts applied to 1,4-polybutadiene. *Phys. Chem. Chem. Phys.* **2009**, *11*, 1942–1948. [CrossRef] [PubMed]

377. Vettorel, T.; Meyer, H. Coarse graining of short polythylene chains for studying polymer crystallization. *J. Chem. Theory Comput.* **2006**, *2*, 616–629. [CrossRef] [PubMed]

378. Yelash, L.; Müller, M.; Paul, W.; Binder, K. How well can coarse-grained models of real polymers describe their structure? The case of polybutadiene. *J. Chem. Theory Comput.* **2006**, *2*, 588–597. [CrossRef] [PubMed]

379. Fu, C.-C.; Kulkarni, P.M.; Scott Shell, M.; Gary Leal, L. A test of systematic coarse-graining of molecular dynamics simulations: Thermodynamic properties. *J. Chem. Phys.* **2012**, *137*. [CrossRef] [PubMed]

380. Baron, R.; Trzesniak, D.; de Vries, A.H.; Elsener, A.; Marrink, S.J.; van Gunsteren, W.F. Comparison of thermodynamic properties of coarse-grained and atomic-level simulation models. *ChemPhysChem* **2007**, *8*, 452–461. [CrossRef] [PubMed]

381. Betancourt, M.R.; Omovie, S.J. Pairwise energies for polypeptide coarse-grained models derived from atomic force fields. *J. Chem. Phys.* **2009**, *130*. [CrossRef] [PubMed]

382. Mullinax, J.W.; Noid, W.G. Extended ensemble approach for deriving transferable coarse-grained potentials. *J. Chem. Phys.* **2009**, *131*. [CrossRef]

383. Patrone, P.N.; Rosch, T.W.; Phelan, F.R., Jr. Bayesian calibration of coarse-grained forces: Efficiently addressing transferability. *J. Chem. Phys.* **2016**, *144*. [CrossRef] [PubMed]

384. Unadkat, J.D.; Beal, S.L.; Sheiner, L.B. Bayesian calibration. *Anal. Chim. Acta* **1986**, *181*, 27–36. [CrossRef]

385. Padding, J.T.; Briels, W.J. Uncrossability constraints in mesoscopic polymer melt simulations: Non-rouse behavior of C120H242. *J. Chem. Phys.* **2001**, *115*, 2846–2859. [CrossRef]

386. Padding, J.T.; Briels, W.J. Time and length scales of polymer melts studied by coarse-grained molecular dynamics simulations. *J. Chem. Phys.* **2002**, *117*, 925–943. [CrossRef]

387. Padding, J.T.; Briels, W.J.; Stukan, M.R.; Boek, E.S. Review of multi-scale particulate simulation of the rheology of wormlike micellar fluids. *Soft Matter* **2009**, *5*, 4367–4375. [CrossRef]

388. Padding, J.T.; Briels, W.J. Coarse-grained molecular dynamics simulations of polymer melts in transient and steady shear flow. *J. Chem. Phys.* **2003**, *118*, 10276–10286. [CrossRef]

389. Pérez-Aparicio, R.; Colmenero, J.; Alvarez, F.; Padding, J.T.; Briels, W.J. Chain dynamics of poly(ethylene-alt-propylene) melts by means of coarse-grained simulations based on atomistic molecular dynamics. *J. Chem. Phys.* **2010**, *132*. [CrossRef] [PubMed]

390. Liu, L.; Padding, J.T.; Den Otter, W.K.; Briels, W.J. Coarse-grained simulations of moderately entangled star polyethylene melts. *J. Chem. Phys.* **2013**, *138*. [CrossRef] [PubMed]

391. Maiti, A.; McGrother, S. Bead-bead interaction parameters in dissipative particle dynamics: Relation to bead-size, solubility parameter, and surface tension. *J. Chem. Phys.* **2004**, *120*, 1594–1601. [CrossRef] [PubMed]

392. Kacar, G.; Peters, E.; de With, G. A generalized method for parameterization of dissipative particle dynamics for variable bead volumes. *Europhys. Lett.* **2013**, *102*. [CrossRef]

393. Johnston, K.; Harmandaris, V. Hierarchical multiscale modeling of polymer-solid interfaces: Atomistic to coarse-grained description and structural and conformational properties of polystyrene-gold systems. *Macromolecules* **2013**, *46*, 5741–5750. [CrossRef]

394. Pan, G.; Manke, C.W. Developments toward simulation of entangled polymer melts by dissipative particle dynamics (DPD). *Int. J. Mod. Phys. B* **2003**, *17*, 231–235. [CrossRef]

395. Sirk, T.W.; Slizoberg, Y.R.; Brennan, J.K.; Lisal, M.; Andzelm, J.W. An enhanced entangled polymer model for dissipative particle dynamics. *J. Chem. Phys.* **2012**, *136*, 134903. [CrossRef] [PubMed]

396. Nikunen, P.; Vattulainen, I.; Karttunen, M. Reptational dynamics in dissipative particle dynamics simulations of polymer melts. *Phys. Rev. E* **2007**, *75*, 36713. [CrossRef] [PubMed]

397. Doi, M.; Edwards, S.F. *The Theory of Polymer Dynamics*; Clarendon Press: Oxford, UK, 1986.

398. Gooneie, A.; Schuschnigg, S.; Holzer, C. Coupled orientation and stretching of chains in mesoscale models of polydisperse linear polymers in startup of steady shear flow simulations. *Macromol. Theory Simul.* **2016**, *25*, 170–186. [CrossRef]

399. Murat, M.; Kremer, K. From many monomers to many polymers: Soft ellipsoid model for polymer melts and mixtures. *J. Chem. Phys.* **1998**, *108*, 4340–4348. [CrossRef]

400. D'Adamo, G.; Pelissetto, A.; Pierleoni, C. Coarse-graining strategies in polymer solutions. *Soft Matter* **2012**, *8*, 5151–5167. [CrossRef]

401. D'Adamo, G.; Pelissetto, A.; Pierleoni, C. Polymers as compressible soft spheres. *J. Chem. Phys.* **2012**, *136*. [CrossRef] [PubMed]

402. Vettorel, T.; Besold, G.; Kremer, K. Fluctuating soft-sphere approach to coarse-graining of polymer models. *Soft Matter* **2010**, *6*, 2282–2292. [CrossRef]

403. Zhang, G.; Daoulas, K.C.; Kremer, K. A New Coarse Grained Particle-To-Mesh Scheme for Modeling Soft Matter. *Macromol. Chem. Phys.* **2013**, *214*, 214–224. [CrossRef]

404. Kindt, P.; Briels, W.J. A single particle model to simulate the dynamics of entangled polymer melts. *J. Chem. Phys.* **2007**, *127*. [CrossRef] [PubMed]

405. Briels, W.J. Transient forces in flowing soft matter. *Soft Matter* **2009**, *5*, 4401–4411. [CrossRef]

406. Zhu, Y.-L.; Liu, H.; Lu, Z.-Y. A highly coarse-grained model to simulate entangled polymer melts. *J. Chem. Phys.* **2012**, *136*. [CrossRef] [PubMed]

407. Sprakel, J.; Padding, J.T.; Briels, W.J. Transient forces and non-equilibrium states in sheared polymer networks. *Europhys. Lett.* **2011**, *93*. [CrossRef]

408. Sprakel, J.; Spruijt, E.; van der Gucht, J.; Padding, J.T.; Briels, W.J. Failure-mode transition in transient polymer networks with particle-based simulations. *Soft Matter* **2009**, *5*, 4748–4756. [CrossRef]

409. Savin, T.; Briels, W.J.; öttinger, H.C. Thermodynamic formulation of flowing soft matter with transient forces. *Rheol. Acta* **2013**, *52*, 23–32. [CrossRef]

410. Padding, J.T.; van Ruymbeke, E.; Vlassopoulos, D.; Briels, W.J. Computer simulation of the rheology of concentrated star polymer suspensions. *Rheol. Acta* **2010**, *49*, 473–484. [CrossRef]

411. Padding, J.T.; Mohite, L.V.; Auhl, D.; Briels, W.J.; Bailly, C. Mesoscale modeling of the rheology of pressure sensitive adhesives through inclusion of transient forces. *Soft Matter* **2011**, *7*, 5036–5046. [CrossRef]

412. Padding, J.T.; Mohite, L.V.; Auhl, D.; Schweizer, T.; Briels, W.J.; Bailly, C. Quantitative mesoscale modeling of the oscillatory and transient shear rheology and the extensional rheology of pressure sensitive adhesives. *Soft Matter* **2012**, *8*, 7967–7981. [CrossRef]

413. Schweizer, K.S.; Curro, J.G. Integral equation theories of the structure, thermodynamics, and phase transitions of polymer fluids. *Adv. Chem. Phys.* **1997**, *98*, 1–142.

414. McCarty, J.; Guenza, M.G. Multiscale modeling of binary polymer mixtures: Scale bridging in the athermal and thermal regime. *J. Chem. Phys.* **2010**, *133*. [CrossRef] [PubMed]

415. McCarty, J.; Lyubimov, I.Y.; Guenza, M.G. Effective soft-core potentials and mesoscopic simulations of binary polymer mixtures. *Macromolecules* **2010**, *43*, 3964–3979. [CrossRef]

416. McCarty, J.; Lyubimov, I.Y.; Guenza, M.G. Multiscale modeling of coarse-grained macromolecular liquids. *J. Phys. Chem. B* **2009**, *113*, 11876–11886. [CrossRef] [PubMed]

417. Guenza, M.G. Theoretical models for bridging timescales in polymer dynamics. *J. Phys.: Condens. Matter* **2007**, *20*, 033101. [CrossRef]

418. Clark, A.J.; McCarty, J.; Lyubimov, I.Y.; Guenza, M.G. Thermodynamic consistency in variable-level coarse graining of polymeric liquids. *Phys. Rev. Lett.* **2012**, *109*. [CrossRef] [PubMed]

419. McCarty, J.; Clark, A.J.; Lyubimov, I.Y.; Guenza, M.G. Thermodynamic consistency between analytic integral equation theory and coarse-grained molecular dynamics simulations of homopolymer melts. *Macromolecules* **2012**, *45*, 8482–8493. [CrossRef]

420. Santangelo, G.; Di Matteo, A.; Müller-Plathe, F.; Milano, G. From mesoscale back to atomistic models: A fast reverse-mapping procedure for vinyl polymer chains. *J. Phys. Chem. B* **2007**, *111*, 2765–2773. [CrossRef] [PubMed]

421. Parker, A.J.; Rottler, J. Using soft potentials for the simulation of block copolymer morphologies. *Macromol. Theory Simul.* **2014**, *23*, 401–409. [CrossRef]

422. Sliozberg, Y.R.; Kröger, M.; Chantawansri, T.L. Fast equilibration protocol for million atom systems of highly entangled linear polyethylene chains. *J. Chem. Phys.* **2016**, *144*. [CrossRef] [PubMed]

423. Chen, X.; Carbone, P.; Santangelo, G.; Di Matteo, A.; Milano, G.; Müller-Plathe, F. Backmapping coarse-grained polymer models under sheared nonequilibrium conditions. *Phys. Chem. Chem. Phys.* **2009**, *11*, 1977–1988. [CrossRef] [PubMed]

424. Carbone, P.; Ali Karimi-Varzaneh, H.; Müller-Plathe, F. Fine-graining without coarse-graining: An easy and fast way to equilibrate dense polymer melts. *Faraday Discuss.* **2009**, *144*, 25–42. [CrossRef]

425. Tschöp, W.; Kremer, K.; Halm, O.; Batoulis, J.; Bürger, T. Simulation of polymer melts. II. From coarse-grained models back to atomistic description. *Acta Polym.* **1998**, *49*, 75–79. [CrossRef]

426. Kotelyanskii, M.; Wagner, N.J.; Paulaitis, M.E. Building large amorphous polymer structures: Atomistic simulation of glassy polystyrene. *Macromolecules* **1996**, *29*, 8497–8506. [CrossRef]

427. Harmandaris, V.A.; Mavrantzas, V.G.; Theodorou, D.N. Atomistic molecular dynamics simulation of stress relaxation upon cessation of steady-state uniaxial elongational flow. *Macromolecules* **2000**, *33*, 8062–8076. [CrossRef]

428. Queyroy, S.; Neyertz, S.; Brown, D.; Müller-Plathe, F. Preparing relaxed systems of amorphous polymers by multiscale simulation: Application to cellulose. *Macromolecules* **2004**, *37*, 7338–7350. [CrossRef]

429. Hess, B.; León, S.; van der Vegt, N.; Kremer, K. Long time atomistic polymer trajectories from coarse grained simulations: Bisphenol-A polycarbonate. *Soft Matter* **2006**, *2*, 409–414. [CrossRef]

430. Karimi-Varzaneh, H.A.; Carbone, P.; Müller-Plathe, F. Fast dynamics in coarse-grained polymer models: The effect of the hydrogen bonds. *J. Chem. Phys.* **2008**, *129*. [CrossRef] [PubMed]

431. Wu, C. Multiscale simulations of the structure and dynamics of stereoregular poly(methyl methacrylate)s. *J. Mol. Model.* **2014**, *20*. [CrossRef] [PubMed]

432. Handgraaf, J.-W.; Serral Gracia, R.; Nath, S.K.; Chen, Z.; Chou, S.-H.; Ross, R.B.; Schultz, N.E.; Fraaije, J. A multiscale modeling protocol to generate realistic polymer surfaces. *Macromolecules* **2011**, *44*, 1053–1061. [CrossRef]

433. Bleha, T.; Gajdos, J.; Karasz, F.E. Energetics of strain-induced conformational transitions in polymethylene chains. *Macromolecules* **1990**, *23*, 4076–4082. [CrossRef]

434. Ghanbari, A.; Böhm, M.C.; Müller-Plathe, F. A simple reverse mapping procedure for coarse-grained polymer models with rigid side groups. *Macromolecules* **2011**, *44*, 5520–5526. [CrossRef]

435. Abraham, F.F.; Broughton, J.Q.; Bernstein, N.; Kaxiras, E. Spanning the length scales in dynamic simulation. *Comput. Phys.* **1998**, *12*, 538–546. [CrossRef]

436. Stillinger, F.H.; Weber, T.A. Computer simulation of local order in condensed phases of silicon. *Phys. Rev. B Condens. Matter Mater. Phys.* **1985**, *31*, 5262–5271. [CrossRef]

437. Rudd, R.E.; Broughton, J.Q. Concurrent coupling of length scales in solid state systems. *Phys. Status Solidi B* **2000**, *217*, 251–291. [CrossRef]

438. Nakano, A.; Bachlechner, M.E.; Kalia, R.K.; Lidorikis, E.; Vashishta, P.; Voyiadjis, G.Z.; Campbell, T.J.; Ogata, S.; Shimojo, F. Multiscale simulation of nanosystems. *Comput. Sci. Eng.* **2001**, *3*, 56–66. [CrossRef]

439. Broughton, J.Q.; Abraham, F.F.; Bernstein, N.; Kaxiras, E. Concurrent coupling of length scales: Methodology and application. *Phys. Rev. B Condens. Matter Mater. Phys.* **1999**, *60*, 2391–2403. [CrossRef]

440. Abraham, F.F.; Broughton, J.Q.; Bernstein, N.; Kaxiras, E. Spanning the continuum to quantum length scales in a dynamic simulation of brittle fracture. *Europhys. Lett.* **1998**, *44*, 783–787. [CrossRef]

441. Curtin, W.A.; Miller, R.E. Atomistic/continuum coupling in computational materials science. *Model. Simul. Mater. Sci. Eng.* **2003**, *11*, R33–R68. [CrossRef]

442. Miller, R.E.; Tadmor, E.B. A unified framework and performance benchmark of fourteen multiscale atomistic/continuum coupling methods. *Model. Simul. Mater. Sci. Eng.* **2009**, *17*, 53001. [CrossRef]

443. Badia, S.; Parks, M.; Bochev, P.; Gunzburger, M.; Lehouc, Q. On atomistic-to-continuum coupling by blending. *Multiscale Model. Simul.* **2008**, *7*, 381–406. [CrossRef]

444. Shenoy, V.B.; Miller, R.; Tadmor, E.B.; Rodney, D.; Phillips, R.; Ortiz, M. An adaptive finite element approach to atomic-scale mechanics—The quasicontinuum method. *J. Mech. Phys. Solids* **1999**, *47*, 611–642. [CrossRef]

445. Li, X.; Ming, P. On the effect of ghost force in the quasicontinuum method: Dynamic problems in one dimension. *Commun. Comput. Phys.* **2014**, *15*, 647–676. [CrossRef]

446. Ortner, C.; Zhang, L. Atomistic/continuum blending with ghost force correction. *Siam J. Sci. Comput.* **2016**, *38*, A346–A375. [CrossRef]

447. Shimokawa, T.; Mortensen, J.J.; Schiøtz, J.; Jacobsen, K.W. Matching conditions in the quasicontinuum method: Removal of the error introduced at the interface between the coarse-grained and fully atomistic region. *Phys. Rev. B Condens. Matter Mater. Phys.* **2004**, *69*, 214104. [CrossRef]

448. Lu, J.; Yang, J.Z. Uniform accuracy of the quasicontinuum method. *Phys. Rev. B* **2006**, *74*. [CrossRef]

449. Klein, P.A.; Zimmerman, J.A. Coupled atomistic-continuum simulations using arbitrary overlapping domains. *J. Comput. Phys.* **2006**, *213*, 86–116. [CrossRef]

450. Tadmor, E.B.; Ortiz, M.; Phillips, R. Quasicontinuum analysis of defects in solids. *Philos. Mag. A Phys. Condens. Matter Struct. Defects Mech. Prop.* **1996**, *73*, 1529–1563. [CrossRef]

451. Tadmor, E.B.; Phillips, R.; Ortiz, M. Mixed atomistic and continuum models of deformation in solids. *Langmuir* **1996**, *12*, 4529–4532. [CrossRef]

452. Rudd, R.E.; Broughton, J.Q. Coarse-grained molecular dynamics and the atomic limit of finite elements. *Phys. Rev. B* **1998**, *58*, R5893–R5896. [CrossRef]

453. Shenoy, V.B.; Miller, R.; Tadmor, E.B.; Phillips, R.; Ortiz, M. Quasicontinuum models of interfacial structure and deformation. *Phys. Rev. Lett.* **1998**, *80*, 742–745. [CrossRef]

454. Rodney, D.; Martin, G. Dislocation pinning by small interstitial loops: A molecular dynamics study. *Phys. Rev. Lett.* **1999**, *82*, 3272–3275. [CrossRef]

455. Rodney, D.; Phillips, R. Structure and Strength of Dislocation Junctions: An Atomic Level Analysis. *Phys. Rev. Lett.* **1999**, *82*, 1704–1707. [CrossRef]

456. Tadmor, E.B.; Smith, G.S.; Bernstein, N.; Kaxiras, E. Mixed finite element and atomistic formulation for complex crystals. *Phys. Rev. B* **1999**, *59*, 235–245. [CrossRef]

457. Miller, R.; Ortiz, M.; Phillips, R.; Shenoy, V.; Tadmor, E.B. Quasicontinuum models of fracture and plasticity. *Eng. Fract. Mech.* **1998**, *61*, 427–444. [CrossRef]

458. Miller, R.; Tadmor, E.B.; Phillips, R.; Ortiz, M. Quasicontinuum simulation of fracture at the atomic scale. *Model. Simul. Mater. Sci. Eng.* **1998**, *6*, 607–638. [CrossRef]

459. Tadmor, E.B.; Miller, R.; Phillips, R.; Ortiz, M. Nanoindentation and incipient plasticity. *J. Mater. Res.* **1999**, *14*, 2233–2250. [CrossRef]

460. Binder, A.; Luskin, M.; Perez, D.; Voter, A.F. Analysis of transition state theory rates upon spatial coarse-graining. *Multiscale Model. Simul.* **2015**, *13*, 890–915. [CrossRef]

461. Eidel, B.; Stukowski, A. A variational formulation of the quasicontinuum method based on energy sampling in clusters. *J. Mech. Phys. Solids* **2009**, *57*, 87–108. [CrossRef]

462. Miller, R.E.; Tadmor, E.B. Hybrid continuum mechanics and atomistic methods for simulating materials deformation and failure. *MRS Bull.* **2007**, *32*, 920–926. [CrossRef]

463. Iacobellis, V.; Behdinan, K. Comparison of concurrent multiscale methods in the application of fracture in nickel. *J. Appl. Mech. Trans. ASME* **2013**, *80*. [CrossRef]

464. Xiao, S.P.; Belytschko, T. A bridging domain method for coupling continua with molecular dynamics. *Comput. Methods Appl. Mech. Eng.* **2004**, *193*, 1645–1669. [CrossRef]

465. Datta, D.K.; Picu, C.; Shephard, M.S. Composite Grid Atomistic Continuum Method: An Adaptive Approach to Bridge Continuum with Atomistic Analysis. *Int. J. Multiscale Comput. Eng.* **2004**, *2*, 71–90. [CrossRef]

466. Rudd, R.E.; Broughton, J.Q. Coarse-grained molecular dynamics: Nonlinear finite elements and finite temperature. *Phys. Rev. B Condens. Matter Mater. Phys.* **2005**, *72*. [CrossRef]

467. Curtarolo, S.; Ceder, G. Dynamics of an inhomogeneously coarse grained multiscale system. *Phys. Rev. Lett.* **2002**, *88*, 2555041–2555044. [CrossRef] [PubMed]

468. Dupuy, L.M.; Tadmor, E.B.; Miller, R.E.; Phillips, R. Finite-temperature quasicontinuum: Molecular dynamics without all the atoms. *Phys. Rev. Lett.* **2005**, *95*. [CrossRef] [PubMed]

469. Tang, Z.; Zhao, H.; Li, G.; Aluru, N.R. Finite-temperature quasicontinuum method for multiscale analysis of silicon nanostructures. *Phys. Rev. B Condens. Matter Mater. Phys.* **2006**, *74*. [CrossRef]

470. Marian, J.; Venturini, G.; Hansen, B.L.; Knap, J.; Ortiz, M.; Campbell, G.H. Finite-temperature extension of the quasicontinuum method using Langevin dynamics: Entropy losses and analysis of errors. *Model. Simul. Mater. Sci. Eng.* **2010**, *18*. [CrossRef]

471. Kohlhoff, S.; Gumbsch, P.; Fischmeister, H.F. Crack propagation in b.c.c. crystals studied with a combined finite-element and atomistic model. *Philos. Mag. A Phys. Condens. Matter Struct. Defects Mech. Prop.* **1991**, *64*, 851–878. [CrossRef]

472. Shilkrot, L.E.; Miller, R.E.; Curtin, W.A. Coupled atomistic and discrete dislocation plasticity. *Phys. Rev. Lett.* **2002**, *89*, 255011–255014. [CrossRef] [PubMed]

473. Shilkrot, L.E.; Miller, R.E.; Curtin, W.A. Multiscale plasticity modeling: Coupled atomistics and discrete dislocation mechanics. *J. Mech. Phys. Solids* **2004**, *52*, 755–787. [CrossRef]

474. Luan, B.Q.; Hyun, S.; Molinari, J.F.; Bernstein, N.; Robbins, M.O. Multiscale modeling of two-dimensional contacts. *Phys. Rev. E Stat. Nonlinear Soft Matter Phys.* **2006**, *74*. [CrossRef] [PubMed]

475. Badia, S.; Bochev, P.; Lehoucq, R.; Parks, M.L.; Fish, J.; Nuggehally, M.A.; Gunzburger, M. A force-based blending model foratomistic-to-continuum coupling. *Int. J. Multiscale Comput. Eng.* **2007**, *5*, 387–406. [CrossRef]

476. Fish, J.; Nuggehally, M.A.; Shephard, M.S.; Picu, C.R.; Badia, S.; Parks, M.L.; Gunzburger, M. Concurrent AtC coupling based on a blend of the continuum stress and the atomistic force. *Comput. Methods Appl. Mech. Eng.* **2007**, *196*, 4548–4560. [CrossRef]

477. Hughes, T.; Feijóo, G.R.; Mazzei, L.; Quincy, J.-B. The variational multiscale method—A paradigm for computational mechanics. *Comput. Methods Appl. Mech. Eng.* **1998**, *166*, 3–24. [CrossRef]

478. Qian, D.; Wagner, G.J.; Liu, W.K. A multiscale projection method for the analysis of carbon nanotubes. *Comput. Methods Appl. Mech. Eng.* **2004**, *193*, 1603–1632. [CrossRef]

479. Wagner, G.J.; Liu, W.K. Coupling of atomistic and continuum simulations using a bridging scale decomposition. *J. Comput. Phys.* **2003**, *190*, 249–274. [CrossRef]

480. Park, H.S.; Liu, W.K. An introduction and tutorial on multiple-scale analysis in solids. *Comput. Methods Appl. Mech. Eng.* **2004**, *193*, 1733–1772. [CrossRef]

481. Tan, V.; Zeng, X.S.; Deng, M.; Lim, K.M.; Tay, T.E. Multiscale modeling of polymers—The Pseudo Amorphous Cell. *Comput. Methods Appl. Mech. Eng.* **2008**, *197*, 536–554. [CrossRef]

482. Theodorou, D.N.; Suter, U.W. Detailed molecular structure of a vinyl polymer glass. *Macromolecules* **1985**, *18*, 1467–1478. [CrossRef]

483. Theodorou, D.N.; Suter, U.W. Geometrical considerations in model systems with periodic boundaries. *J. Chem. Phys.* **1985**, *82*, 955–966. [CrossRef]

484. Su, Z.C.; Tay, T.-E.; Chen, Y.; Tan, V. Multiscale modeling for amorphous materials—Mapping atomistic displacements to macroscopic deformation. *Intl. J. Appl. Mech.* **2012**, *4*. [CrossRef]

485. Codina, R. Stabilization of incompressibility and convection through orthogonal sub-scales in finite element methods. *Comput. Methods Appl. Mech. Eng.* **2000**, *190*, 1579–1599. [CrossRef]

486. Castillo, E.; Codina, R. Stabilized stress-velocity-pressure finite element formulations of the Navier-Stokes problem for fluids with non-linear viscosity. *Comput. Methods Appl. Mech. Eng.* **2014**, *279*, 554–578. [CrossRef]

487. Castillo, E.; Codina, R. Variational multi-scale stabilized formulations for the stationary three-field incompressible viscoelastic flow problem. *Comput. Methods Appl. Mech. Eng.* **2014**, *279*, 579–605. [CrossRef]

488. Koo, B.; Subramanian, N.; Chattopadhyay, A. Molecular dynamics study of brittle fracture in epoxy-based thermoset polymer. *Compos. Part B* **2016**, *95*, 433–439. [CrossRef]

489. Büyüköztürk, O.; Buehler, M.J.; Lau, D.; Tuakta, C. Structural solution using molecular dynamics: Fundamentals and a case study of epoxy-silica interface. *Int. J. Solids Struct.* **2011**, *48*, 2131–2140. [CrossRef]

490. Jo, W.H.; Yang, J.S. Molecular simulation approaches for multiphase polymer systems. In *Molecular Simulation Fracture Gel Theory*; Springer: Berlin, Germany, 2002.

491. Li, C.; Chou, T.-W. Elastic moduli of multi-walled carbon nanotubes and the effect of van der Waals forces. *Compos. Sci. Technol.* **2003**, *63*, 1517–1524. [CrossRef]

492. Li, C.; Chou, T.-W. Multiscale modeling of compressive behavior of carbon nanotube/polymer composites. *Compos. Sci. Technol.* **2006**, *66*, 2409–2414. [CrossRef]

493. Montazeri, A.; Naghdabadi, R. Study the effect of viscoelastic matrix model on the stability of CNT/polymer composites by multiscale modeling. *Polym. Compos.* **2009**, *30*, 1545–1551. [CrossRef]

494. De, S.; Fish, J.; Shephard, M.S.; Keblinski, P.; Kumar, S.K. Multiscale modeling of polymer rheology. *Phys. Rev. E* **2006**, *74*, 30801. [CrossRef] [PubMed]

495. Guenza, M.G. Advancements in multi scale modeling: Adaptive resolution simulations and related issues. *Eur. Phys. J.* **2015**, *224*, 2491–2495. [CrossRef]

496. Kreis, K.; Fogarty, A.C.; Kremer, K.; Potestio, R. Advantages and challenges in coupling an ideal gas to atomistic models in adaptive resolution simulations. *Eur. Phys. J.* **2015**, *224*, 2289–2304. [CrossRef]

497. Zavadlav, J.; Podgornik, R.; Praprotnik, M. Adaptive resolution simulation of a DNA molecule in salt solution. *J. Chem. Theory Comput.* **2015**, *11*, 5035–5044. [CrossRef] [PubMed]

498. Wang, H.; Agarwal, A. Adaptive resolution simulation in equilibrium and beyond. *Eur. Phys. J.* **2015**, *224*, 2269–2287. [CrossRef]

499. Youn Park, J.; Park, C.-H.; Shin Park, J.; Kong, K.-J.; Chang, H.; Im, S. Multiscale computations for carbon nanotubes based on a hybrid QM/QC (quantum mechanical and quasicontinuum) approach. *J. Mech. Phys. Solids* **2010**, *58*, 86–102. [CrossRef]

500. Praprotnik, M.; Delle Site, L.; Kremer, K. A macromolecule in a solvent: Adaptive resolution molecular dynamics simulation. *J. Chem. Phys.* **2007**, *126*, 134902. [CrossRef] [PubMed]

501. Nielsen, S.O.; Srinivas, G.; Klein, M.L. Incorporating a hydrophobic solid into a coarse grain liquid framework: Graphite in an aqueous amphiphilic environment. *J. Chem. Phys.* **2005**, *123*, 124907. [CrossRef] [PubMed]

502. Praprotnik, M.; Delle Site, L.; Kremer, K. Adaptive resolution molecular-dynamics simulation: Changing the degrees of freedom on the fly. *J. Chem. Phys.* **2005**, *123*. [CrossRef] [PubMed]

503. Praprotnik, M.; Delle Site, L.; Kremer, K. Adaptive resolution scheme for efficient hybrid atomistic-mesoscale molecular dynamics simulations of dense liquids. *Phys. Rev. E* **2006**, *73*. [CrossRef] [PubMed]

504. Praprotnik, M.; Matysiak, S.; Site, L.D.; Kremer, K.; Clementi, C. Adaptive resolution simulation of liquid water. *J. Phys.* **2007**, *19*. [CrossRef]

505. Praprotnik, M.; Site, L.D.; Kremer, K. Multiscale simulation of soft matter: From scale bridging to adaptive resolution. *Annu. Rev. Phys. Chem.* **2008**, *59*, 545–571. [CrossRef] [PubMed]

506. Praprotnik, M.; Poblete, S.; Delle Site, L.; Kremer, K. Comment on "adaptive multiscale molecular dynamics of macromolecular fluids". *Phys. Rev. Lett.* **2011**, *107*. [CrossRef] [PubMed]

507. Delle Site, L.; Leon, S.; Kremer, K. BPA-PC on a Ni(111) Surface: The Interplay between Adsorption Energy and Conformational Entropy for Different Chain-End Modifications. *J. Am. Chem. Soc.* **2004**, *126*, 2944–2955. [CrossRef] [PubMed]

508. Fritsch, S.; Poblete, S.; Junghans, C.; Ciccotti, G.; Delle Site, L.; Kremer, K. Adaptive resolution molecular dynamics simulation through coupling to an internal particle reservoir. *Phys. Rev. Lett.* **2012**, *108*. [CrossRef] [PubMed]

509. Delle Site, L. Some fundamental problems for an energy-conserving adaptive-resolution molecular dynamics scheme. *Phys. Rev. E* **2007**, *76*. [CrossRef] [PubMed]

510. Poma, A.B.; Delle Site, L. Classical to path-integral adaptive resolution in molecular simulation: Towards a smooth quantum-classical coupling. *Phys. Rev. Lett.* **2010**, *104*. [CrossRef] [PubMed]

511. Fritsch, S.; Junghans, C.; Kremer, K. Structure formation of toluene around C60: Implementation of the adaptive resolution scheme (AdResS) into GROMACS. *J. Chem. Theory Comput.* **2012**, *8*, 398–403. [CrossRef] [PubMed]

512. Poblete, S.; Praprotnik, M.; Kremer, K.; Delle Site, L. Coupling different levels of resolution in molecular simulations. *J. Chem. Phys.* **2010**, *132*. [CrossRef] [PubMed]

513. Mukherji, D.; van der Vegt, N.; Kremer, K. Preferential solvation of triglycine in aqueous urea: An open boundary simulation approach. *J. Chem. Theory Comput.* **2012**, *8*, 3536–3541. [CrossRef] [PubMed]

514. Lambeth, B.P., Jr.; Junghans, C.; Kremer, K.; Clementi, C.; Site, L.D. Communication: On the locality of Hydrogen bond networks at hydrophobic interfaces. *J. Chem. Phys.* **2010**, *133*, 221101. [CrossRef] [PubMed]

515. Poma, A.B.; Site, L.D. Adaptive resolution simulation of liquid para-hydrogen: Testing the robustness of the quantum-classical adaptive coupling. *Phys. Chem. Chem. Phys.* **2011**, *13*, 10510–10519. [CrossRef] [PubMed]

516. Potestio, R.; Delle Site, L. Quantum locality and equilibrium properties in low-temperature parahydrogen: A multiscale simulation study. *J. Chem. Phys.* **2012**, *136*, 54101. [CrossRef] [PubMed]

517. Mukherji, D.; van der Vegt, N.; Kremer, K.; Delle Site, L. Kirkwood-buff analysis of liquid mixtures in an open boundary simulation. *J. Chem. Theory Comput.* **2012**, *8*, 375–379. [CrossRef] [PubMed]

518. Mukherji, D.; Kremer, K. Coil-globule-coil transition of PNIPAm in aqueous methanol: Coupling all-atom simulations to semi-grand canonical coarse-grained reservoir. *Macromolecules* **2013**, *46*, 9158–9163. [CrossRef]

519. Agarwal, A.; Zhu, J.; Hartmann, C.; Wang, H.; Site, L.D. Molecular dynamics in a grand ensemble: Bergmann-Lebowitz model and adaptive resolution simulation. *New J. Phys.* **2015**, *17*. [CrossRef]

520. Wang, H.; Hartmann, C.; Schütte, C.; Site, L.D. Grand-canonical-like molecular-dynamics simulations by using an adaptive-resolution technique. *Phys. Rev. X* **2013**, *3*. [CrossRef]

521. Nielsen, S.O.; Moore, P.B.; Ensing, B. Adaptive multiscale molecular dynamics of macromolecular fluids. *Phys. Rev. Lett.* **2010**, *105*. [CrossRef] [PubMed]

522. Heyden, A.; Truhlar, D.G. Conservative algorithm for an adaptive change of resolution in mixed atomistic/coarse-grained multiscale simulations. *J. Chem. Theory Comput.* **2008**, *4*, 217–221. [CrossRef] [PubMed]

523. Park, J.H.; Heyden, A. Solving the equations of motion for mixed atomistic and coarse-grained systems. *Mol. Simul.* **2009**, *35*, 962–973. [CrossRef]

524. Potestio, R.; Fritsch, S.; Español, P.; Delgado-Buscalioni, R.; Kremer, K.; Everaers, R.; Donadio, D. Hamiltonian adaptive resolution simulation for molecular liquids. *Phys. Rev. Lett.* **2013**, *110*. [CrossRef] [PubMed]

525. Potestio, R.; Español, P.; Delgado-Buscalioni, R.; Everaers, R.; Kremer, K.; Donadio, D. Monte carlo adaptive resolution simulation of multicomponent molecular liquids. *Phys. Rev. Lett.* **2013**, *111*. [CrossRef] [PubMed]

526. Voter, A.F. A method for accelerating the molecular dynamics simulation of infrequent events. *J. Chem. Phys.* **1996**, *106*, 4665–4677. [CrossRef]

527. Voter, A.F. Hyperdynamics: Accelerated molecular dynamics of infrequent events. *Phys. Rev. Lett.* **1997**, *78*, 3908–3911. [CrossRef]

528. Voter, A.F.; Montalenti, F.; Germann, T.C. Extending the time scale in atomistic simulation of materials. *Annu. Rev. Mater. Sci.* **2002**, *32*, 321–346. [CrossRef]

529. Voter, A.F. Parallel replica method for dynamics of infrequent events. *Phys. Rev. B* **1998**, *57*, R13985–R13988. [CrossRef]

530. Sørensen, M.R.; Voter, A.F. Temperature-accelerated dynamics for simulation of infrequent events. *J. Chem. Phys.* **2000**, *112*, 9599–9606. [CrossRef]

531. Hänggi, P.; Talkner, P.; Borkovec, M. Reaction-rate theory: Fifty years after Kramers. *Rev. Mod. Phys.* **1990**, *62*, 251–341. [CrossRef]

532. Elber, R.; Karplus, M. A method for determining reaction paths in large molecules: Application to myoglobin. *Chem. Phys. Lett.* **1987**, *139*, 375–380. [CrossRef]

533. Elber, R.; Karplus, M. Multiple conformational states of proteins: A molecular dynamics analysis of myoglobin. *Science* **1987**, *235*, 318–321. [CrossRef] [PubMed]

534. Elber, R.; Ghosh, A.; Cárdenas, A. Long time dynamics of complex systems. *Acc. Chem. Res.* **2002**, *35*, 396–403. [CrossRef] [PubMed]

535. Dellago, C.; Bolhuis, P.G.; Csajka, F.S.; Chandler, D. Transition path sampling and the calculation of rate constants. *J. Chem. Phys.* **1998**, *108*, 1964–1977. [CrossRef]

536. Brooks, B.R.; Brooks, C.L., III; MacKerell, A.D., Jr.; Nilsson, L.; Petrella, R.J.; Roux, B.; Won, Y.; Archontis, G.; Bartels, C.; Boresch, S.; et al. CHARMM: The biomolecular simulation program. *J. Comput. Chem.* **2009**, *30*, 1545–1614. [CrossRef] [PubMed]

537. Christen, M.; van Gunsteren, W.F. On searching in, sampling of, and dynamically moving through conformational space of biomolecular systems: A review. *J. Comput. Chem.* **2008**, *29*, 157–166. [CrossRef] [PubMed]

538. Escobedo, F.A.; Borrero, E.E.; Araque, J.C. Transition path sampling and forward flux sampling. Applications to biological systems. *J. Phys. Condens. Matter* **2009**, *21*. [CrossRef] [PubMed]

539. Klenin, K.; Strodel, B.; Wales, D.J.; Wenzel, W. Modelling proteins: Conformational sampling and reconstruction of folding kinetics. *Biochim. Biophys. Acta Proteins Proteomics* **2011**, *1814*, 977–1000. [CrossRef] [PubMed]

540. E, W.; Ren, W.; Vanden-Eijnden, E. Finite temperature string method for the study of rare events. *J. Phys. Chem. B* **2005**, *109*, 6688–6693. [CrossRef] [PubMed]

541. Vanden-Eijnden, E.; Ren, W.; Vanden-Eijnden, E. Transition pathways in complex systems: Reaction coordinates, isocommittor surfaces, and transition tubes. *Chem. Phys. Lett.* **2005**, *413*, 242–247.

542. Weinan, E.; Vanden-Eijnden, E. Transition-path theory and path-finding algorithms for the study of rare events. *Annu. Rev. Phys. Chem.* **2010**, *61*, 391–420.

543. Ren, W.; Vanden-Eijnden, E.; Maragakis, P.; Vanden-Eijnden, E. Transition pathways in complex systems: Application of the finite-temperature string method to the alanine dipeptide. *J. Chem. Phys.* **2005**, *123*, 134109. [CrossRef] [PubMed]

544. Passerone, D.; Parrinello, M. Action-derived molecular dynamics in the study of rare events. *Phys. Rev. Lett.* **2001**, *87*, 108302. [CrossRef] [PubMed]

545. Branduardi, D.; Gervasio, F.L.; Parrinello, M. From A to B in free energy space. *J. Chem. Phys.* **2007**, *126*. [CrossRef] [PubMed]

546. Dellago, C.; Bolhuis, P.G. Transition path sampling and other advanced simulation techniques for rare events. In *Advanced Computer Simulation Approaches for Soft Matter Sciences III*; Springer: Berlin, Germany, 2009.

547. Dellago, C.; Bolhuis, P.G.; Geissler, P.L. Transition path sampling. *Annu. Rev. Phys. Chem.* **2002**, *53*, 291–318.

548. Schwetlick, H.; Zimmer, J. Calculation of long time classical trajectories: Algorithmic treatment and applications for molecular systems. *J. Chem. Phys.* **2009**, *130*. [CrossRef] [PubMed]

549. Wales, D.J. Discrete path sampling. *Mol. Phys.* **2002**, *100*, 3285–3305. [CrossRef]

550. Zaloj, V.; Elber, R. Parallel computations of molecular dynamics trajectories using the stochastic path approach. *Comput. Phys. Commun.* **2000**, *128*, 118–127. [CrossRef]

551. Laio, A.; Parrinello, M. Escaping free-energy minima. *Proc. Natl. Acad. Sci. USA* **2002**, *99*, 12562–12566. [CrossRef] [PubMed]

552. Kamerlin, S.; Vicatos, S.; Dryga, A.; Warshel, A. Coarse-grained (multiscale) simulations in studies of biophysical and chemical systems. *Annu. Rev. Phys. Chem.* **2011**, *62*, 41–64. [CrossRef] [PubMed]

553. Neri, M.; Anselmi, C.; Cascella, M.; Maritan, A.; Carloni, P. Coarse-grained model of proteins incorporating atomistic detail of the active site. *Phys. Rev. Lett.* **2005**, *95*. [CrossRef] [PubMed]

554. Van Gunsteren, W.F.; Bakowies, D.; Baron, R.; Chandrasekhar, I.; Christen, M.; Daura, X.; Gee, P.; Geerke, D.P.; Glättli, A.; Hünenberger, P.H.; et al. Biomolecular modeling: Goals, problems, perspectives. *Angew. Chem. Int. Ed.* **2006**, *45*, 4064–4092. [CrossRef] [PubMed]

555. Tuckerman, M.E.; Martyna, G.J.; Berne, B.J. Molecular dynamics algorithm for condensed systems with multiple time scales. *J. Chem. Phys.* **1990**, *93*, 1287–1291. [CrossRef]